Title
SLIP MECHANISMS IN SINGLE CRYSTALS OF HEXAGONAL CLOSE-PACKED PHASES

Authors
Dorn, John E.
Mitchell, Jack B.

Publication Date
1964-06-15

UCRL-11418

University of California

Ernest O. Lawrence Radiation Laboratory

SLIP MECHANISMS IN SINGLE CRYSTALS OF HEXAGONAL CLOSE-PACKED PHASES

Berkeley, California

DISCLAIMER

UCRL-11418

UNIVERSITY OF CALIFORNIA
Lawrence Radiation Laboratory
Berkeley, California
AEC Contract No. W-7405-eng-48

SLIP MECHANISMS IN SINGLE CRYSTALS OF HEXAGONAL CLOSE-PACKED PHASES

John E. Dorn[1] and Jack B. Mitchell[2]

Prepared for Presentation

at the

Second International Symposium on Materials

University of California
Berkeley, California

June 15-18, 1964

[1]Professor of Materials Science of the Department of Mineral Technology and Research Metallurgist of the Inorganic Materials Research Division of the Lawrence Radiation Laboratory, University of California, Berkeley.

[2]Research Metallurgist, Inorganic Materials Research Division of the Lawrence Radiation Laboratory, University of California, Berkeley.

I. INTRODUCTION

Whereas a large number of metals and alloys crystallize in the face-centered and body-centered cubic lattices only relatively few metals and intermediate phases, as shown in Table I, crystallize in the hexagonal close-packed system. For this reason, perhaps, only a modest amount of research has been directed toward uncovering the dislocation mechanisms that hexagonal alloys can undertake, in contrast to the extensive investigations that have already been completed on the face-centered and body-centered cubic materials. It might also be thought that basic research on hexagonal systems is being somewhat neglected because their greater anisotropy implies greater complexity of dislocation behavior. This deduction is not necessarily true; frequently, it is easier to isolate and identify operative mechanisms of deformation in hexagonal than in cubic crystals.

Although some hexagonal alloys often exhibit other unique and desirable engineering properties, they are at present not particularly noted for their high strength. On the other hand, there is no theoretical reason why hexagonal alloys of high strength cannot be developed. As in the cubic systems, the highest strength commercial hexagonal alloys are dispersion hardened. The major problem in increasing their strength concerns maintaining adequate ductility. As shown by von Mises[2] at least five independent slip systems must operate in order to mitigate the stress concentrations of groups of blocked dislocations. Because of the limited slip systems they have, this problem is much more difficult to solve in hexagonal metals than in cubic metals which always have an adequate number of operative slip systems to satisfy von Mises condition.

TABLE I

Hexagonal Close-Packed Metals and Alloys[1]

A. Elements

Element	Lattice constants (Å) a	c	Axial Ratio c/a
∝-Be	2.281	3.576	1.567
Cd	2.972	5.605	1.886
Ce	3.62	5.99	1.65
Co	2.502	4.061	1.623
Dy	3.590	5.648	1.573
Er	3.558	5.587	1.570
Gd	3.636	5.782	1.590
∝-Hf	3.194	5.0511	1.581
Ho	3.577	5.616	1.569
Lu	3.503	5.551	1.579
Mg	3.203	5.200	1.623
Os	2.729	4.310	1.579
Re	2.760	4.458	1.615
Ru	2.700	4.273	1.582
Sc	3.309	5.273	1.594
Tb	3.601	5.694	1.501
Tc	2.735	4.388	1.604
∝-Ti	2.950	4.683	1.587
∝-Tl	3.449	5.514	1.598
Tm	3.538	5.554	1.570
Y	3.647	5.730	1.571
Zn	2.659	4.936	1.856
∝-Zr	3.231	5.147	1.593

B. Intermediate Phases

Phase	a	c	c/a
γ - Ag_2Al	2.879	4.573	1.588
β - AgAs	2.891	4.722	1.633

TABLE I (Cont.)

δ-$AgCd_3$	3.060	4.810	1.572
Ag_3Ga	-----	-----	-----
β-AgHg	2.964	4.831	1.631
β-Ag-Sn(14.2 at.%)	2.928	4.774	1.630
δ-$AgZn_3$	2.818	4.451	1.579
α_2-Au_2Cd	2.916	4.822	1.655
Au_3Hg	2.910	4.791	1.647
Au_4In	2.908	4.777	1.643
β-Au_4Sn	2.928	4.763	1.627
Au_2Ti	2.79	4.77	1.71
ϵ - $AuZn_8$	2.809	4.369	1.555
β-Pb-Bi(28.83 at.%)	3.501	5.705	1.629
β^1-Cd_3Li(23 at.% Li)	3.083	4.88	1.586
Cd_3Mg (ordered)	6.220	5.034	0.809
$CdMg_3$ (ordered)	6.300	5.064	0.803
Co_3Mo (ordered)	5.12	4.11	0.805
Co_3W (ordered)	5.12	4.12	0.804
ϵ-CrIr	2.670	4.259	1.595
Rh-Cr(50 at.%)	2.669	4.249	1.592
β^1-Cu_3Ga	2.593	4.228	1.630
CuGe(18 at.%)	2.609	4.229	1.621
CuGe	-----	-----	-----
G-CuSb(18.1 at.%) (partially ordered)	10.896	8.660	0.794
ϵ-ZnCu(21 at.%)	2.73	4.28	1.567
β^{11}-Fe_3Sn (ordered)	5.447	4.352	0.799
MnGe(23.8 at.%) (ordered)	5.336	4.365	0.8165
γ - $InNi_3$ (ordered)	5.320	4.242	0.798
ϵ -IrMo(46.3 at.%)	2.754	4.409	1.601
β-IrW(36.1 at.%)	2.753	4.399	1.598
$Mn_{11}Sn_3$ (ordered)	5.650	4.506	0.798
ϵ-MoPt(33 at.%)	2.795	4.492	1.607
G-MoRh(31.5 at.%)	2.737	4.376	1.599

TABLE I (Cont.)

β-Ni_3Sn (ordered)	5.282	4.235	0.8018
$PbTi_4$ (ordered)	5.97	4.836	0.8096
Pt_3U (ordered)	5.752	4.889	0.851
Rh_3V_2	-----	-----	-----
$(Sb_{0.8}$-$Ti_{0.2})Ti_3$ (ordered)	5.946	4.798	0.807
$(Si_{0.72}$-$Ta_{0.28})Ta_3$ (ordered)	6.09	4.90	1.61
$SnTi_3$ (ordered)	5.916	4.764	0.805
Ag_3In (ordered)			0.813
$Mn_{3.25}Ge$ (ordered)			0.8165
$(Ti_{0.2}$-$Pb_{0.8})Ti_3$ (ordered)			0.8096

It is the objective of this survey to review the current status of knowledge on dislocation mechanisms of slip on each of several slip systems in the hope that this information will shed some light on what factors control slip and how slip mechanisms might be modified in order to provide more operative slip systems so as to establish the preliminary basis for the future development of higher strength hexagonal alloys with adequate ductility. Although the phenomena of twinning and fracturing are also significant to the development of high strength hexagonal metals, these issues will not be emphasized here since the major problem appears a fortiori to be concerned with slip mechanisms. Furthermore, only those papers that impinge strongly on the objective of this survey will be discussed.

II. DISLOCATIONS AND STACKING FAULTS IN CLOSE-PACKED HEXAGONAL PHASES

Frank and Nicholas[3] and also Berghizan, Fourdeux and Amelinckx[4] demonstrated that a greater variety of dislocations are possible in hexagonal close-packed phases than in the face-centered or body-centered cubic lattices. The issues involved were reviewed in detail by Price[5] and are merely summarized here for future reference.

As shown in Fig. 1, there are six types of dislocations in hexagonal close-packed crystals to each of which belong a number of dislocations as shown without regard to sign in column C. An estimate of the energy of each type of dislocation based on the ideal axial ratio is also shown in the figure where elastic anisotropy is neglected and the energy is assumed to be proportional to the square of the Burgers vector. As noted, dislocations of the type AB will dissociate into their partials by the reaction

$$AB \rightarrow A\sigma + \sigma B \qquad \Delta u = -a^2 + 2/3a^2 = -a^2/3 \tag{1}$$

since the energy is reduced. The possibility of the dissociation

$$AS \rightarrow A\sigma + \sigma S \qquad \Delta u = -a^2 + \frac{2a^2}{3} + \frac{a^2}{3} = 0 \tag{2}$$

is dictated principally by elastic anisotropy. Whereas the change in energy for the dissociation,

$$AS + TB \rightarrow AB + TS \qquad \Delta u = -\frac{11}{3}a^2 + a^2 + 8/3\ a^2 = 0 \tag{3}$$

is zero, this reaction is nevertheless expected as a result of the continued dissociation of AB as given by Eq. 1. On this basis, the most commonly encountered dislocations are expected to be types of $A\sigma$, ST, AS, and σS.

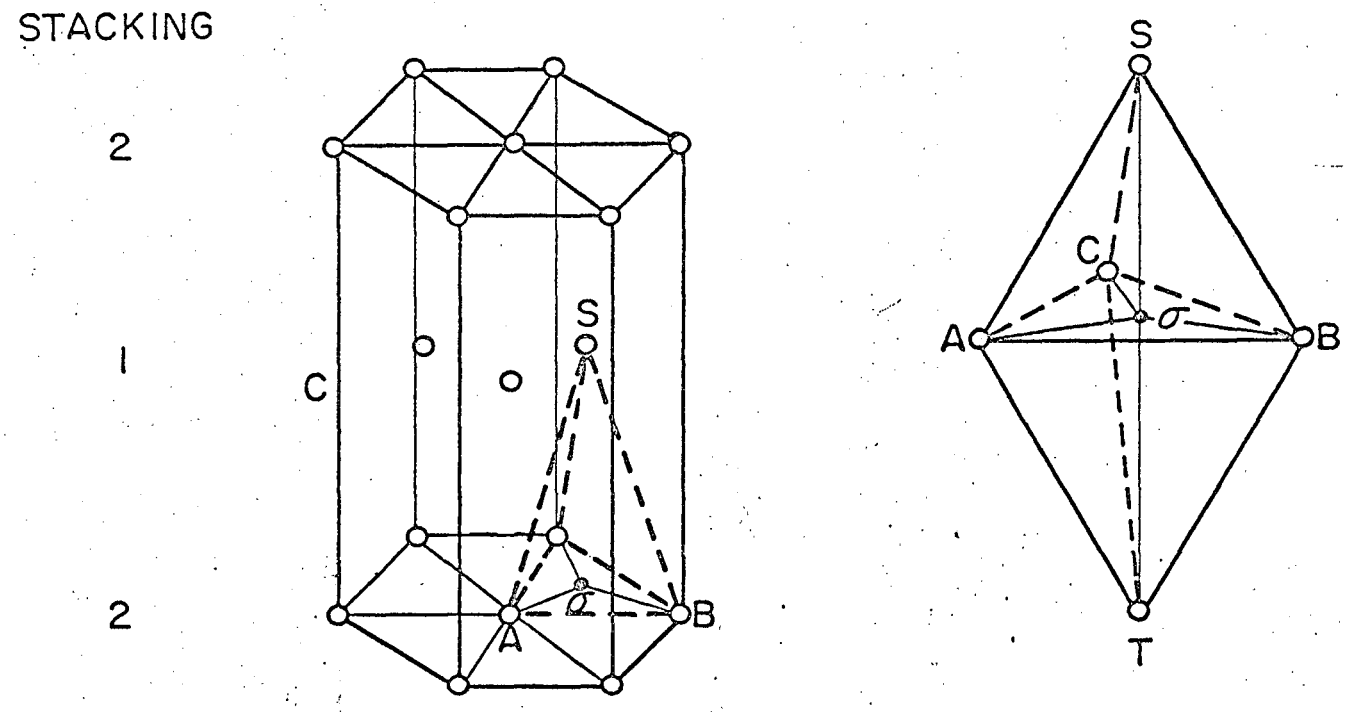

KIND	TYPE	NO.	ENERGY, U
PERFECT	AB = a	6	a^2
	ST = c	1	$c^2 = 8a^2/3$
	SA + BT = c+a	6	$11a^2/3$
IMPERFECT	Aσ = p	3.	$a^2/3$
	σS = 1/2 c	2	$2a^2/3$
	AS = 1/2 c+p	3	a^2

FIG. 1 DISLOCATIONS IN HEXAGONAL CLOSE-PACKED CRYSTALS.

The various imperfect dislocations are associated with stacking faults on the basal plane, as documented in Fig. 2, where the close-packed hexagonal stacking is designated by 1212 and the face-centered cubic is 123123. The faults shown in Fig. 2a and 2b occur when perfect dislocations of type AB dissociate into two imperfect dislocations of type $A\sigma$. As indicated by the arrows these faults introduce two violations of next nearest neighbors. Stacking faults can also be produced by the condensation of vacancies into platelets on the basal plane leading to the high energy sequency--121121--which brings two similar layers into contact. More likely, the lower energy dipole of partial dislocations of type type σS will be formed as shown in Fig. 2c. This is also a high energy stacking fault because, as shown by the arrows, it contains three next nearest neighbor violations. Therefore, the yet lower energy configurations (shown in Figs. 2d and 2e) resulting in the formation of type AS or AT dipoles are expected which have only a single next nearest neighbor violation. The types of stacking faults obtained by condensation of interstitials on the basal plane are shown in Figs. 2f and 2g; these become more stable when swept out by SA type dipoles as shown in Figs. 2h and 2i.

The various dislocations that have been observed by electron microscopy and slip trace techniques are recorded in Table II. These observations reveal that all of the various stable dislocations predicted do, in fact, exist although all types have not yet been observed in each case.

Dislocations of the type AB remain perfect on all planes excepting the basal plane. When they lie in the basal plane, however, they dissociate into a pair of partials, as shown by Eq. 1, with a

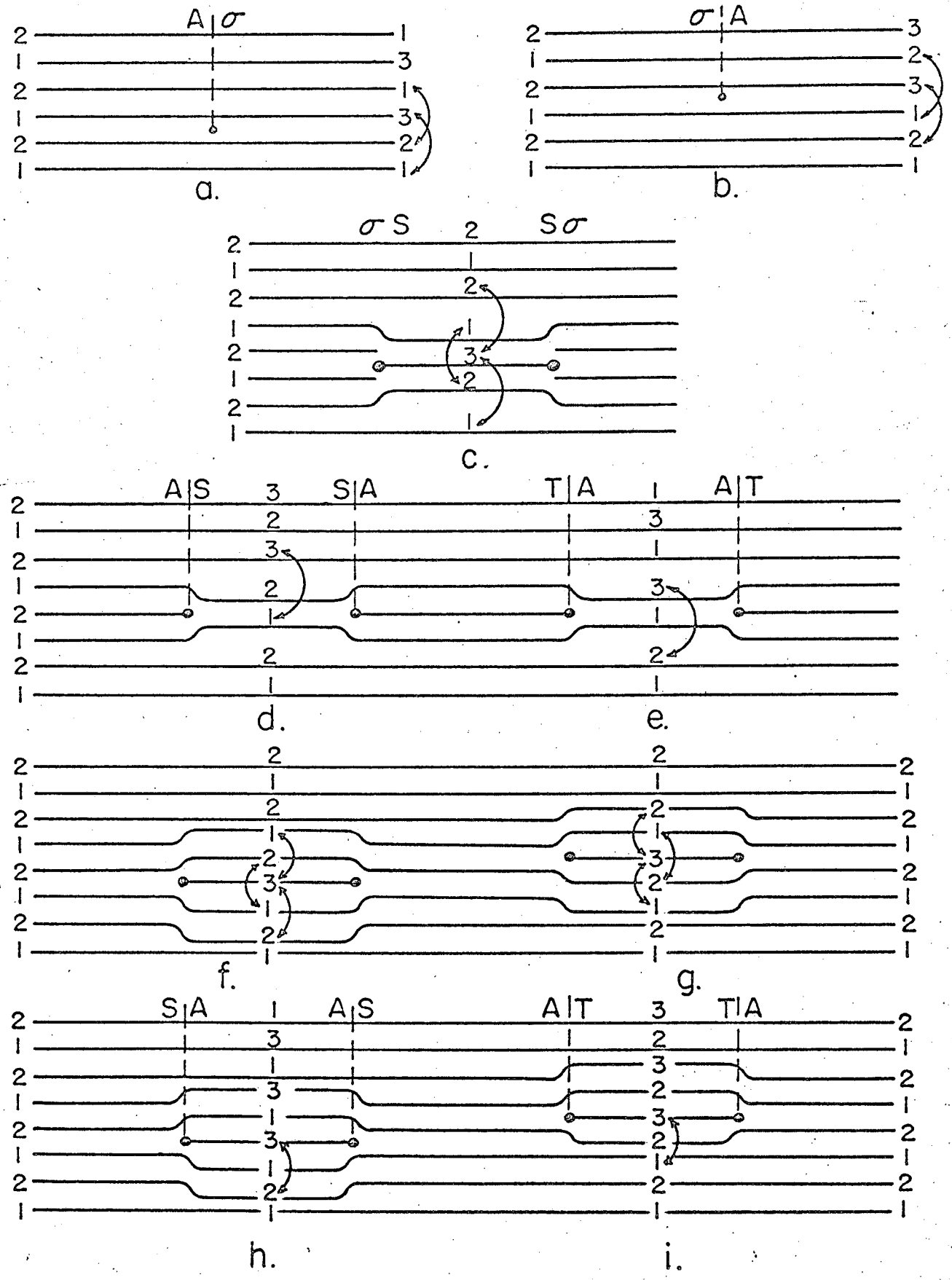

FIG. 2 STACKING FAULTS IN HEXAGONAL CLOSE-PACKED METALS.

TABLE II

Observed Dislocations and Slip Modes*

Metal or Alloy	c/a	Burgers Vector	Slip Plane	Reference	Remarks
Cd	1.89	a	$(0001)^P$	$(10)^{SM}(5)^E$	
		a	$(10\bar{1}0)$	$(11)^{SU}$	Prism slip in bulk single crystals above 165°C (11)
		a	$(10\bar{1}1)$	$(12)^E(14)^E$	
		c + a	$(11\bar{2}2)$	$(10)^{SM}(13,14)^E(15)^{SU}(16)^{SU}$	Pyramidal slip in bent or compressed single crystals but not in tension (15) Thin foils strained in the electron microscope or rolled and thinned polycrystals
		c	?	$(5)^E$	
		p	(0001)	$(5)^E$	
		c/2 + p	sessile	$(5,17)^E$	
Zn	1.86	a	$(0001)^P$	$(18)^{SU}(19)^{SU}$	Prism glide in bulk single crystals above 250°C (19)
		a	$(10\bar{1}0)$	$(19)^{SU}(24)^{SU}$	
		c + a	$(11\bar{2}2)$	$(20)^{SU}(21,22)^E(23)^{SU}$	
		c	?	$(5)^E$	Thin foils strained in electron microscope or rolled and thinned polycrystals
		p	(0001)	$(4)^E$	
		c/2 + p	sessile	$(4)^E$	
Mg	1.62	a	$(0001)^P$	$(25)^{SM}(26)^{SU}(27)^{SU}(28)^{SU}$ $(29)^{SU}(30)^{SU}$	Pyramidal and prism slip observed in region of stress concentrations below ambient temperature (25)
		a	$(10\bar{1}0)$	$(25)^{SM}(31)^E(32)^{SU}$	
		a	$(10\bar{1}1)$	$(33)^{SU}(26)^{SU}(27)^{SU}(34)^{SU}$ $(35)^{SU}(36)^{SU}$	Prism slip above 450°K in single crystals (32)
		$\langle 10\bar{1}0\rangle$	$(11\bar{2}2)$	$(37)^{SU}$	

TABLE II (Cont.)

Ti	1.59	a	(0001)	$(38)^{SU}(39)^{SM}$	
		a	$(10\bar{1}0)^{P}$	$(40)^{SM}(38)^{SM}$	
		a	$(10\bar{1}1)$	$(40)^{SM}(38)^{SM}$	
Zr	1.59	a	(0001)	$(41)^{SM}$	
		a	$(10\bar{1}0)^{P}$	$(41)^{SM}$	
Be	1.57	a	$(0001)^{P}$	$(42)^{SU}(43)^{SU}(44)^{SU}(45)^{SU}$	Pyramidal slip observed above 500°K (40) Other non-basal slip observed above 800°C (47)
		a	$(10\bar{1}0)$	$(42)^{SU}(43)^{SU}(45)^{SU}(46)^{SM}$	
		a	$(10\bar{1}1)$	$(45)^{SU}(46)^{SM}(47)^{SM}$	
		c + a	$(11\bar{2}4)$	$(45)^{SU}$	
		c + a	$(11\bar{2}2)$	$(45)^{SU}$	
		a	$(10\bar{1}4)$	$(47)^{SM}$	
		c + a	$(10\bar{1}0)$	$(47)^{SM}(56)^{E}$	
Mg-Li (14 at. %) solid solution	1.61	a	$(0001)^{P}$	$(48)^{SM}(49)^{SU}$	
		a	$(10\bar{1}0)$	$(48)^{SU}(49)^{SU}$	
γ Ag_2Al intermediate phase	1.588	a	$(0001)^{P}$	$(50)^{SU}$	
		a	$(10\bar{1}0)$	$(50)^{SU}(51)^{SU}$	
ϵ Ag-Zn solid solution	1.557 to 1.571	a	$(0001)^{P}$	$(52)^{SU}$	Tendancy for non-basal slip increased with decreasing c/a
		a	$(10\bar{1}0)$	$(52)^{SM}$	
		a	$(10\bar{1}1)$	$(52)^{SM}$	
ζ Cu-Ge Solid solution	1.633	a	(0001)	$(53)^{SU}$	

TABLE II (Cont.)

Cd-Mg solid solution	1.80-1.89	a	$(0001)^P$	$(10)^{SM}$	Slip direction not determined for pyramid plane
		?	$(11\bar{2}2)$	$(10)^{SM}$	
Cd-Mg solid solution	1.64-1.77	a	$(0001)^P$	$(10)^{SM}$	Prismatic slip at grain corners
		a	$(10\bar{1}0)$	$(10)^{SM}$	
Mg_3Cd solid solution	1.627	a	$(0001)^P$	$(54)^{SM}$	Disordered condition c/a not reported
Mg_3Cd	0.8038	a	$(0001)^P$	$(54)^{SM}$	Ordered State Non-basal slip directions not reported
		?	$(10\bar{1}0)$	$(54)^{SM}$	
		?	$(10\bar{1}1)$	$(54)^{SM}$	
		?	$(11\bar{2}2)$	$(54)^{SM}$	

*E = observed by electron microscopy

S = observed by slip trace technique

P = predominant slip mode at ambient temperature

M = polycrystals

U = single crystals

reduction of energy. As the partials separate, a stacking fault ribbon of the kind shown in Figs. 2a and 2b is formed having an energy γ per unit area due to the two next nearest neighbor violations for hexagonal packing. At equilibrium the repulsion arising from the two partial dislocations is balanced by the attraction due to the stacking fault and for two straight parallel dislocations.

$$\gamma \sim \frac{Gb^2}{24\pi d}\left\{\left(3 - \frac{1}{1-u}\right)\cos^2\theta + \left(\frac{3}{1-u} - 1\right)\sin^2\theta\right\} \qquad (4)$$

where d is the separation of the partials, G and u are the shear modulus and Poisson's ratio respectively, and θ is the angle between the dislocation line and its total Burger's vector. Although Eq. 4 can be used to determine the stacking fault energy, Whelan's method,[6] using extended and contracted modes, is usually preferred. The stacking fault energies that have been estimated by electron microscopy are summarized in Table III. These data suggest that in general the stacking fault energies in hexagonal close-packed metals is high and in many cases so high that the separation of the partial dislocations is less than the resolution of the electron microscope. In these cases, as will be developed later, the stacking fault energies can be deduced from the kinetics of intersection and cross-slip mechanisms as determined from mechanical behavior. As suggested by Marcinkowski,[9] ordered DO_{19} hexagonal close-packed phases should exhibit higher stacking fault energies than random solution due to the additional energy of the antiphase boundary thus produced.

TABLE III

Stacking Fault Energies

Metal	c/a	Energy	Ref.	Remarks
Cd	1.886	15-30 ergs/cm^2	(5)	Stacking fault energies of Zn, Cd and Be estimated from electron microscope observations and that of Mg from analysis of basal slip in single crystals.
Zn	1.856	15.30 ergs/cm^2	(5)	
Mg	1.623	~60 ergs/cm^2	(7)	
Be	1.567	~180 ergs/cm^2	(8)	

III. MODES OF SLIP

The various modes of slip that have been observed in hexagonal close-packed metals and alloys are summarized in Table II. A distinction is made between observations based on electron microscopy and those based on the more macroscopic method of slip trace techniques because the observations by electron microscopy may identify infrequent and local events whereas slip line traces are only observed where rather extensive slip over one or a cluster of nearby slip planes has taken place. An additional distinction is also made regarding whether the observations were made on single crystals or polycrystalline aggregates because as a result of high stress concentrations polycrystalline specimens occasionally exhibit some of the difficult modes of deformation which are not necessarily observed in single crystals. Furthermore, the sessile dislocations are appropriately identified in the slip plane column. Although it is possible that the absence of a mode merely refers to the fact that it has not been observed, it is more likely that in those examples that have been subjected to detailed scrutiny, the absence of data on any one mode of slip seriously implies that the crtical resolved shear stress for slip by this mode is extremely high.

The á priori prediction of the planes on which slip might take place is much less accurate than predictions of the possible Burger's vectors of dislocations. This stems from the fact that different mechanisms of deformation might serve to hinder the motion of dislocations on the different planes. It is generally agreed, however, that slip will not readily occur on those planes for which the Peierls stress[55] is extremely high. Nabarro,[56] assuming elastic isotropy and a simple tetragonal

lattice, suggested that the Peierls stress at the absolute zero, τ_p°, is approximated by

$$\tau_p^\circ \simeq \frac{2G}{(1-u)} e^{-\frac{2\pi d}{b(1-u)}} \quad (5)$$

where G = the shear modulus of elasticity and u = Poisson's ratio, d = the interplanar spacing, and b = the Burgers vector. Therefore, in general agreement with the experimental observations in Table II, slip should take place on planes having low indices, for which d has its largest values. Although Eq. 5 is quantitatively in error and gives theoretical Peierls' stresses that are much in excess of the flow stresses usually observed in single crystals, it has, nevertheless, been used in the absence of other approaches as a crude qualitative guide for judging the relative orders of facile slip by different modes of deformation. On the basis of the Nabarro estimate, the Peierls stress is expected to be high on high index planes which would not therefore serve as operative slip planes. Furthermore, it might be expected that whereas crystals having a large c/a ratio should slip with relative ease on the basal plane, those having lower c/a ratio might exhibit more facile slip on the prismatic or pyramidal planes. This trend appears to be observed as the c/a ratio decreases from 1.86 for Zn to 1.59 for Zr, but Be which has an axial ratio of c/a = 1.57 appears to be an exception to this expectation. It is not known whether the strong elastic anisotropy of Be might be responsible for this anomaly. Levine, Kaufmann and Aronin[42] have shown that the critical resolved shear stress in Be for both the $\langle 11\bar{2}0\rangle \{0001\}$ and $\langle 11\bar{2}0\rangle \{10\bar{1}0\}$ modes of slip decreases with increasing purity; the ratio of the critical resolved shear stress

for prismatic to basal slip increased from 5/1 to 38/1 with increasing purity over the range of impurities that were investigated. This first suggests that impurity hardening is very pronounced in Be and secondly that even high purity Be is an exception to the general trend that prismatic slip becomes more favorable as the c/a ratio is reduced. Other exceptions have also been observed. For example, Stoloff and Davies[52] have shown that ϵ-Ag-Zn alloys which have an axial ratio from 1.55 to 1.57 deformed principally by basal slip with only modest amounts of prismatic and first type pyramidal slip. Therefore, the Nabarro analysis of the Peierls stress merely serves to discount the possibility of slip on very high index planes but it cannot be employed, in its present state of development, for discriminating between various permissible modes of deformation on low index planes.

As shown in Table II, dislocations of the type a that have Burgers vectors $b = a/3 \langle 11\bar{2}0 \rangle$ have been observed to slip on the $\{0001\}$, $\{10\bar{1}0\}$ and the $\{10\bar{1}1\}$ planes. It is interesting to speculate on the relative ease of these mechanisms of deformation. Under preliminary straining to induce either prismatic or pyramidal slip, dislocations having edge components may move out of the crystal whereas dislocation segments that achieve the screw orientation will become trapped because they will dissociate into a pair partial dislocation on the basal plane. If additional dislocations are generated on the prismatic or pyramidal planes at points of stress concentration, they also will become trapped causing, in the absence of other aleviating mechanisms, strain hardening. Stress concentrations due to piled-up dislocations might therefore be expected to promote early fracturing. It appears, at present, that the only

mechanism that might aleviate this condition is dynamic cross slip of the dissociated screw dislocations trapped on the basal planes. As shown by Friedel,[57] the activation energy for cross slip increases with the constriction and recombination energies. Consequently, the ease of slip on the prismatic or pyramidal planes as a result of dislocations of type a should increase as the stacking fault energy increases or as the separation of the partial dislocations decreases. On this basis alone, prismatic slip should be least prevalent in Be, and its frequency should increase with the series Zn, Cd and Mg. With the exception of Be, which exhibits some prismatic slip, this is the observed trend. On the other hand, the stacking fault energy is not the only significant factor involved. Even when the constriction and recombination energies are low, glide may yet be extremely difficult on the prismatic and pyramidal planes as a result of high activation energies for slip (e.g. that due to the Peierls mechanism) on these planes. Price[14] has shown that the resolved shear stress for slip on non-basal planes below room temperature in Zn and Cd is lowest for $(11\bar{2}2)\ \langle 11\bar{2}3\rangle$ glide, intermediate for $(10\bar{1}1)\ \langle 11\bar{2}0\rangle$ glide and highest for $(10\bar{1}0)\ \langle 11\bar{2}0\rangle$ glide whereas at higher temperatures the shear stress for $(11\bar{2}2)\ \langle 11\bar{2}3\rangle$ glide is higher than that for $(10\bar{1}1)\ \langle 11\bar{2}0\rangle$ glide. Consequently, generalizations concerning operative slip modes must await detailed evidence regarding the strain-rate controlling mechanisms of slip on the various planes. Some preliminary investigations on these issues will be reviewed in the following sections of this summary.

As mentioned previously at least five independent slip systems are required in order to insure extensive ductility in polycrystalline aggregates. A number of possible modes of slip are identified in Table IV.

As documented in Table II, the first four modes have been detected experimentally and the last two are shown merely to indicate additional possible, but yet undetected, modes. Slip by the $\{0001\}\ \langle 11\bar{2}0\rangle$ systems contribute only two independent modes since the third Burgers vector of type a lying in the basal plane is equal to the sum of the other two and consequently does not provide an independent mode. Twinning on the most frequently observed $\{11\bar{2}2\}$ twin plane provides 6 more modes in one direction each but, as has been observed in the low temperature deformation of pure polycrystalling Mg, basal slip plus twinning, permits only a few percent strain before fracture takes place since the shear strains due to twinning are limited in sense and extent.[25] Prismatic slip by the $\{1\bar{1}00\}\ \langle 11\bar{2}0\rangle$ systems provides three modes of deformation but only two of these are independent. Consequently, simultaneous basal and prismatic slip by Burger's vectors of the type a provides four modes of deformation and does not allow for shear straining parallel to the c axis. It has been shown that alpha solid solution alloy additions above about 8 at.% Li induce extensive prismatic slip in polycrystalline Mg in addition to basal slip.[48] Such alloys exhibit up to 12% elongation even at 4°K whereas the pure Mg polycrystals having the same grain size fracture at about 5% elongation. The mechanism whereby Li additions to Mg lower the critical resolved shear stress for slip by the $\{1\bar{1}00\}\ \langle 11\bar{2}0\rangle$ modes of slip will be discussed later in this summary.

The changes of shape which can be produced by the first type pyramidal slip in the family $\{10\bar{1}1\}\ \langle 11\bar{2}0\rangle$ are precisely the same as those which can be produced by the simultaneous and independent operation of both basal and prismatic slip. The operation of this mode together with

TABLE IV

Modes of Slip in Hexagonal Metals

No.	Burgers Vector Type	Slip Direction	Slip Plane Type	Slip Plane	Number Independent Systems [58]
1	a	$\langle 1\bar{2}10\rangle$	basal	$\{0001\}$	2
2	a	$\langle 1\bar{2}10\rangle$	prismatic 1st type	$\{10\bar{1}0\}$	2
3	a	$\langle 1\bar{2}10\rangle$	pyramidal 1st type	$\{10\bar{1}1\}$	4
4	c + a	$\langle \bar{1}\bar{1}23\rangle$	pyramidal 2nd type	$\{11\bar{2}2\}$	5
5	c	$\langle 0001\rangle$	prismatic 1st type	$\{10\bar{1}0\}$	2
6	c	$\langle 0001\rangle$	prismatic 2nd type	$\{11\bar{2}0\}$	2

basal and prismatic slip provides only four independent slip systems. Slip by the fourth mode documented in Table IV provides all of the independent modes of deformation for assuring ductility in polycrystalline aggregates. The fact that only minor contributions of this mode have been observed in Zn suggests that its critical resolved shear stress is quite high and it may be this factor that accounts for the notorious lack of ductility in polycrystalline Zn at room temperature. The fourth mode of deformation has been observed to take place to a greater extent in Cd and this might in part account for the better ductility that polycrystalline Cd exhibits.[10,15] Simultaneous action of only the first three modes does not provide for shearing parallel to the c axis. Consequently, they must be supplimented by relatively easy action of one or more of the last three modes in order to provide extensive ductility. Twinning can assist only in a limited way in providing some of the needed shear strains parallel to the c axis.

IV. MECHANISMS OF DEFORMATION

Mechanisms of deformation refer to the athermal or thermally activated processes that determine the critical resolved shear stress for the various modes of slip. Up to the present, investigations on mechanisms of slip have been limited to basal and prismatic slip by the first two modes given in Table IV. Each of these modes of slip can exhibit a series of different mechanisms of slip dependent on which is the more difficult and thus controls the deformation. It will be shown that different mechanisms control the deformation by a given mode over different ranges of temperature in a given metal or alloy. Furthermore, the controlling mechanism of a given mode can occasionally be changed by appropriate alloying and the controlling mechanism is frequently different over identical ranges of temperature for the different modes.

A. Basal Slip

The effect of temperature on the critical resolved shear stress for slip by the $\{0001\}\ \langle 11\bar{2}0\rangle$ mode for Zn, Cd, Mg and Be are given in Fig. 3. Two ranges of behavior are clearly revealed. Deformation over Region I, where the flow stress decreases almost linearly with an increase in temperature, is controlled by a thermally activated mechanism; over Region II, where the flow stress appears to decrease mildly and proportional to the decrease in the shear modulus of elasticity with increasing temperature, deformation is controlled by an athermal mechanism. At higher temperatures, a second thermally activated mechanism, undoubtedly dynamic recovery, is controlling.

Whereas strain hardening increases the flow stress in each of these ranges, it is most readily isolated from other effects in Region II

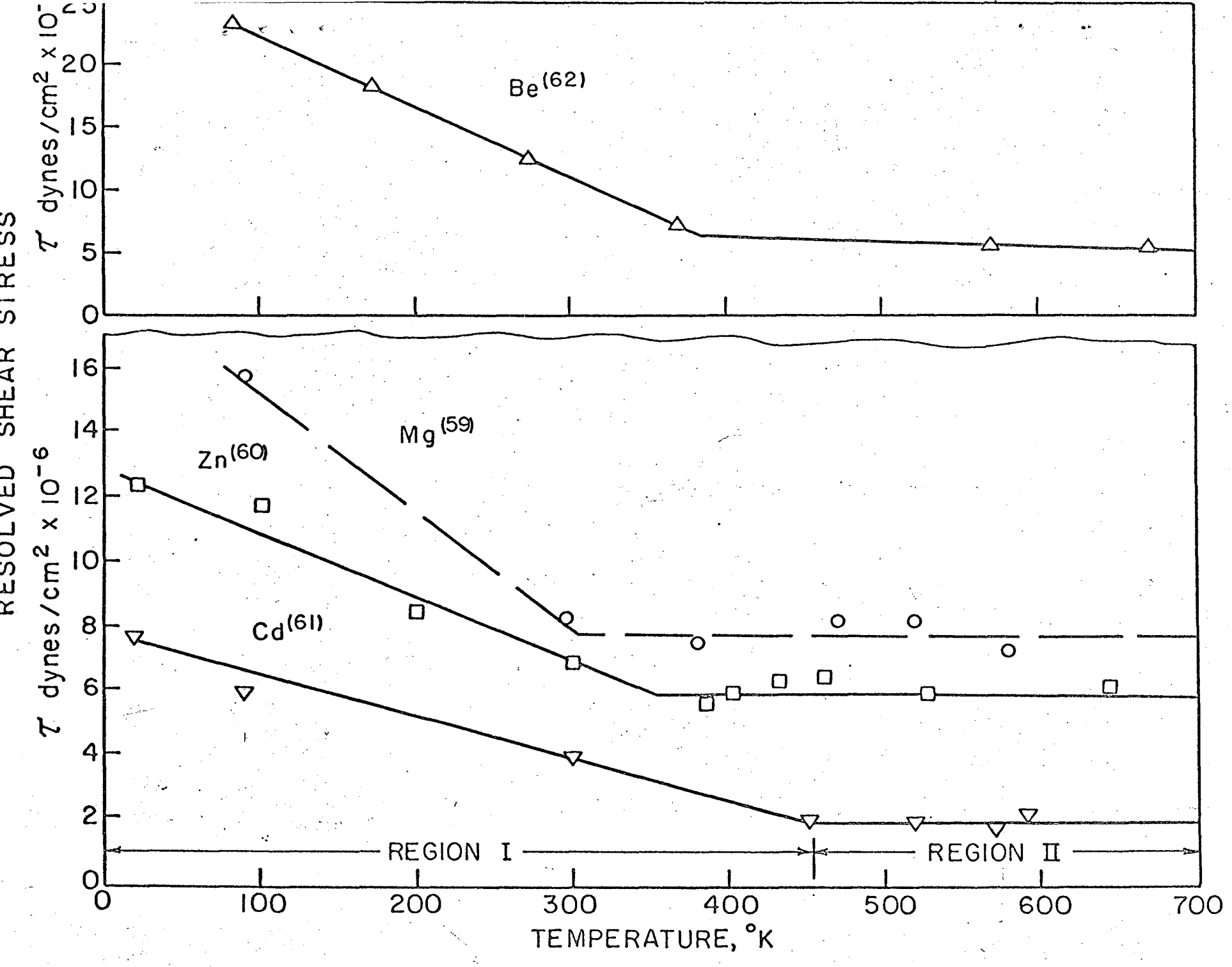

FIG. 3 RESOLVED SHEAR STRESS vs. TEMPERATURE FOR BASAL SLIP FOR Cd, Zn, Mg AND Be.

where it is the major factor that modifies the critical resolved shear stress for slip. The thermally activated mechanism that determines slip over Region I occurs with such rapidity at the higher temperatures of Region II that it no longer affects the flow stress in this range. In general the rate of strain hardening on the basal plane is small, the flow stress increasing linearly with the strain over the lower temperatures of Region II in a manner analogous to the strain-hardening observed during easy-glide of face-centered cubic metals. As shown in the Parker-Washburn experiment on the motion of a low-angle boundary in Zn,[63] dislocations undertaking basal slip encounter barriers. Price[5] noted that occasionally dislocations become blocked at barriers that are not resolved by the electron microscope. Other barriers, however, have been identified by Seeger and Trauble[18] and also Price.[5] Mechanically polygonized low angle boundaries and mechanically produced twist boundaries are seen. Dislocations from different sources on slightly different slip planes form piled-up arrays of dislocations. Occasionally, tensile stress fields due to the arrays are sufficiently high to induce fracturing on the basal plane about midway between the two glide planes of the arrays. Superjogs are formed by double cross slip from the basal to prismatic to another basal plane. Dislocations having screw components exhibit cusps when under a stress probably due to unit jogs or small superjogs. Such cusped dislocations have been observed to move by jumps under a stress suggesting that vacancies are produced. Dislocations having jogs of an intermediate size form the usual dipoles as a result of the mutual interactions of the branches of the dipoles and the two branches of a dislocation having large superjogs continue under a stress to spiral about the jog. Dislocation loops due to the

condensation of mechanically produced vacancies are prevalent in electron micrographs of deformed hexagonal crystals. Seeger and Trauble[18] have observed that Zn single crystals tested above about 243°K exhibit a range of much higher strain hardening following an easy glide stage than crystals tested below this temperature. They attributed this to the interaction of the glide dislocations of type a on the basal plane with loops of dislocations of the type 1/2c + p produced by the condensation of vacancies.

Glide dislocations of the type a on the basal plane do not interact with forest dislocations of the type c since their Burgers vectors are mutually perpendicular. When glide dislocations on the basal plane of the type a form junctions with dislocations of the same type on the prism plane they form another dislocation of type a on the basal plane. If the dislocation on the prism plane is almost normal to the basal plane the junction is small and will be easily eliminated by a minor modification of the usual intersection mechanism; and when the dislocation on the prism plane makes a small angle with the basal plane, a long junction having a Burgers vector of type a is produced which can then slip on the basal plane. Thus only very modest stresses are required to decompose junctions that are produced by interactions between glide dislocations on the basal plane having Burgers vectors of type a with forest dislocations on the prism plane having the same type of Burgers vector. Both attractive and repulsive junctions can be formed between glide dislocations on the basal plane having Burgers vectors of the type a and forest dislocations on the pyramidal plane having Burgers vectors of the type c + a. The interaction here is somewhat analogous to that described by Saada for face-centered cubic metals.[64] He has shown that the piercing

of attractive junctions formed by intersecting dislocations results in an athermal contribution to the flow stress which is decidedly higher than in the case of repulsive junctions. The stress to complete intersection of the dislocations that have formed an attractive junction is given by

$$\tau = \frac{\gamma G b}{d} \qquad (6)$$

where d is the average spacing between the "forest" dislocations of type c + a. If the forest dislocations are spaced close together γ is approximately 2.0; however, if the forest dislocations which satisfy the required geometrical conditions to form attractive junctions with glide dislocation are widely spaced, γ is about 0.4. It is difficult to estimate what contribution this mechanism makes to the flow stress during basal glide in hcp metals since little is known concerning the density and distribution of c + a dislocations. It is expected that because the energy of the c + a dislocation is relatively high, the grown in density of these dislocations might be small and therefore the athermal contribution to the flow stress during basal glide by the junction reaction might be negligible. If, However, $\langle 11\bar{2}3\rangle$ glide becomes active during deformation, as it might in polycrystalline metals, the frequency of junction reactions might increase to the point where they would make a significant contribution to the flow stress. In zinc and cadmium where $(11\bar{2}2)\langle 11\bar{2}3\rangle$ glide is known to be an active slip mode, this mechanism may be of significant importance, but in several other hcp metals c + a glide dislocations are not observed at atmospheric temperatures and a strain hardening contribution by this mechanism would probably be small. It therefore appears that the temperature independent flow stress exhibited in Region II arises

principally as a result of long range stress fields of groups of dislocations plus the interactions between glide dislocations and sessile loops lying in the basal planes.

B. Thermally Activated Intersection

Conrad and Robertson[29] and Conrad, Hays, Schoeck and Wiedersich[30] have rather clearly demonstrated that the thermally activated mechanism for basal slip in Mg over Region I arises from the intersection of dislocations. The similarity of the stress-temperature diagrams for basal slip of the other hexagonal metals suggests that their deformation at low temperatures is also controlled by the intersection mechanism. As previously mentioned, however, the mechanical behavior of Be single crystals during basal slip in Region I is influenced by interactions of solute atoms with the glide dislocations. Seeger[65] has shown that the strain rate that is obtained by the intersection mechanism is given by

$$\dot{\gamma} = \dot{\gamma}_o \in^{-U/kT} \qquad (7)$$

where $\dot{\gamma}$ is the shear strain rate, $\dot{\gamma}_o$ = NAbν (where N is the number of points of contact per unit volume between glide and forest dislocations, A is the area swept out per successful intersection, and ν is the frequency of vibration of the intersecting dislocation) U is the additional energy that must be supplied by a thermal fluctuation to complete intersection and kT has its usual meaning of the Boltzmann constant times the temperature of test. Defining τ_G as the local stress field a dislocation must surmount athermally the net stress, τ^*, aiding the thermal fluctuation in completing intersection is given by

$$\tau^* = \tau - \tau_G \qquad (8)$$

where τ is the applied shear stress. Taking L as the average distance between contacted forest dislocations, a force

$$F = \tau^* L b \tag{9}$$

acts to aid intersection and consequently $U = U\{F\}$. Detailed statistics of the mechanism have not yet been completely formulated and the terms of Eq. 9 must therefore be taken as appropriate smeared values.

In his early discussions of intersection Seeger[65] assumed that the activation energy decreased linearly with the stress according to

$$U = U_i - \tau^* L b d \tag{10}$$

where U_i is the total energy for intersection and d is the distance the force $\tau^* Lb$ has to move to complete the process. On this basis

$$\tau^* = \tau - \tau_G = \frac{U_i}{Lbd} - \frac{kT}{Lbd} \ln \frac{\dot{\gamma}_0}{\dot{\gamma}} \qquad T < T_c \tag{11}$$

revealing that the flow stress should decrease linearly with temperature over Region I and that

$$\tau = \tau_G \tag{12}$$

over Region II where $\tau^* = 0$ and

$$T_c = \frac{U_i}{k \ln (\dot{\gamma}_0/\dot{\gamma})} \tag{13}$$

Both τ_G and U_i vary linearly with the shear modulus of elasticity so that

$$\tau_G = \tau_G^{\circ} G/G^{\circ} \tag{14a}$$

and

$$U_i = U_i^{\circ} G/G^{\circ} \tag{14b}$$

where the superscript zero refers to the absolute zero of temperature. Consequently τ_G and U_i decrease slightly and almost linearly with the absolute temperature.

The trends suggested by Eqs. 11 and 12 are in nominal agreement with the experimental data for basal slip recorded in Fig. 3.

Friedel[66] suggested that the distance between the forest dislocations, L, should decrease as the stress τ^* is increased according to the statistically determined relationship

$$L = \frac{3}{2}\left(\frac{L_w^2 Gb}{\tau^*}\right)^{1/3} \tag{15}$$

where Lw is the mean spacing between the forest dislocations. According to this modification Eq. 11 becomes

$$(\tau^*)^{2/3} = \frac{2}{3}\frac{U_i}{(L_w^2 Gb)^{1/3} bd} - \frac{2}{3}\frac{kT}{(L_w^2 Gb)^{1/3} bd} \ln \frac{\dot{\gamma}_o}{\dot{\gamma}} \tag{16}$$

and T_c retains its value given by Eq. 13. Whereas the original Seeger formulation suggests that

$$\tau = \tau_G + \frac{k \ln(\dot{\gamma}_o/\dot{\gamma})}{Lbd}(T_c - T) \tag{17}$$

Friedel's modification gives

$$\tau = \tau_G + \left\{\frac{\gamma k \ln(\dot{\gamma}_o/\dot{\gamma})}{3(L_w^3 Gb)^{1/3} bd}\right\}^{3/2}(T_c - T)^{3/2} \tag{18}$$

The original data of CHSW[30] giving τ^* as a function of T are shown in Fig. 4. The decreasing values of T_c with strain rate are in accord with the suggestion of Eq. 13 which is valid for the Seeger and Friedel approximations as well as other models for intersection. Thus, the total activation energy for intersection can be determined from the effect of strain rate on T_c, namely

$$\frac{\dot{\gamma}_2}{\dot{\gamma}_1} = \frac{e^{-\frac{U_i^o G/G^o}{k T_{c2}}}}{e^{-\frac{U_i^o G/G^o}{k T_{c1}}}} \tag{19}$$

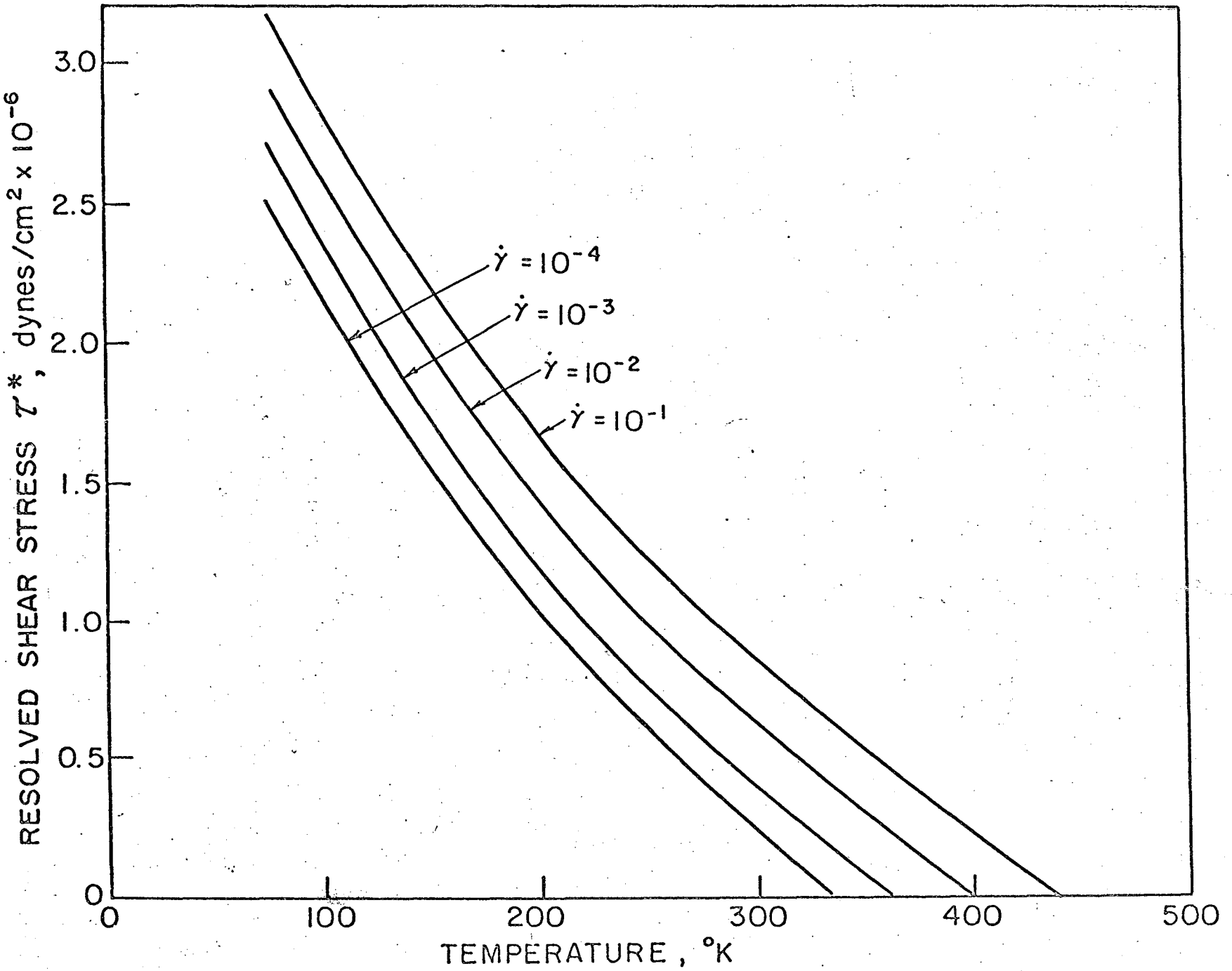

FIG. 4 EFFECT OF TEMPERATURE AND STRAIN RATE ON THE FLOW STRESS τ^* FOR BASAL GLIDE OF Mg SINGLE CRYSTAL.

Using CHSW's data of $T_{c_2} = 440°K$ for $\dot{\gamma}_2 = 10^{-1}$ per sec and $T_{c_1} = 335°K$ for $\dot{\gamma}_1 = 10^{-4}$, and the effect of T on G for Mg given by Roberts,[88] $U_i^0 = 13.1 \times 10^{-13}$ ergs which is in good agreement with the value obtained by CHSW by an alternate procedure. Furthermore from

$$\dot{\gamma}_1 = \dot{\gamma}_0 e^{-\frac{U_i^0 G/G^0}{k T_{c1}}} \tag{20}$$

the value of $\dot{\gamma}_0 = 1.0 \times 10^7$ per sec is obtained. Assuming that

$$\dot{\gamma}_0 = \rho A b v = \left(\frac{\rho}{2}\right) L^2 b \left(\frac{v_0 b}{L}\right) = \rho b^2 \nu_0 \tag{21}$$

where ρ is the density of the glide dislocations and ν_0 is the Debye frequency taken to be 10^{13} per sec, the slightly high but not unreasonable value of $\rho \approx 10^9$ is obtained. Introducing the value of $\dot{\gamma}_0$ obtained above into Eq. 7 and calculating U for the various strain rates that were employed by CHSW gives U as a linear function of T as shown in Fig. 5. Furthermore, the U vs τ^* curve can now be obtained from the data given in Figs. 4 and 5 as shown in Fig. 6. Although the analytical technique that was employed here differs from that originally used by CHSW, the results agree well with their analyses.

Basinki[67] has shown that the activation energy for intersection does not necessarily decrease linearly with the stress (as was originally suggested by Seeger) but it can be represented by a force displacement (F- λ) diagram shown schematically in Fig. 7. Accordingly the energy that must be supplied by a thermal fluctuation to aid the stress in completing intersection is

$$U = \int_{\tau^* L b}^{F_m} \lambda \, dF \tag{22}$$

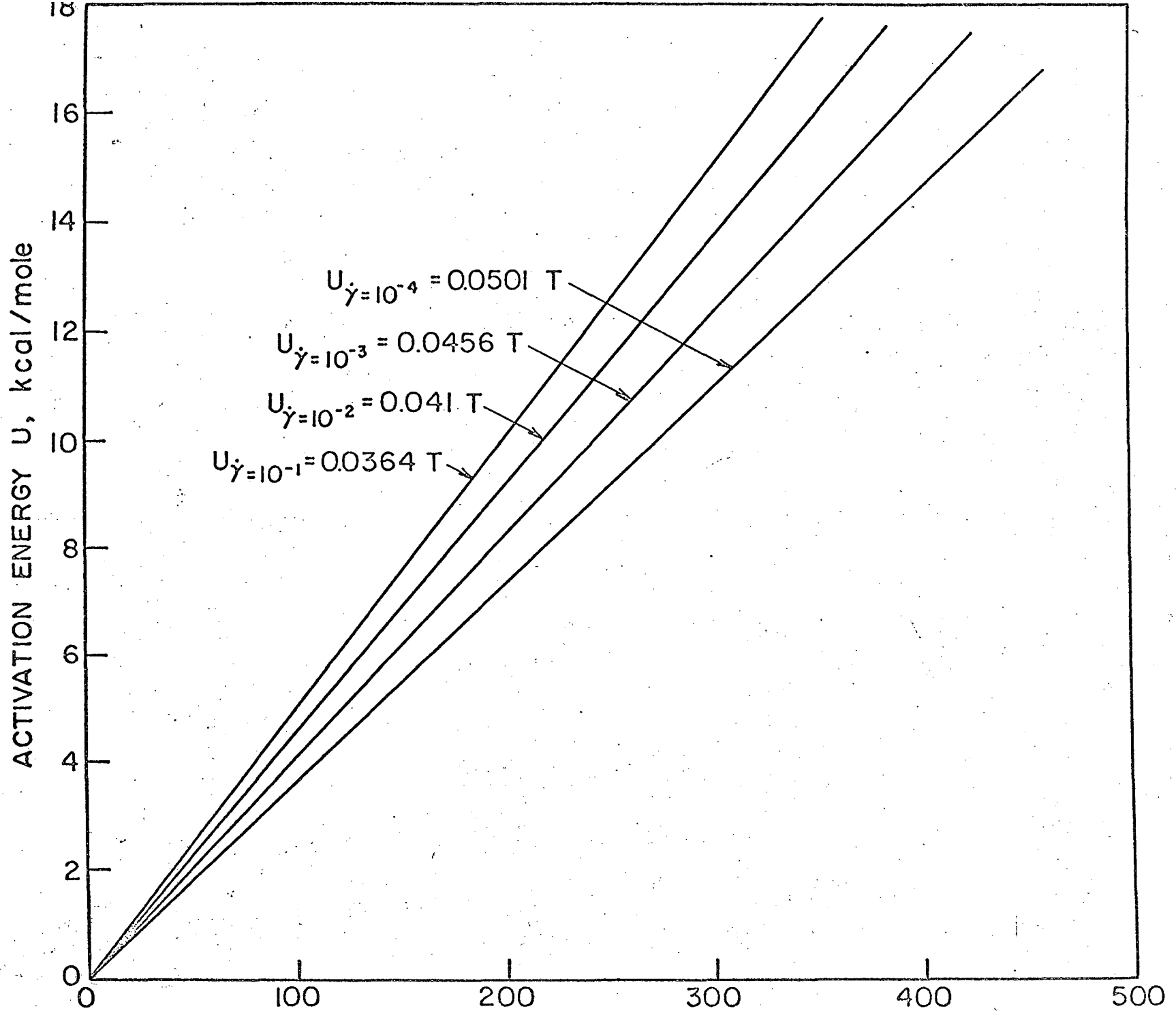

FIG. 5 EFFECT OF TEMPERATURE ON THE ACTIVATION ENERGY FOR BASAL SLIP IN Mg SINGLE CRYSTALS.

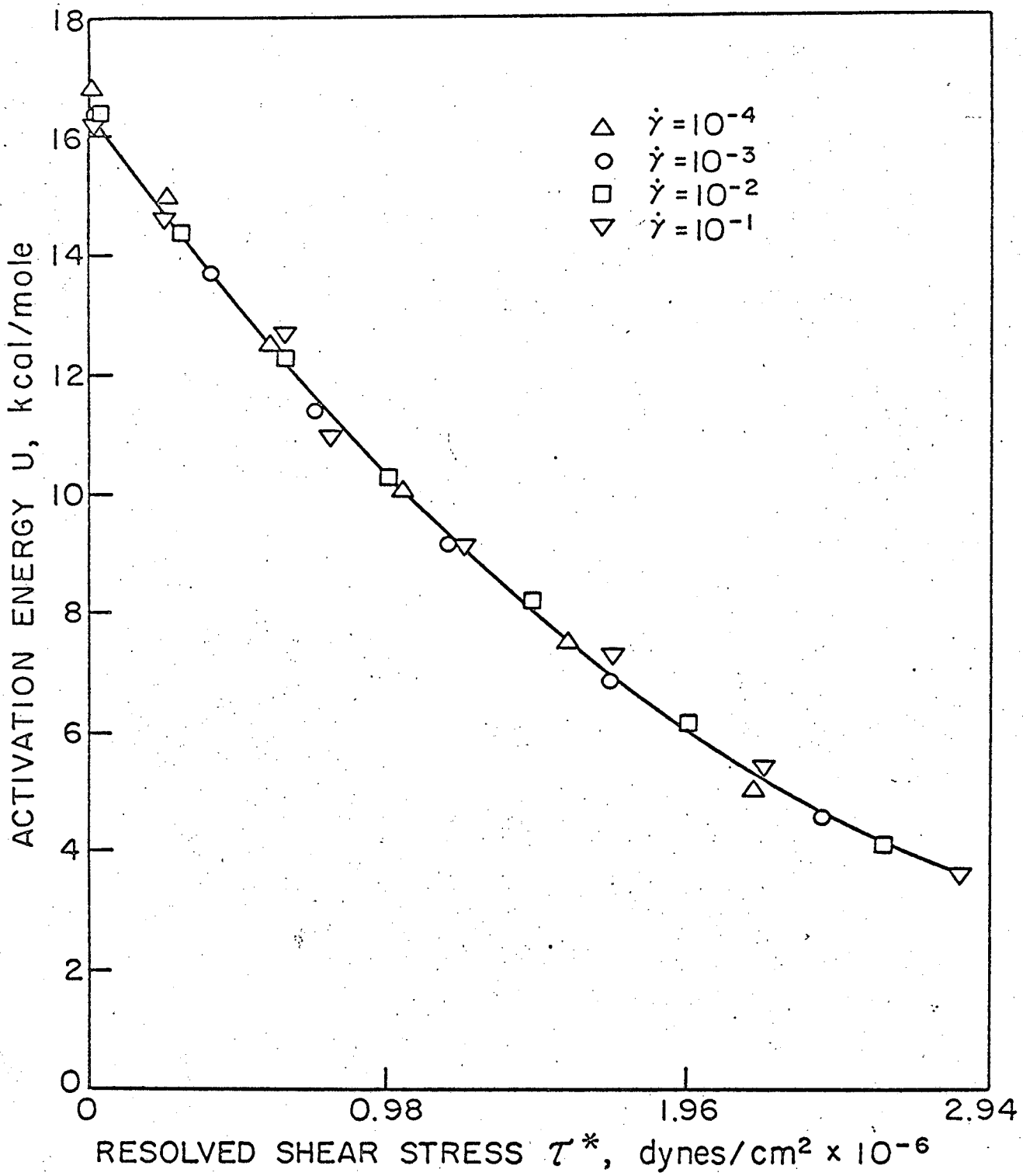

FIG. 6 EFFECT OF STRESS ON THE ACTIVATION ENERGY FOR BASAL SLIP IN Mg SINGLE CRYSTALS.

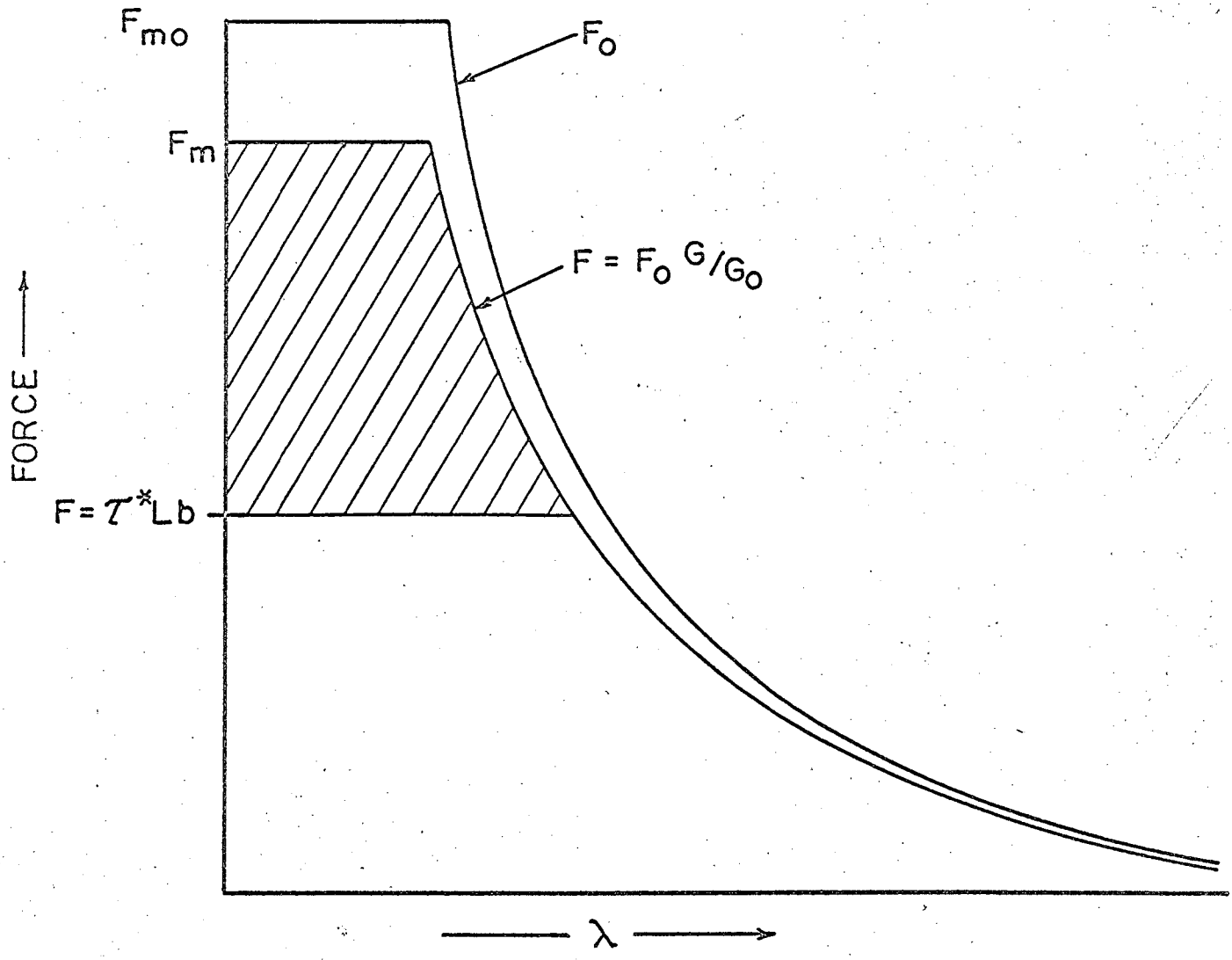

FIG. 7 SCHEMATIC REPRESENTATION OF THE AVERAGE $F-\lambda$ CURVE FOR INTERSECTION.

In order to establish the F-λ diagram from experimental results, the change in strain rate with a change in stress might be used, where

$$\beta = \left(\frac{\partial \ln \dot{\gamma}}{\partial \tau^*}\right)_T = -\frac{1}{kT}\frac{\partial U}{\partial \tau^*} = \frac{A}{kT}\frac{\partial(\tau^* L b)}{\partial \tau^*} \tag{23}$$

If the smeared average values of L can be assumed to be independent of the stress

$$\beta kT = \lambda L b \tag{24}$$

but if Friedel's assumption, given by Eq. 15, is valid

$$\beta kT = \left(\frac{L_0^2 G b}{\tau^*}\right)^{1/3} \lambda b \tag{25}$$

Correspondingly if the smeared average value of L is taken to be constant, the force assisting intersection is

$$F_s = \tau^* L b \tag{26}$$

whereas if Friedel's assumption given by Eq. 15 is valid, this force becomes

$$F_F = \frac{3}{2}(\tau^*)^{2/3}(L_0^2 G b)^{1/3} b \tag{27}$$

Calculations based on the Friedel's assumption gave results that deviated seriously from theoretical expectations of the force-displacement diagram for intersection and, therefore, will not be reproduced here. Rather it will be assumed that the smeared average value of L is substantially constant and that Eqs. 24 and 26 apply.

Using the values of β determined experimentall by CHSW, the τ^* vs $\frac{\beta kT}{b^2}$ curve shown in Fig. 8 was obtained. The ordinates of Fig. 8 are proportional to F and the abscissas are proportional to λ. Therefore, the F-λ curve can be established once the value of L is known.

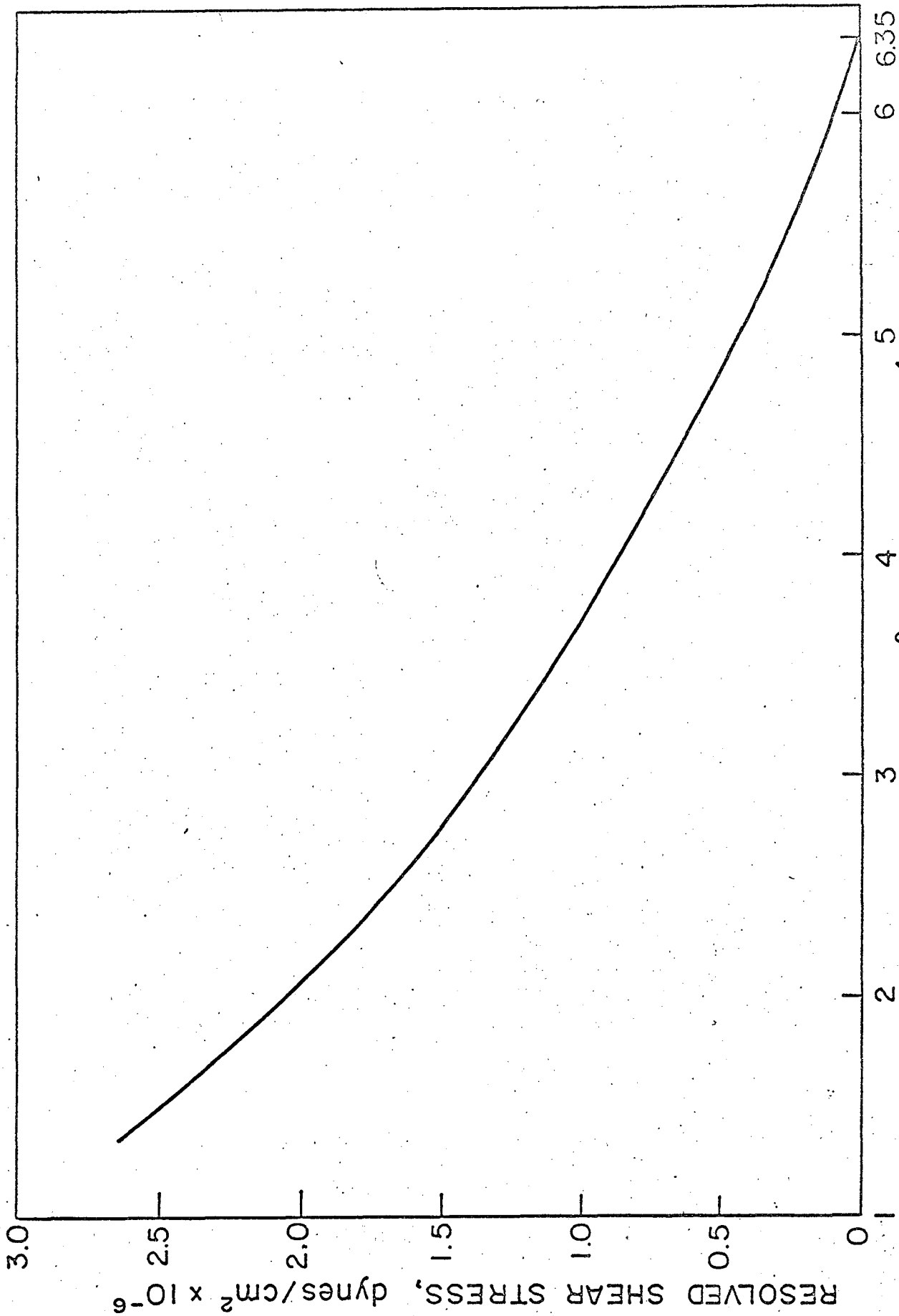

FIG. 8 τ^* vs $\beta kT/b^2$ FOR BASAL GLIDE OF Mg.

An estimate of λ can be duduced from the known theoretical relationship of $U_c/2\Gamma_p y_o$ vs λ/y_o which is developed in the appendix of this paper and is shown by the solid curves given in Fig. 9. Here U_c is the total energy required to form a constriction at the point of intersection of a glide dislocation with a forest dislocation, Γ_p is the line energy per unit length of a partial dislocation and y_o is the equilibrium separation of the partial dislocations. As described in the appendix, the curve for $2c = 0.24$ applies when the total dislocation is in edge orientation whereas that for $2c = 0.12$ applies when the total dislocation is in screw orientation. Since the total intersection energy for Mg was found to be $U_i^0 = 13.1 \times 10^{-13}$ ergs and the jog energy can be approximated to be about $U_j^0 \approx \frac{Gb^3}{12} = 5.05 \times 10^{-13}$ ergs, the constriction energy for Mg, namely $U_c^0 = U_i^0 - U_j^0$, is estimated to be about $U_c^0 = 8.05 \times 10^{-13}$ ergs. Assuming various values of y_o and taking $\Gamma_p^0 = 1/6\ Gb^2$ the experimentally acceptable values of $U_c/2\Gamma_p y_o$ vs λ/y_o for constriction in Mg were also plotted as the broken curve on Fig. 9. The points of intersection of the broken curve with the solid curves give the experimentally deduced value of $y_o \simeq 2b$ as the stacking fault width in pure Mg.

At present it is not known whether some jogging occurs during the last stages of constriction or whether the constriction must be complete before jogging takes place. Therefore, the total displacement for intersection λ_i might be estimated to be $2b \lesssim \lambda_i \lesssim 3b$. Two values $\lambda_i = 2b$ and $\lambda_i = 2.5b$ were assumed for the purpose of comparison. As deduced from Fig. 8 when λ_i is taken to be 2b, $2L = 6.35 \times 10^{-4}$ cm and $L = 3.1 \times 10^{-4}$ whereas when λ_i is taken to be 2.5b, $L = 2.5 \times 10^{-4}$. In either case, the reasonable density of forest dislocations of about 10^7 is

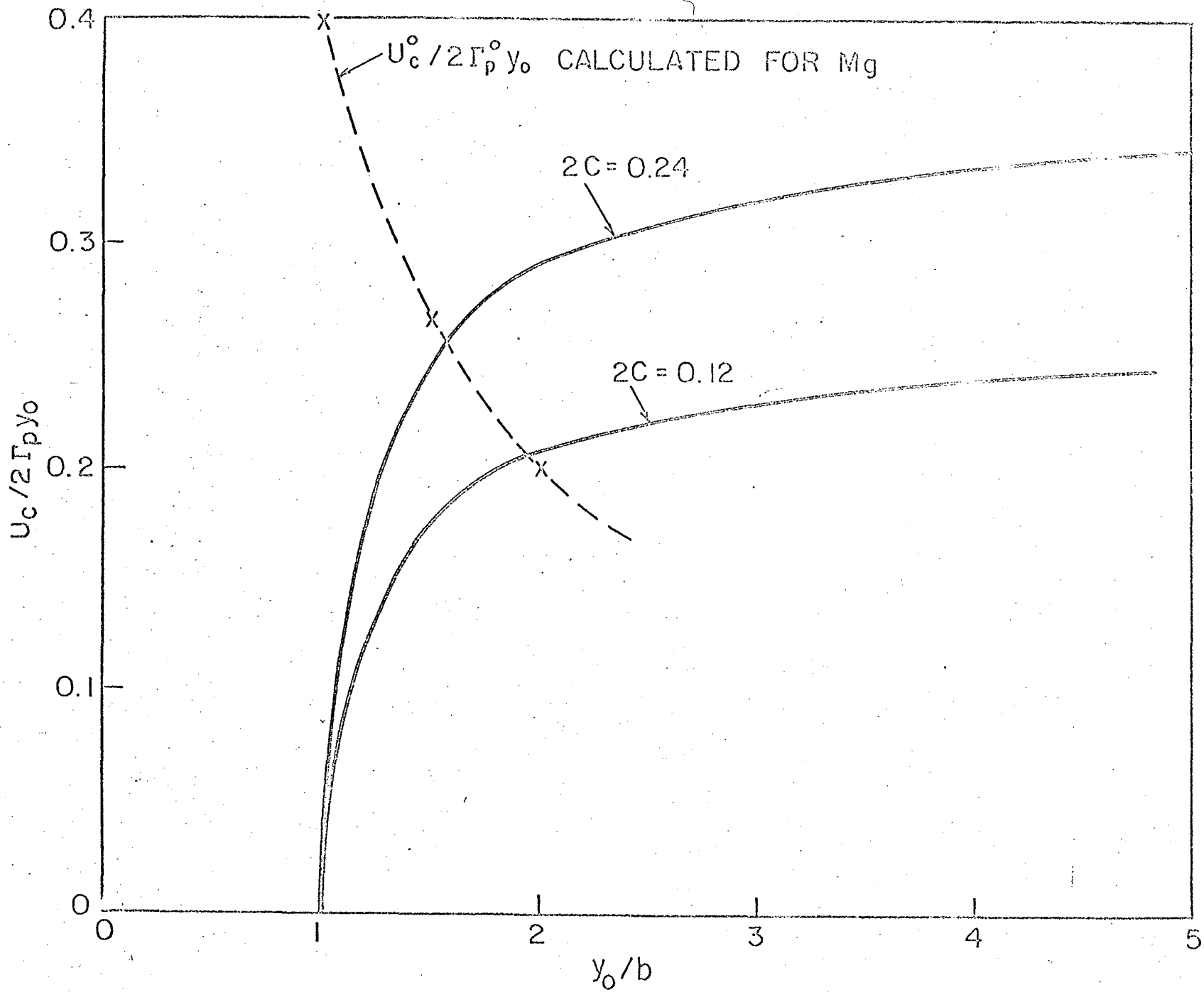

FIG. 9 $U_c/2\Gamma_p y_o$ vs y_o/b FOR CONSTRICTION OF DISLOCATIONS IN EDGE AND SCREW ORIENTATION.

obtained. Using the above mentioned values of L and the experimental data given in Fig. 8, the $F = \tau^* Lb$ vs $\lambda = \beta kT/Lb$ datum points given in Fig. 10 were determined. The solid line refers to the theoretically deduced $F-\lambda$ curve derived in the appendix for constriction alone. The better agreement between theory and experiment when λ_i is taken equal to 2b suggests that some jogging accompanies the last stages of constriction; the fact that the experimentally deduced datum points lie slightly above the theoretical curve for constriction over $o < \lambda < b$ suggests that jogging begins to take place over the final Burger's vector of constriction. Whereas these deductions are somewhat subjective and must be rechecked in the light of better theory and more complete experimental data, they nevertheless conclusively establish the operation of the intersection mechanism for basal slip in Mg and point to a very small separation of the partial dislocations of about $y_o \simeq 2b$.

Up to the present there have been only a few investigations on the effect of alloying on the mechanisms for basal slip in hexagonal alloys. In Fig. 11 are shown the limited data of Quimby, Mote and Dorn[49] on the critical resolved shear stress for basal slip of a 12.5 at.% Li alloy of Mg as a function of temperature for the single strain rate of $\dot{\gamma} = 3 \times 10^{-4}$ per sec. These data reveal that alloying can appreciably increase the flow stress for basal slip. This alloy exhibited a modest yield point, due to Suzuki[68] and possibly also Cottrell[69] locking. The very high value of τ_G for this alloy in contrast to the lower values for pure Mg is believed to arise from Suzuki locking, short-range order hardening and entrapment of a high dislocation density as a result of solute atom interactions. It is not possible at present to say whether the rapid increase in the critical

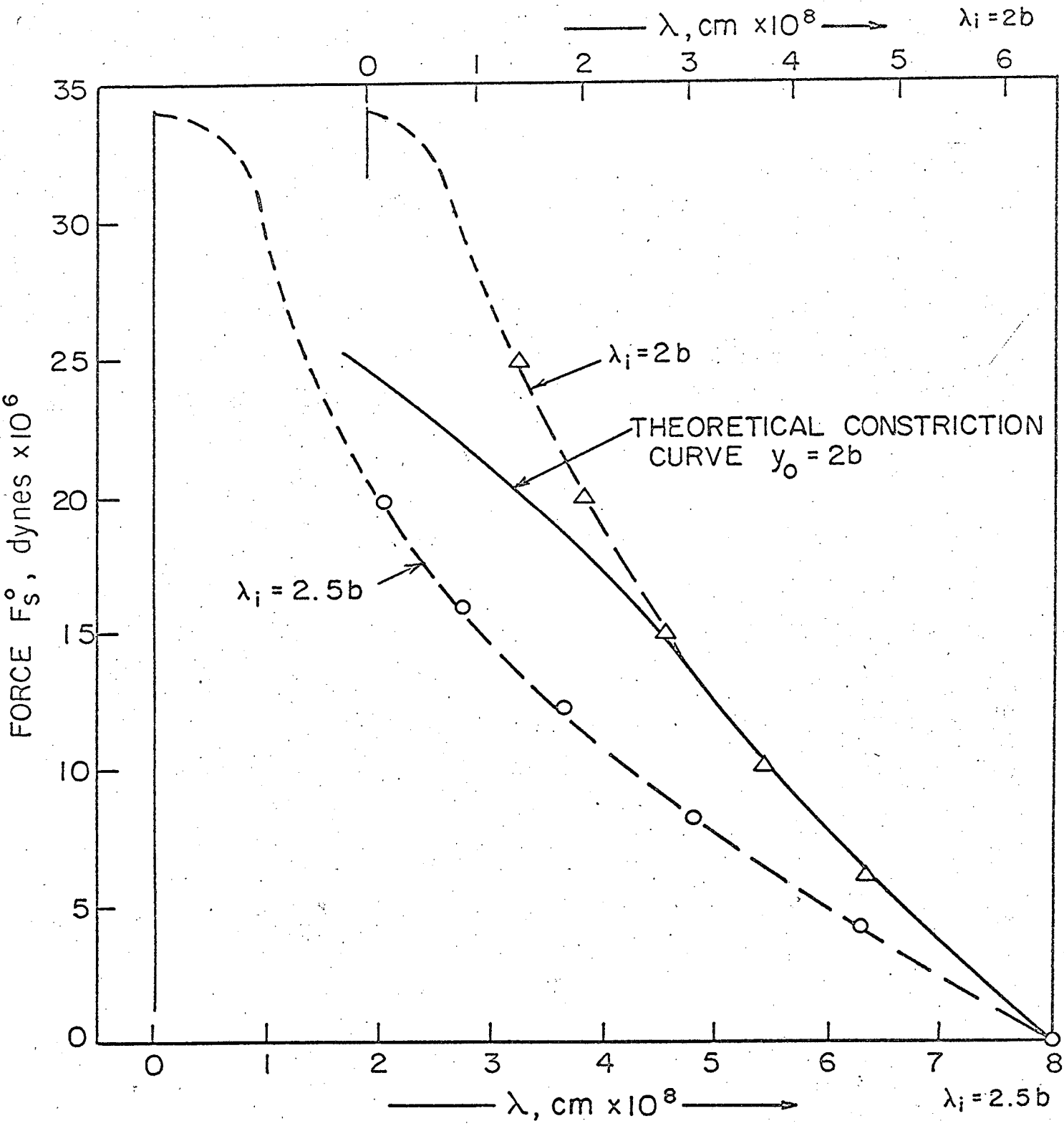

FIG. 10 F - λ CURVES FOR INTERSECTION OF DISSOCIATED GLIDE DISLOCATIONS.

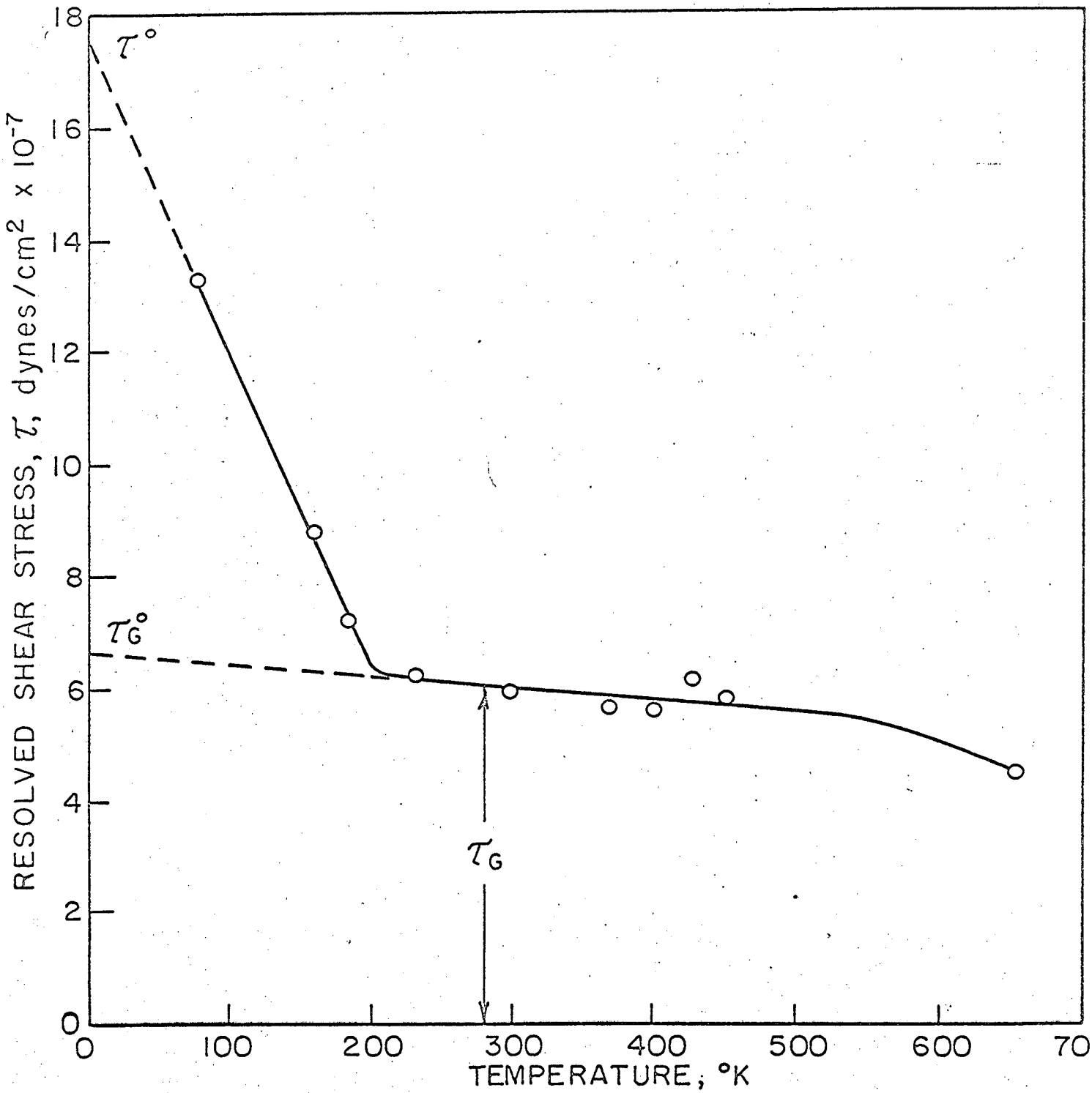

FIG. 11 RESOLVED SHEAR STRESS vs. TEMPERATURE FOR BASAL SLIP IN Mg - 12.5 AT. % Li ALLOY.

resolved shear stress with a decrease in temperature over Region I arises from solute atom effects or from the high density of forest dislocations. If the result is exclusively due to intersection and the intersection energy is about $U_i^0 = 13.1 \times 10^{-13}$ ergs, as previously established for pure Mg, the spacing of the forest dislocation is estimated to be about

$$L \simeq \frac{U_i^0}{(\tau^0 - \tau_e^0)b^2} = 1.2 \times 10^{-5} \text{ cm} \qquad (28)$$

which is within the expected range.

Gilman observed that the critical resolved shear stress for basal slip in Zn containing 0.1 at.% Cd is distinctly different from that for pure Zn as shown in Fig. 12.[19] The decrease in the flow stress that accompanies an increase in temperature over Region I is much more pronounced in the 0.1 at.% Cd alloy of Zn than in pure Zn and whereas the resolved shear stress for basal glide in zinc crystals was insensitive to strain rates from 0.3×10^{-5} to 10×15^5 per sec and insensitive to temperature from about 300° to 680°K, the flow stress for the Zn 0.1 at.% Cd alloy exhibited a strong strain rate and temperature dependence above 540°K in Region III. Although it might be suggested that the intersection mechanism is rate controlling over the low temperature thermally-activated range of Region I (in which event the high sensitivity of the stress to temperature must be ascribed to a substantial increase in the density of the forest dislocations) the data are not adequate to check this postulate. The jerky flow observed in Zn 0.1 at.% Cd alloy over Region II is undoubtedly associated with strain-aging. Both Cottrell and Suzuki locking can contribute to this effect.

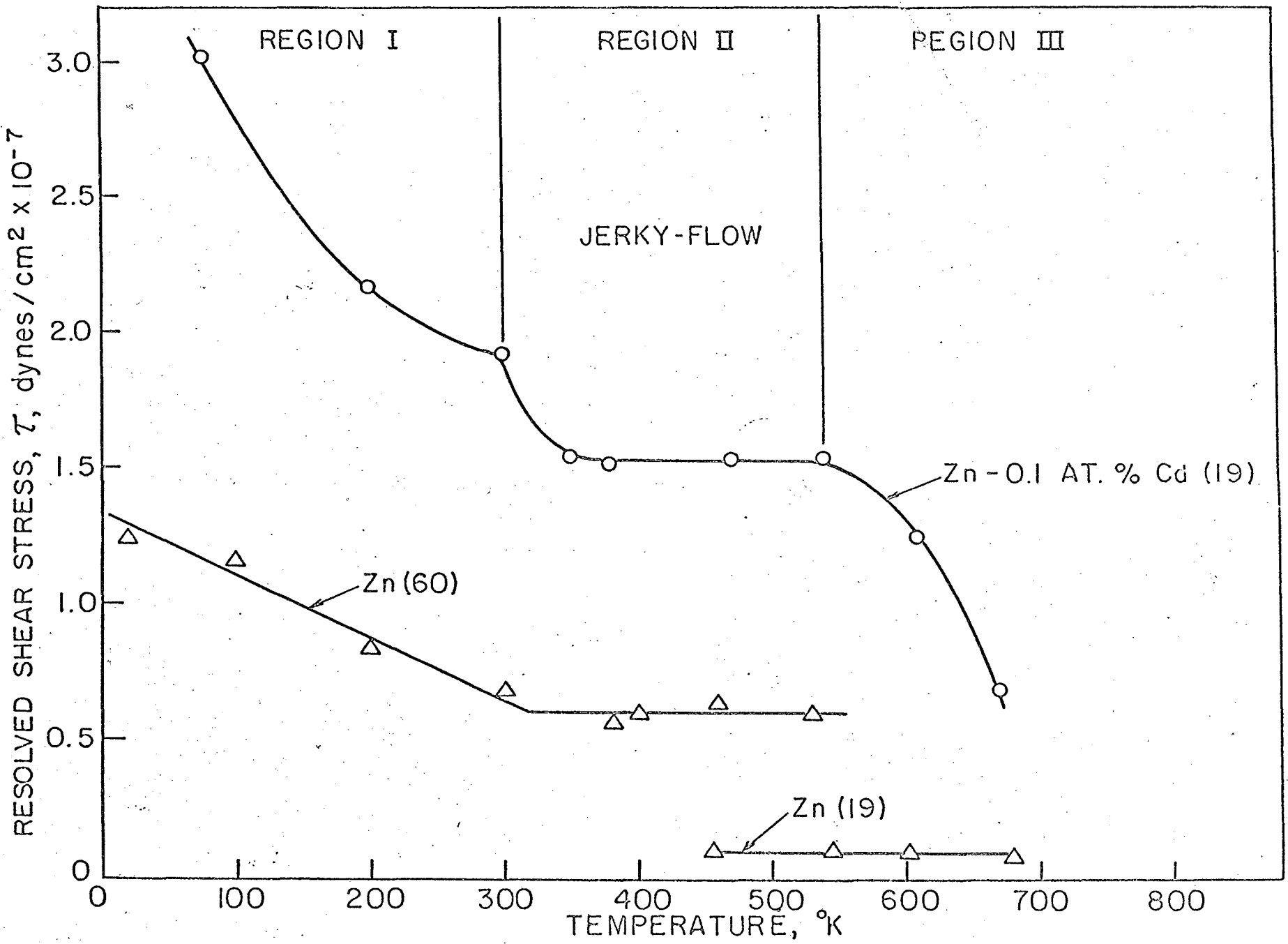

FIG. 12 RESOLVED SHEAR STRESS vs. TEMPERATURE FOR BASAL SLIP IN Zn AND Zn - 0.1 AT. % Cd ALLOY

C. Viscous Creep

In sharp contrast to pure Zn which behaves athermally at high temperatures, the Zn-Cd alloy exhibited a second thermally activated mechanism for basal glide over the high temperature range of Region III. Gilman has shown that over this range the strain rate is given by [19]

$$\dot{\gamma} = 2.2 \times 10^{-16} \tau^{2.7} e^{-21{,}000/RT} \text{ per sec} \qquad (29)$$

where τ is expressed in dynes/cm^2. Such thermally activated processes as intersection, the Peierls mechanism, and thermally activated motion of jogged screw dislocations, which have activation energies that depend on the applied stress, cannot account for these results. Although the stress and temperature dependency of the strain rate might suggest that dislocation climb is the rate controlling mechanism, it appears more likely that the Weertman viscous creep model is operative. The higher flow stress of the 0.1% Cd alloy of Zn above that for pure Zn over Region II and the jerky flow that was observed point to the importance solute atom interactions with dislocations over Region III.

Weertman[70] has shown that at high temperatures where dislocations from separate sources can annihilate each other as a result of facile climb, the shear strain rate for viscous creep is

$$\dot{\gamma} = \frac{2\pi(1-\mu)\tau^3 B}{G^2} \qquad (30)$$

where B is the mobility of a dislocation.

Various mechanisms might account for the mobility. As will be shown later short-range ordering can be the significant factor. In Gilman's experiment, however, this mechanism is unlikely because of the very dilute solutions that were employed. Cottrell atmosphere effects

should prove to be a more likely possibility. Cottrell and Jaswon[71] have shown that the mobility of a dislocation restrained by viscous drag of a solute atmosphere is given by

$$B = \frac{kTD}{\pi r^2 C_o N G^2 [(r'-r)/r]^2} \quad (31)$$

where D is the diffusivity of the solute, C_o is its concentration, N is the number of atoms per cm^3 of the lattice, and r and r' are the atomic radii of solvent and solute atoms respectively. Estimating D to be approximately $b^2 \nu e^{\frac{-\Delta H}{kT}}$ where ν is the Debye frequency and ΔH the activation energy for diffusion of the solute atom, suggests that

$$\dot{\gamma} = A \tau^n e^{-\Delta H/RT} \quad (32)$$

where

$$A = \frac{\pi b^2 (1-\mu) kT}{56 C_o N G^4 [(r'-r)/r]^2} \quad (33)$$

and n = 3

Equation 32 compares favorably with Gilman's experimental results since ΔH for the diffusion of Cd in Zn is expected to be near 21,000cal/mole and the theoretical value of n = 3 does not differ excessively from Gilman's experimentally determined value of 2.7. Furthermore, A is estimated theoretically to be $5.6 \times 10^{-17} \frac{cm^6}{dynes^3 sec}$ (using $\nu = 10^{13}$/sec, $\mu = 1/3$, T = 660°K, $C_o = 1 \times 10^{-3}$, $N = 6.6 \times 10^{22} \frac{atoms}{cc}$, $G = 10^{11}$ dynes/cm^2, $r_{Zn} = 1.33 \times 10^{-8}$cm and $r'_{Cd} = 1.49 \times 10^{-8}$cm) which is in fair agreement with Gilman's experimentally deduced value.

Thus we suggest that the deformation of Zn-0.1 at.% Cd in Region III is controlled by the viscous drag of solute cadmium atmospheres on dislocations.

D. Suzuki Locking

Because dislocations of type a dissociate into two partial dislocations on the basal plane and are separated by a faulted region consisting of two layers of face-centered cubic stacking, basal slip in hexagonal alloys can exhibit Suzuki locking.[68] At temperatures above about 0.4 of the melting temperature, the atoms will redistribute themselves between the faulted region and the matrix, in a manner analogous to the partition of atoms between two phases, resulting in a lowering of the free energy of the system. When dislocations are moved from the ribbon of concentration difference work must be done to increase the free energy of the system. Suzuki has shown that the process is not thermally activated and that the yield strength is given by

$$\tau = \tau_G + \frac{2h}{bV}\left\{(F^f - F)_c - (F^f - F)_{cf}\right\} \qquad (34)$$

where τ is the total yield strength τ_G is the dislocation stress fields that must be surmounted athermally plus the stress necessary to overcome short-range order, h is the height of a single layer of atoms lying on the slip plane, $(F^f\text{-}F)_c$ is the increase in free energy per mole for the faulted region above the unfaulted matrix for a composition c of the matrix and $(F^f\text{-}F)_{cf}$ is the same quantity where c_f is the composition of the fault, and V is the molar volume. Once the dislocations have been separated from the ribbon of the composition difference, the last term in Eq. 34 vanishes and the flow stress decreases to τ_G. Consequently, Suzuki locked alloys exhibit an athermal yield point. The small yield point that was obtained during basal slip of the 12.5 at.% Li alloy of Mg over both Regions I and II (vide Fig. 11) is probably due in a large part to Suzuki

locking; Cottrell solute atom locking in this alloy would be weak and thermally activatable.

Mote, Tanaka and Dorn[50] have shown that basal slip in the intermediate hexagonal solid solution phase having the congruent melting composition of about Ag_2Al (33 at. % Al) provides an interesting example of the behavior expected as a result of Suzuki locking. Single crystals, so oriented that the Schmid angles for basal slip are $\chi_o = \lambda_o = 45°$, were tested in tension. This alloy exhibited, within the limit of experimental scatter, identical stress strain curves from 77° to 450°K. A typical example is shown in Fig. 13. It is significant to note that the upper yield point is about 50 times higher than the yield strength commonly obtained in pure metals. Upon yielding a single Luder's band having a Luder's strain of 130% traversed the gage length, following which a modest degree of strain hardening was observed. As shown in Fig. 14, the yield point for the tension tests were independent of temperature up to about 450°K. Above 450°K, specimens tested in tension at $\dot{\gamma} \sim 10^{-4}$ per sec slipped on the prismatic plane in spite of the much more favorable orientation for basal slip. Dynamic tests in compression and shear were conducted by Larsen, Rajnak, Hauser and Dorn[72] (vide also[73, 74]) over the entire range of temperatures using modified Kolsky thin wafer[87] techniques. Under dynamic conditions, the thermally activated prismatic slip was completely suppressed and only basal slip took place. The data given in Fig. 14 clearly reveal that the flow stress is insensitive to temperature from 4°K to 450°K and that it is insensitive to changes of strain rate from $\sim 10^{-4}$ to $\sim 10^{4}$. Above one-half of the melting temperature the shear stress for basal slip increased with temperature even as

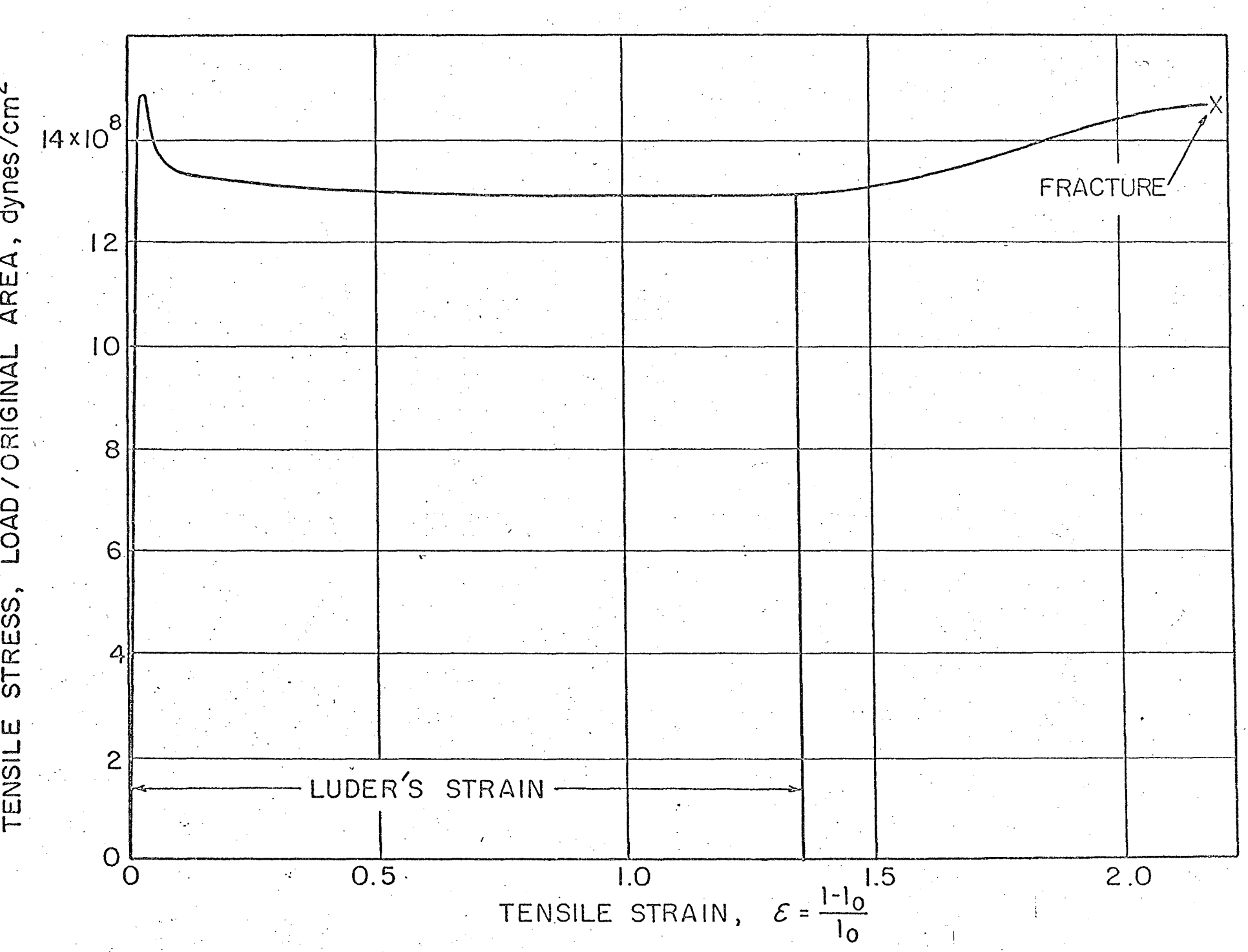

FIG. 13 TENSILE STRESS - TENSILE STRAIN DIAGRAM FOR BASAL SLIP IN Ag_2Al AT 77-450 °K FOR $\dot{\varepsilon} \simeq 10^{-4}$ SEC.$^{-1}$

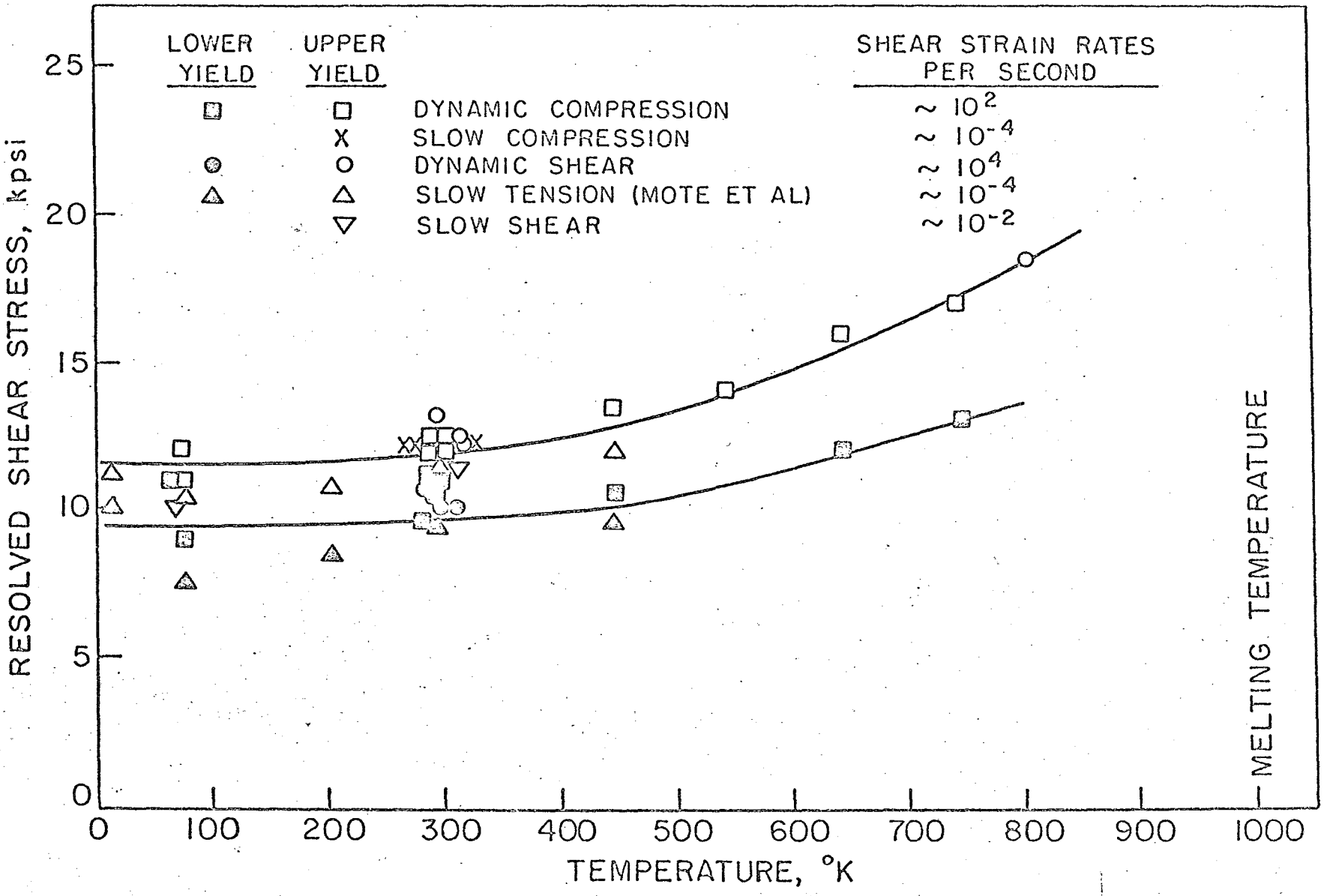

FIG. 14 RESOLVED SHEAR STRESS vs. TEMPERATURE FOR BASAL SLIP IN Ag_2Al.

the melting temperature was approached. The yield point, large Luder's band strain and the athermal behavior could only be rationalized in terms of Suzuki locking; Cottrell locking is undoubtedly absent because of the identity of the atomic radii of Ag and Al.

Unfortunately thermodynamic data are not currently available to provide an accurate analysis of the problem. If, however, the solid solutions in both the hexagonal matrix and the stacking fault are assumed to be ideal

$$\tau - \tau_G = \frac{2h}{bV}(c - c_f)\Delta F \tag{35}$$

$$\frac{c_f}{1 - c_f} = \frac{c}{1 - c} e^{-\Delta F/RT} \tag{36}$$

$$\Delta F = \left(F_{Al}^{f} - F_{Al}\right) - \left(F_{Ag}^{f} - F_{Ag}\right) \tag{37}$$

$$\frac{2h\Delta F}{V} = \gamma_{Al} - \gamma_{Ag} \tag{38}$$

where γ_{Al} is the stacking fault energy in hexagonal Al and γ_{Ag} that in hexagonal Ag.

It is reasonable to assume that the equilibrium condition of Eq. 35 applies only above about 0.4 of the melting temperature (i.e. above about 450°K). Below 450°K, $c_f - c$ is expected to remain constant at the composition that is frozen in at about 450°K. Consequently τ is expected to remain constant over the range from 4°K to about 450°K as was observed experimentally.

Assuming $\tau_G = 0$, Eqs. 35, 36, 37, and 38 can be solved simultaneously to give an upper bound to $\gamma_{Al} - \gamma_{Ag}$ in terms of the experimentally determined values of τ. The two sets of results that were obtained are recorded in Fig. 15. Since the stacking fault energy in face-centered cubic Al is positive and greater than that in face-centered Ag, it is expected that $\gamma_{Al} - \gamma_{Ag}$ will be negative for faults in the hexagonal phases of these metals. On this basis, the solid lower curve of Fig. 15 represents the estimated trends in the differences in the stacking fault energies, $\gamma_{Al} - \gamma_{Ag}$. The magnitude of the stacking fault energies so obtained appear quite reasonable in view of the fact that smaller absolute values would have been obtained if τ_G is actually greater than zero.

A recent investigation of the mechanical properties of hcp phase Cu-Ge alloys by Thornton[53] indicates that the strengthening mechanism for basal slip in this alloy may also be due to Suzuki locking. Thornton found that deformation occurred exclusively by basal slip in this alloy. The alloy exhibited a pronounced yield drop at low temperatures which appeared to be due to the unpinning of locked dislocations and the yield stress appeared to be insensitive to the strain rate. At high temperatures, the yield point dissappeared and the yield stress increased with increased strain rate suggesting a decreasing magnitude of Suzuki locking with increasing temperatures.

E. Prismatic Slip

When dislocations of type a move on the prismatic plane into screw orientation they dissociate into a pair of partial dislocations on the basal plane separated by a stacking fault. For this reason Friedel[57] suggested that continued slip on the prismatic plane is, therefore,

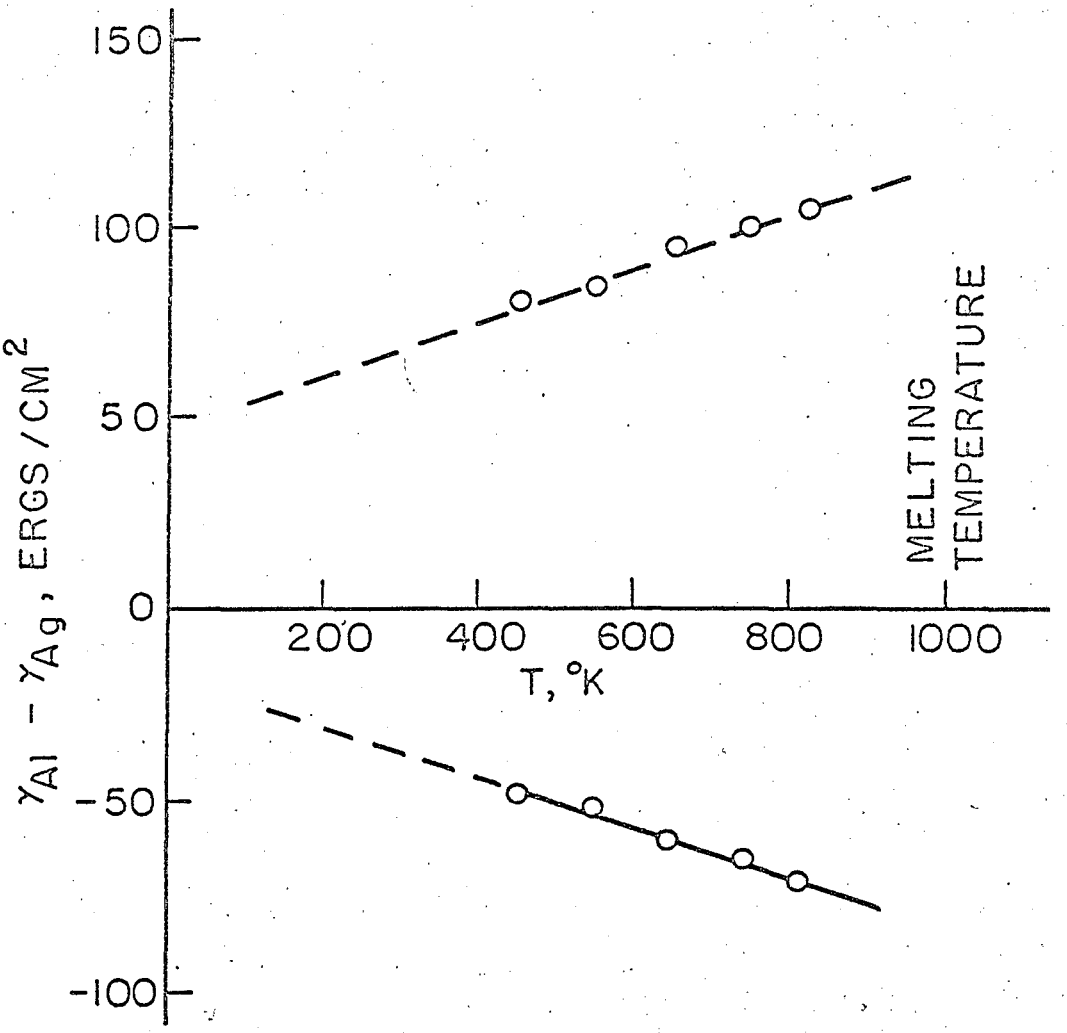

FIG. 15 STACKING FAULT ENERGIES vs. TEMPERATURE IN Ag_2Al.

dependent upon dynamic recovery by cross-slip from the basal to the prismatic plane. As shown in Fig. 16, this involves the energy of formation of a constriction U_c, the energy of recombination, R, of the partial dislocations over length L, and the increase in the line energy as the line bows out on the prismatic plane, where Γ is the line energy per cm length, and the negative of the work done by the applied stress. Under a given local stress, τ^*, the radius of curvature of the bowed-out section of the dislocations is fixed and the saddle-point free energy for cross slip depends on the critical value for $\theta_c = (\frac{2R}{\Gamma})^{1/2}$ at which point the energy for cross slip reaches its maximum value. On this basis Friedel determined that the shear strain rate for cross-slip is given by

$$\dot{\gamma} = \frac{N L_s A b^4 \nu \tau^{*2}}{8 \Gamma R} \epsilon^{-\frac{U_c}{kT} + \frac{2^{3/2}(\Gamma R^3)^{1/2}}{3 \tau^* b k T}} \qquad (39)$$

where N is the number of screw segments of dissociated dislocations on the basal plane per unit volume of the crystal, each having a total length L_s, A is the area swept out per unit activation, ν is the Debye frequency, and τ^* is the local shear stress on the prismatic plane in the direction of the Burgers vector b. The same expression, also applies to cross slip on other planes of the zone containing dissociated screw dislocations. On the other hand, this cross slip mechanism will control the deformation only when other mechanisms such as for example the Peierls process are more facile.

Flynn, Mote and Dorn[32] investigated prismatic slip in Mg under conditions where the basal planes were parallel to the tension axis and thus were subjected to zero shear stress. Their results are recorded in Fig. 17 where it is shown that $\frac{1}{\tau^* T}$ decreased linearly with 1/T over

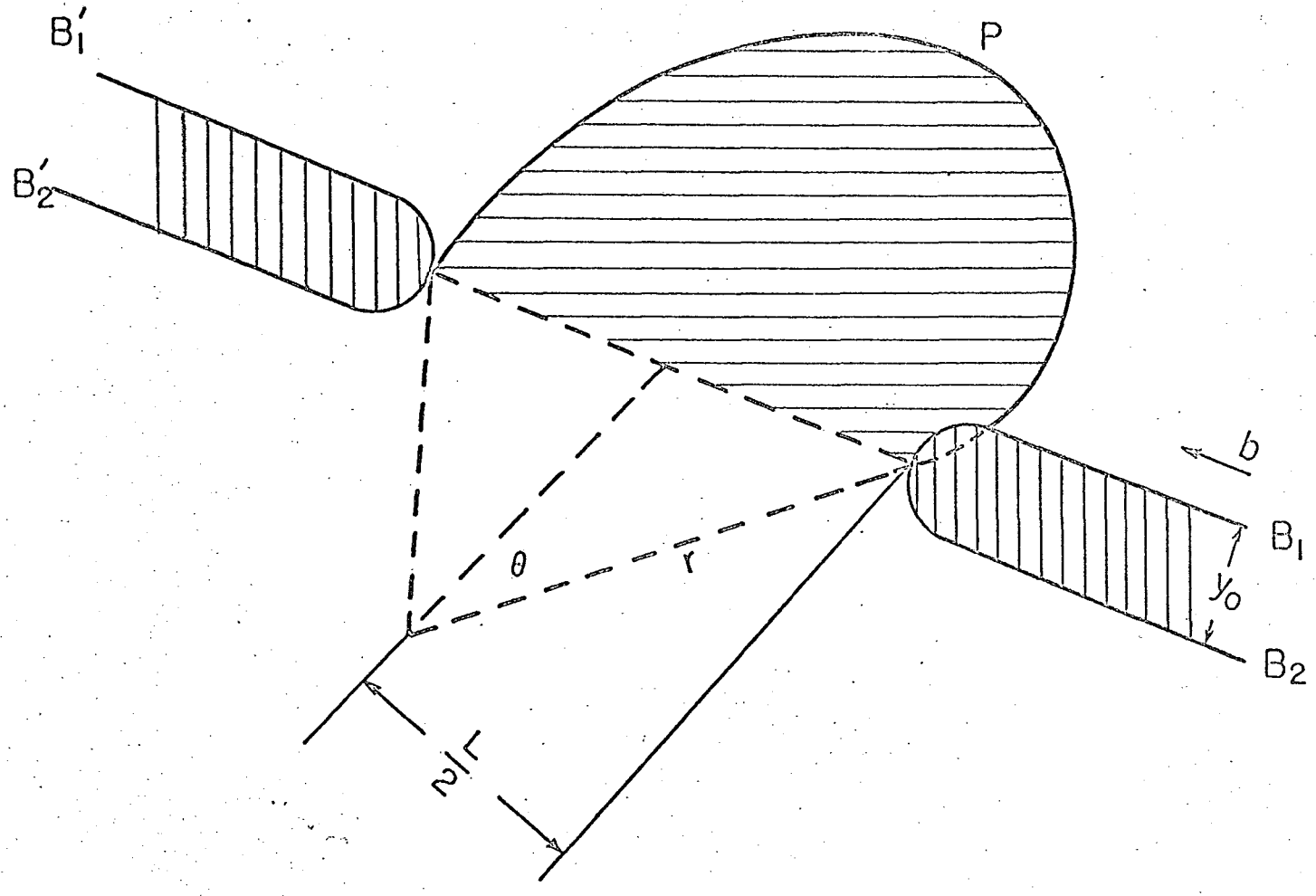

FIG. 16 NUCLEATION OF CROSS SLIP AS A RESULT OF RECOMBINATION OF THE PARTIALS B_1 AND B_2 ON THE BASAL PLANE ALONG LENGTH L AND BOWING OUT OF THE RECOMBINED SECTION P ON THE PRISM PLANE.

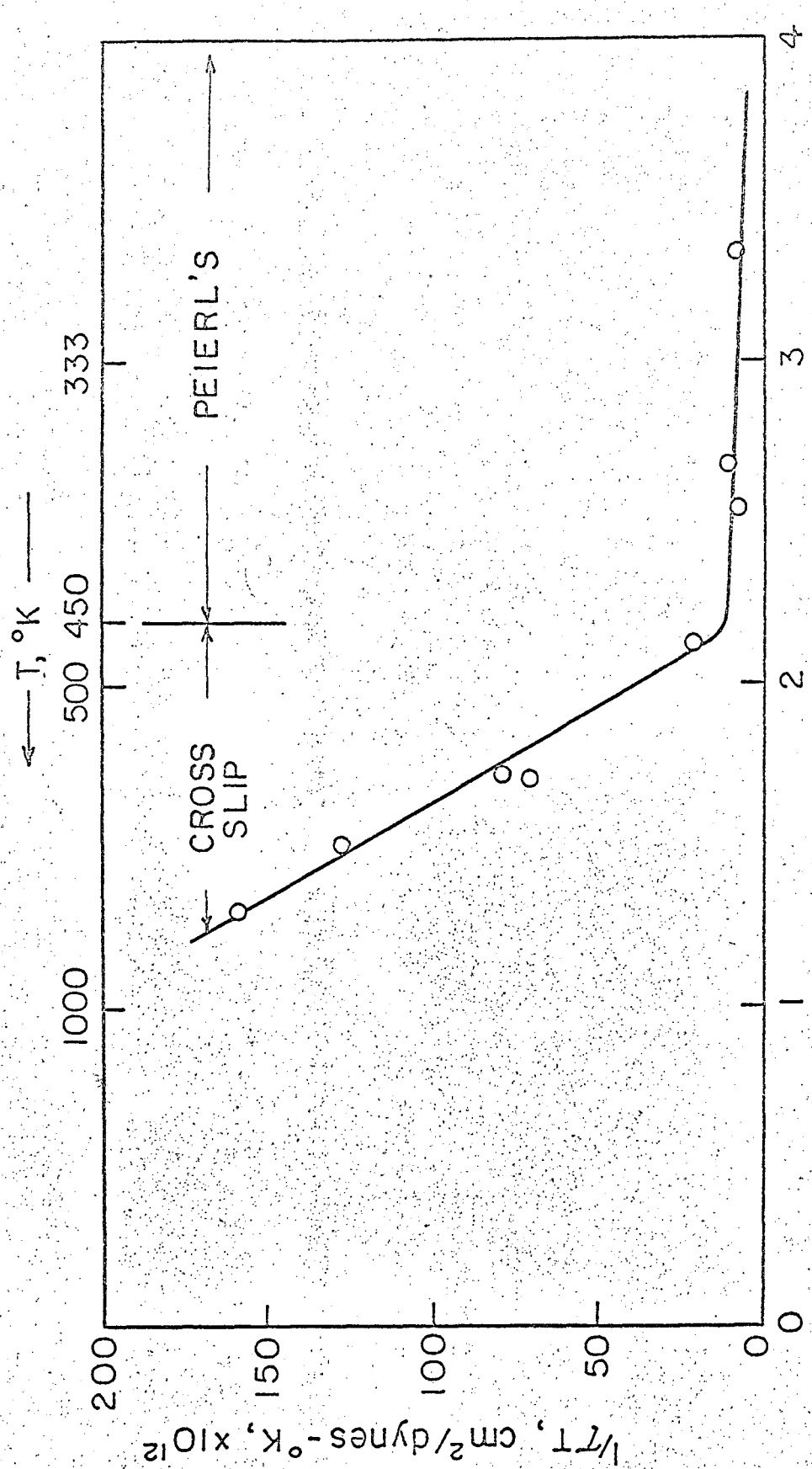

FIG. 17 $1/\tau T$ vs. $1/T$ FOR PRISMATIC SLIP IN MAGNESIUM.

the region where only prismatic slip took place. As shown by Eq. 39 when prismatic slip is controlled by cross slip the slope of Fig. 17 is approximately $bU_c/2(2\Gamma R^3)^{1/2} = 11.3 \frac{cm^2}{dyne}$.

In addition, the effect of changes in strain rate on the flow stress were obtained where

$$\left(T, \frac{\partial \tau^*}{\partial \ln \dot{\gamma}}\right) = \alpha T = \frac{AT}{\tau^*} + \frac{2^{3/2}(\Gamma R^3)^{1/2}}{3\tau^{*2}b} \qquad (40)$$

which can be rewritten to give

$$(R^3\Gamma)^{1/2} = \frac{3\cdot 4kT\tau^{*2}b}{2^{3/2}} - \frac{3\tau^* bAT}{2^{3/2}} \qquad (41)$$

Employing $\Gamma = \frac{Gb^2}{2} = 6.6 \times 15^5 erg/cm$ together with experimentally determined values of τ^*, T, and β gave $R = 6.5 \times 10^{-8} erg/cm$. Using the well known recombination energy equation

$$R/\Gamma \simeq \frac{1}{16} \ln (y_o/b) \qquad (42)$$

the separation of the partial dislocation is deduced to be $y_o/b \simeq 3$. Introducing the values of R and Γ into the expression $bU_c/2(2\Gamma R^3)^{1/2}$ deduced from the $\frac{1}{\tau T}$ vs $\frac{1}{T}$ curve, U_c was estimated to be $2.43 \times 10^{-12} ergs$.

Applying now Strohs[89] equation

$$U_c = \frac{Gb^3}{30}\left(\frac{y_o}{b}\right)\ln(y_o/b)^{1/2} = \frac{\Gamma b}{15}\left(\frac{y_o}{b}\right)\ln(y_o/b)^{1/2} \qquad (43)$$

for the constriction energy gives $y_o/b \simeq 7$. Thus the values of y_o/b for the separation of the partials in Mg are estimated to be:

Slip Mode	Mechanism	Method	y_o/b
Basal	Intersection	F-λ	~2
Prismatic	Cross slip	R	~3
Prismatic	Cross slip	U_c	~7

In general these values appear to agree well within the expectations based on the accuracy of the theory.

On the other hand, Gilman investigated prismatic slip in Zn[19] from 525° to 670°K, in Zn containing 0.1 at.% Cd[19] from 580° to 665°K, and in Cd[11] from 430° to 550°K. He found that

$$\dot{\gamma} = 7.4 \times 10^{-4} \tau^{3} e^{-\frac{31,000}{RT}} \quad \text{per sec for 99.999Zn} \qquad (44a)$$

$$\dot{\gamma} = 1.5 \times 10^{-15.36} \tau^{6} e^{-\frac{46,000}{RT}} \quad \text{per sec for Zn} \pm 0.1 \text{ at.\% Cd} \qquad (44b)$$

$$\dot{\gamma} = 1.2 \times 10^{-11.5} \tau^{2.75} e^{-\frac{29,200}{RT}} \quad \text{per sec for Cd} \qquad (44c)$$

where τ is in dynes/cm^2.

Since the activation energy is independent of the applied stress these data appear to disqualify the cross-slip mechanism, as well as all other mechanisms where the activation energy is sensitive to the stress. Furthermore, the dislocation climb mechanism of Weertman is also disqualified because the activation energies that were optained experimentally for prismatic slip are much higher than those for self diffusion, and because that for Zn increased substantially as a result of alloying with only 0.1 at.% Cd. This observation also disqualified the cross slip mechanism assuming Cd additions only slightly modified the stacking fault energy. The general form of Eqs. 44a, 44b, and 44c suggest that a type of viscous creep is operative, but the details of what type of viscous creep these data might represent have not yet been satisfactorily established. Weertman[70] has suggested that the creep of the high purity Zn is controlled by the motion of dislocations over Peierls' barriers. His formulation

for the strain rate at low stresses assuming the activation energy to be independent of the stress gives the stress dependence as a 2.5 power which is close to that given by Eq. 44a. It might be thought that Gilman's data must nevertheless conform to Friedel's cross-slip mechanism. Friedel[90] has suggested that Gilman's Zn data may correspond to a degenerate formulation of the cross-slip mechanism where the constriction energy U_c is the predominent term in the activation energy and the strain rate is proportional to the stress squared but insurmountable discrepancies were uncovered in attempting a detailed reanalysis of Gilman's data for prismatic slip of Zn, Cd and Zn plus 0.1 at.% Cd in terms of Friedel's cross-slip theory. Furthermore, as will be discussed later, prismatic slip in Ag_2Al does not occur by the Friedel mechanism. Prismatic slip need not always take place by Friedel's cross-slip mechanism in spite of the excellence of the theory. The good possibility that a dislocation slipping on the prismatic plane will not dissociate into partials on the basal plane is clearly revealed by Friedel's analysis. The critical length for nucleating cross slip is given by

$$L_c = 2r_c \sin\theta_c = \frac{2\Gamma}{b\tau^*}\left(\frac{2R}{\Gamma}\right)^{1/2} \qquad (45)$$

If only a segment of a dislocation on the prismatic plane dissociates into its partials on the basal plane, a length $L > L_c$ remains on the prism plane, prismatic slip will continue and the screw segments dissociated into partials on the basal plane will be pulled back onto the prism plane. Consequently Friedel's cross slip theory is limited to those conditions where τ^* is small and therefore it need not always prevail.

F. Prismatic Slip in Ag_2Al

Mote, Tanaka and Dorn[50] have studied prismatic slip by the $\langle 1\bar{2}10\rangle \{10\bar{1}0\}$ mode in single hexagonal close-packed crystals of Ag_2Al. Although

this alloy is not long-range ordered, there is good evidence that it exhibits short-range ordering.[75] Single crystals were tested in tension at a strain rate of 10^{-4} per sec employing Schmid angles of $\lambda_o \simeq \chi_o \simeq 45°$. The critical resolved shear stress for prismatic glide as a function of temperature is shown in Fig. 18. These data show that single crystals near the absolute zero have the remarkably high tensile yield strength of about 90,000 psi. Three ranges of deformation are easily recognized: Over Region I, the critical resolved shear stress for slip decreases precipitously with an increase in temperature revealing that the rate controlling mechanism is thermally activated; over Region II an athermal process controls the deformation and the yield stress decreases modestly with the temperature; and in Region III a second thermally activated mechanism becomes rate controlling.

A detailed study by Rosen, Mote and Dorn[51] has shown that the deformation over the low temperature range of Region I is controlled by the Peierls mechanism. This mechanism has been discussed by Seeger,[76] Seeger, Donth and Pfaff,[77] Lothe and Hirth,[78] Seeger and Schiller,[79] Friedel,[8] and Jøssang, Skylstand and Lothe.[80] For the present example the theory of Dorn and Rajnak[81] was adopted. Peierls suggested that dislocations tend to lie in potential valleys parallel to lines of atoms as shown in Fig. 19. When a dislocation is moved as a unit from one valley to the next, the core energy increases so that the total line energy is Γ_o at the bottom of valley and Γ_c at the top of the Peierls hill. Since the exact shape of the Peierls hill is not known it was assumed to be given by

$$\Gamma(y) = \frac{\Gamma_c - \Gamma_o}{2} + \frac{\Gamma_c - \Gamma_a}{2}\left(\frac{\alpha}{2} + \cos\frac{2\pi y}{a} - \frac{\alpha}{4}\cos\frac{4\pi y}{a}\right) \qquad (46)$$

where α provides for modest variations from a sinusoidal Peierls hill and the remaining symbols are defined in Fig. 19. Consequently, the stress

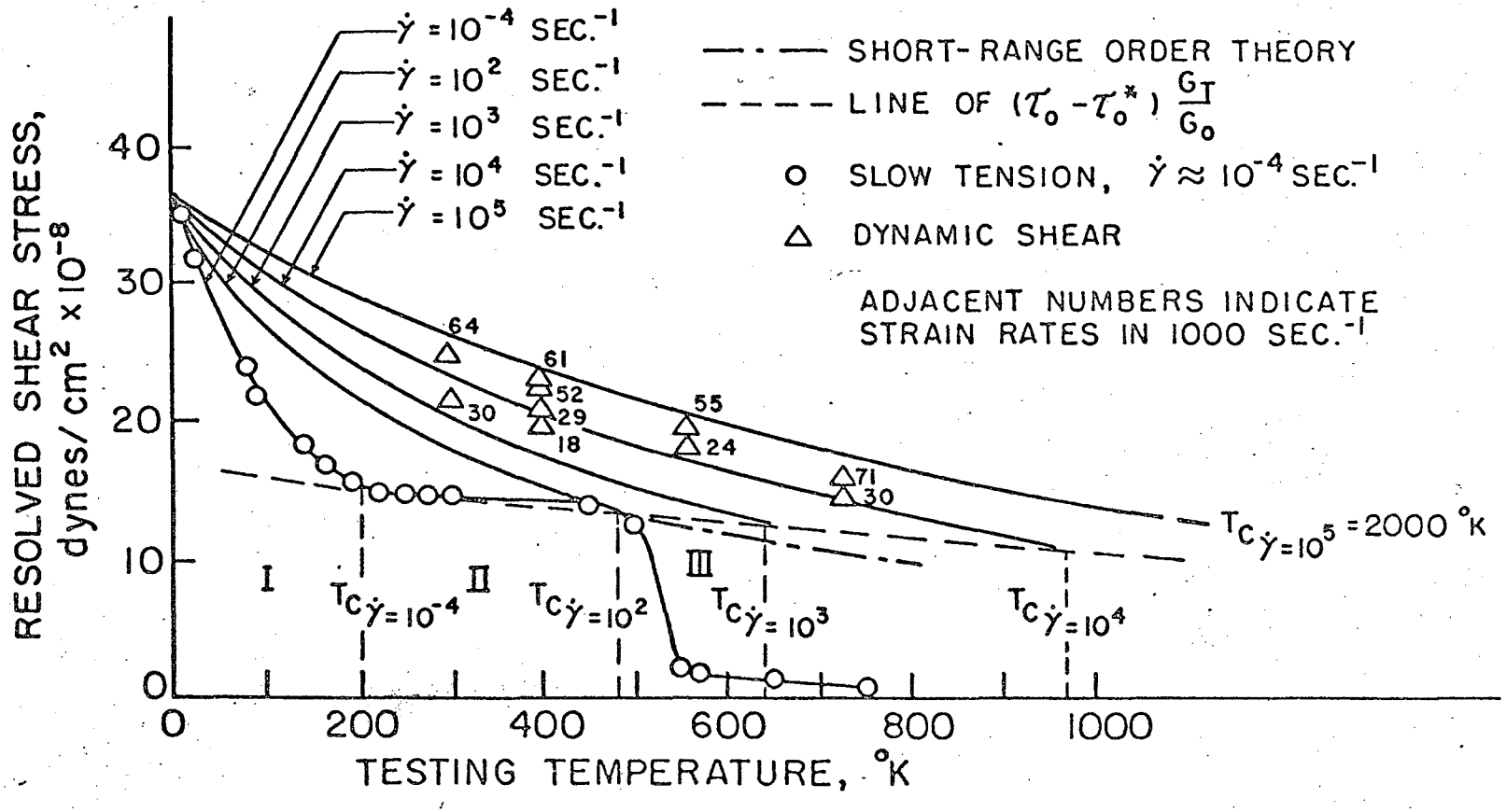

FIG. 18 RESOLVED SHEAR STRESS vs. TEMPERATURE FOR PRISMATIC SLIP IN Ag_2 - Al.

MUB-3113

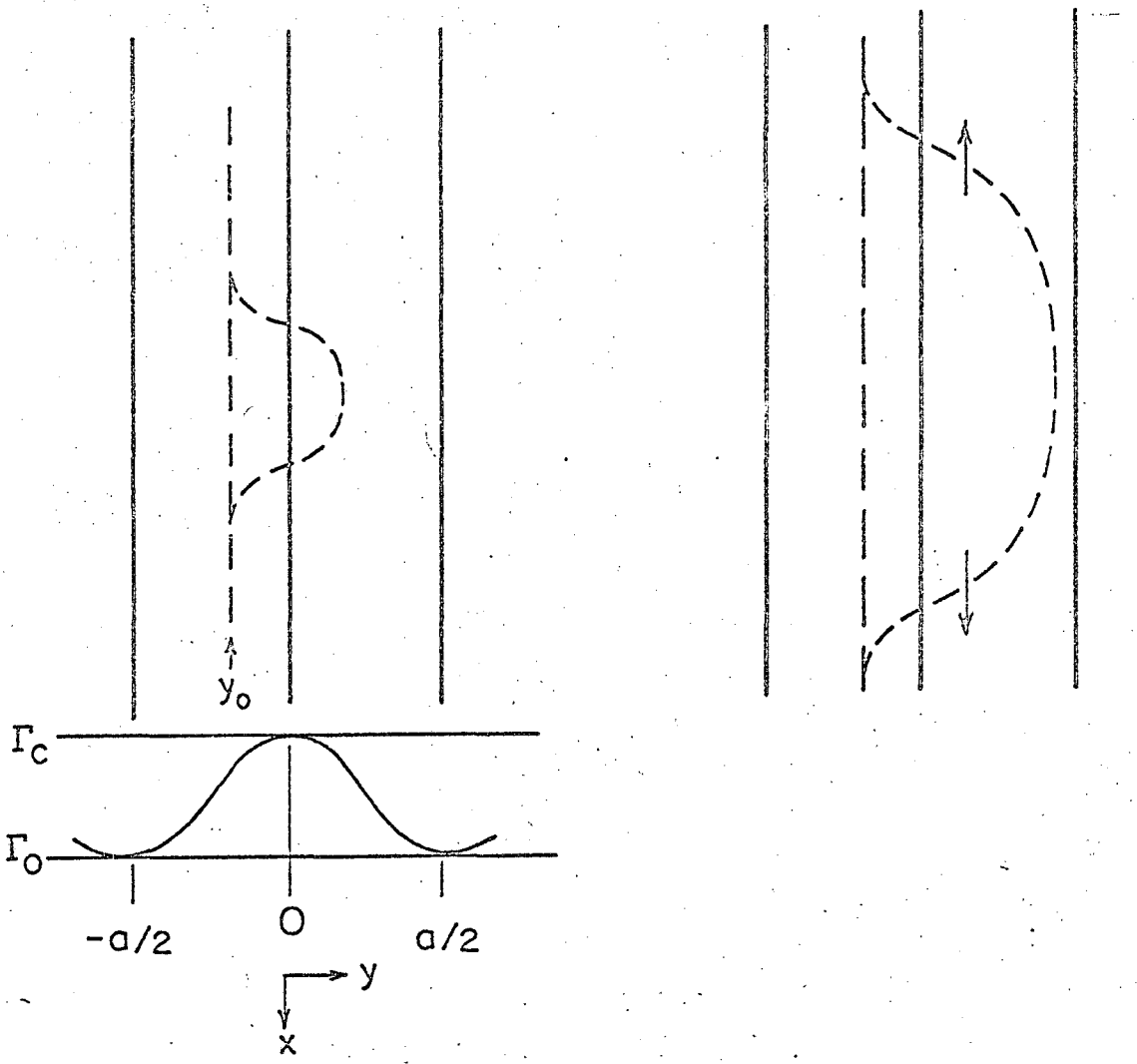

(a) (b)

FIG. 19 THE NUCLEATION OF A PAIR OF KINKS.

needed to move a dislocation to y_o, part way up the Peierls hill is

$$\tau^* b = \left(\frac{\partial \Gamma\{y\}}{\partial y}\right)_{y_o} = -\frac{\pi}{a}(\Gamma_c - \Gamma_o)\sin\frac{2\pi y_o}{a}\left(1 - \alpha\cos\frac{2\pi y_o}{a}\right) \tag{47}$$

and the Peierls stress necessary to cause slip at the absolute zero is the maximum value of τ^*, namely

$$\tau_p^* = \frac{\pi(\Gamma_c - \Gamma_o)}{16\,a\,|\alpha|}\left[3 + (1+8\alpha^2)^{1/2}\right]\left[8\alpha^2 - 2 + 2(1+8\alpha^2)^{1/2}\right]^{1/2} \tag{48}$$

If a stress $\tau^* < \tau_p^*$ is applied to the dislocation, it will be arrested at y_o part way up the Peierls hill as shown by the broken line in Fig. 19a. Permanent plastic strains can only be obtained when a thermal fluctuation is sufficiently great to nucleate a pair of kinks as shown in Fig. 19a. Once this critical energy has been exceeded the pair of kinks so produced will separate to nodal points, jogs, or other barriers, thus advancing a segment of the dislocation the atomic spacing a on the slip plane. (Fig. 19b.)

Dorn and Rajnak assumed a line energy model for this process which accounts indirectly for the attraction of the two kinks. The energy of any embryonic pair of kinks is then given by

$$U = \int_{-\infty}^{\infty}\left\{\Gamma\{y\}\left(1 + \left(\frac{dy}{dx}\right)^2\right)^{1/2} - \Gamma\{y_o\} - \tau^* b(y - y_o)\right\} dx \tag{49}$$

where the first term of the integrand refers to the line energy of the thermally displaced dislocation, $y = y\{x\}$, the second to the original line energy of the dislocation when it was displaced to y_o under the stress τ^* and the third to the work done by the stress as the thermally perturbed dislocation sweeps out the area $\int_{-\infty}^{\infty}(y - y_o)\,dx$. Thus U refers to the energy that must be supplied by a thermal fluctuation to perturb the dislocation to any shape $y = y\{x\}$ from its position $y = y_o$. The perturbations are assumed to center at $x = 0$. If they are too small the pair of embryonic kinks collapse. A saddle-point free energy exists for

the nucleation of a pair of kinks so that all thermal fluctuations greater than this value advances the dislocation segment a distance a. By application of the calculus of variations the saddle-point free energy to nucleate a pair of kinks was found to be given by

$$U_n = 2\int_{y_o}^{\lambda_c} \left(\left[\Gamma\{y\} \right]^2 - \left[\tau^* b (y - y_o) + \Gamma\{y_o\} \right]^2 \right)^{1/2} dy \qquad (50)$$

where λ_c is the critical displacement $y = \lambda_c$ at $x = 0$ for nucleation of a pair of kinks and is given by

$$\Gamma\{\lambda_c\} = \tau^* b (\lambda_c - y_o) + \Gamma\{y_o\} \qquad (51)$$

The energy of a single kink U_k, calculated by the same technique, was found to be in excellent agreement with that previously reported by Seeger[76] and is given by

$$\frac{2 U_k \pi}{a \Gamma_o} = K \left(\frac{\tau_p^* a b}{\pi \Gamma_o} \right)^{1/2} \qquad (52)$$

where K is insensitive to Γ_c / Γ_o and depends only modestly on α as given in Fig. 20. When only a single pair of kinks is nucleated in length L of a dislocation at one time, the strain rate over Region I where the Peierls mechanism controls the deformation is given by

$$\dot{\gamma} = \rho a b \frac{L}{w} \nu e^{-\frac{U_n}{kT}} \qquad (53)$$

where w is approximately the length of the dislocation that is bowed out during a successful fluctuation, ρ is the density of dislocations, and ν is the Debye frequency.

At a critical temperature T_c, analogous to that for intersection, where $\tau^* = 0$, the total energy for kink nucleation is supplied by a thermal fluctuation and

$$(U_n)_{T_c} = 2 U_k \qquad (54)$$

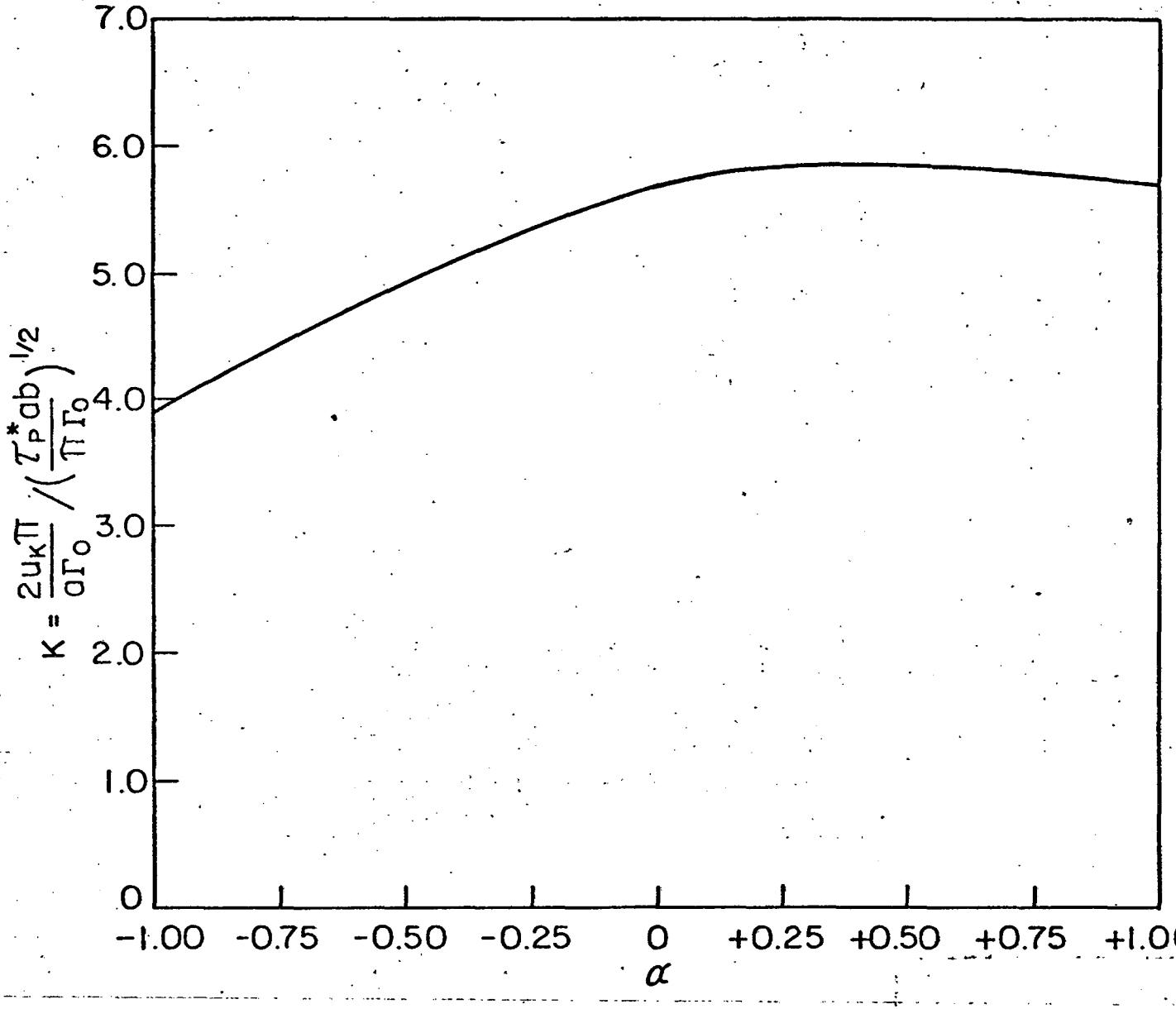

FIG. 20 VARIATION OF K WITH α FOR THE NUCLEATION OF DISLOCATION KINKS.

where U_k is the energy of a single isolated kink. At T_c the strain rate is given by

$$\dot{\gamma} = \rho a b \frac{L}{\omega} \nu e^{-\frac{2U_K}{kT}} \tag{55}$$

Thus the kink energy can be obtained from evaluations of the effect of strain rate on T_c by

$$\frac{\dot{\gamma}_1}{\dot{\gamma}_2} = \frac{e^{-\frac{2U_K}{kT_{c1}}}}{e^{-\frac{2U_K}{kT_{c2}}}} \tag{56}$$

From the kink energy and the Peierls stress, the line energy of a dislocation can be deduced from Eq. 52. Furthermore from tests conducted at the same strain rate where $\frac{\rho a b L \nu}{w}$ is about constant

$$\frac{U_n}{2U_k} \approx \frac{T}{T_c} \tag{57}$$

as shown by Eqs. 53 and 55.

The theoretically deduced ratio $U_n/2U_k$ as a function of τ^*/τ_p^* is shown in Fig. 21. This relationship is very insensitive to Γ_c/Γ_o and only slightly dependent on α and thus represents the dependence of the activation energy for nucleation of pairs of kinks on the applied stress.

A critical characteristic of the Peierls mechanism is the very small activation volumes defined by $v = -\partial U_n/\partial \tau^*$, that are obtained. If β is defined in the usual way

$$\beta = \frac{\partial \ln \dot{\gamma}}{\partial \tau^*} = -\frac{\partial \ln w}{\partial \tau^*} - \frac{1}{kT}\frac{\partial U_n}{\partial \tau^*} \tag{58}$$

The first term following the second equality is negligably small and the activation volume is therefore about

$$v = \beta k T = \frac{2U_K}{\tau_p} \frac{\partial\left(U_n/2U_K\right)}{\partial\left(\tau^*/\tau_p^*\right)} \tag{59}$$

The variation of the activation volume with τ^*/τ_p^* is shown in Fig. 22.

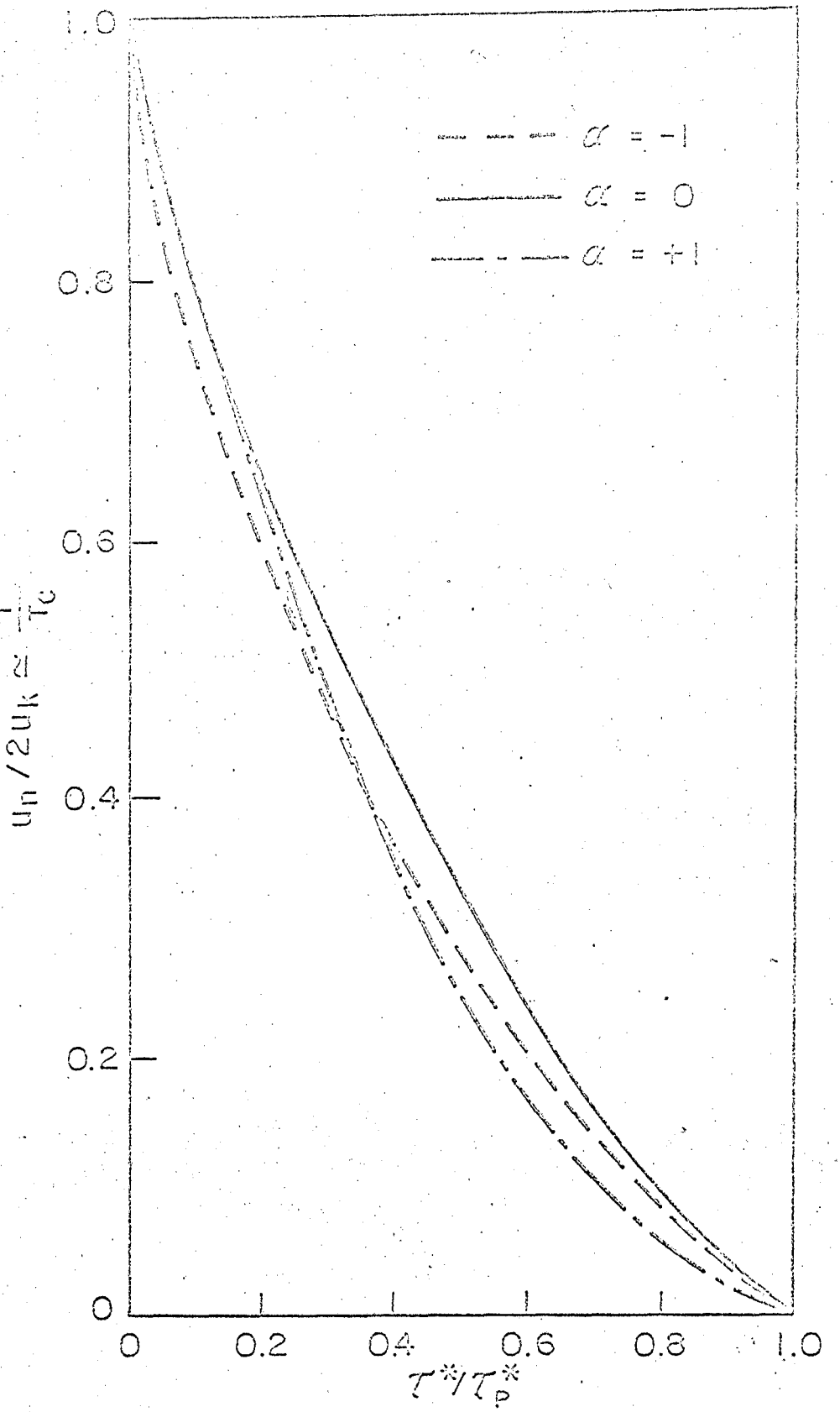

FIG. 21 ENERGY TO NUCLEATE A PAIR OF KINKS AS A FUNCTION OF THE APPLIED STRESS

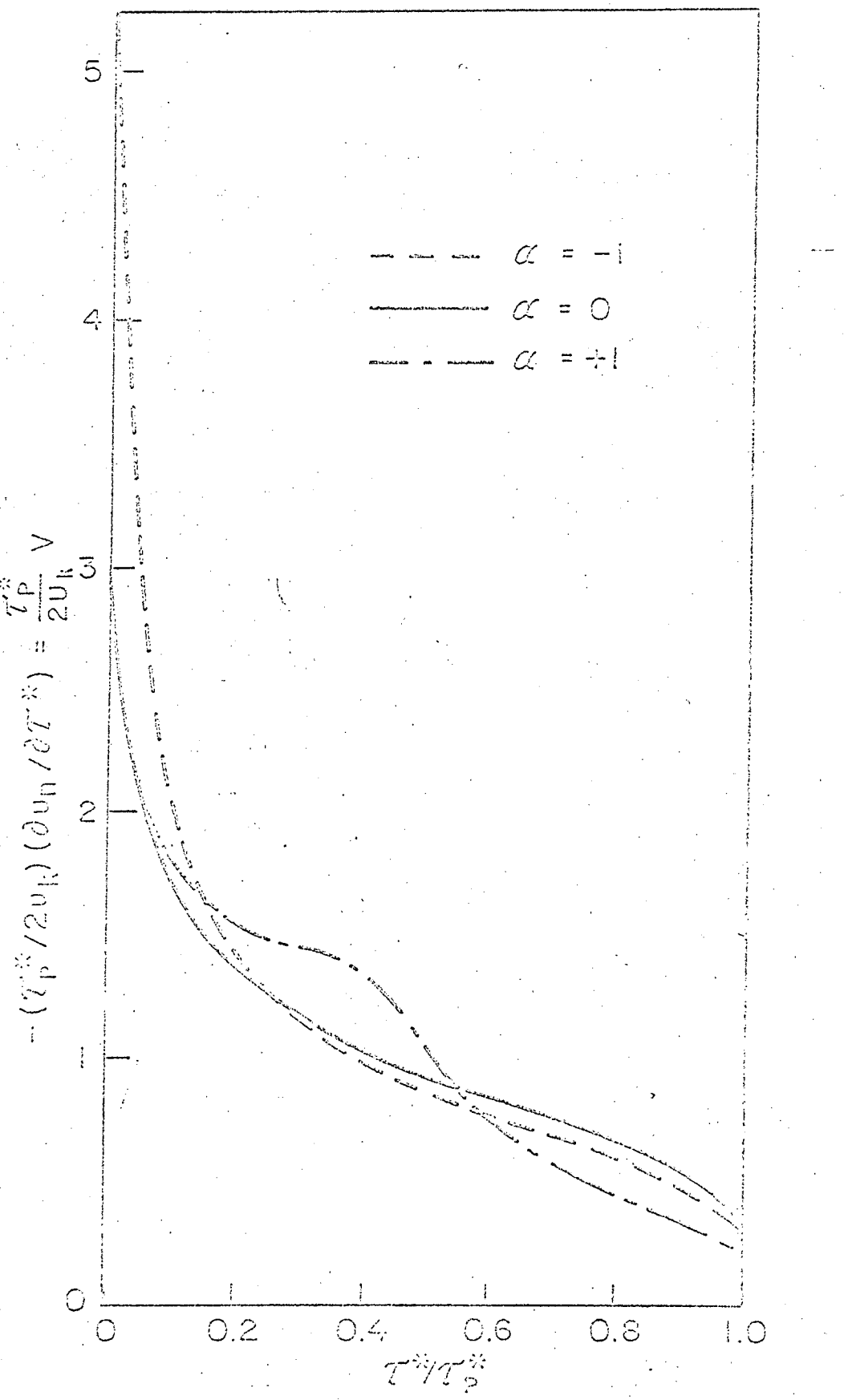

FIG.22 APPARENT ACTIVATION VOLUME VS. STRESS FOR THE PEIERLS MECHANISM

The experimental data obtained by Rosen, Mote and Dorn for the low temperature prismatic slip in Ag_2Al is recorded in Fig. 23, where $\tau^* = \tau - \tau_G^\circ G/G_o$ (i.e. where the athermal stress has already been subtracted from the observed stress). As shown in Fig. 23 $\tau_p^{*\circ} = \tau^{*\circ}$ and the Peierls stress was assumed to be linearly related to the shear modulus of elasticity. The correlation of these data, with the theory from the Peierls mechanism is documented in Fig. 24. From the effect of $\dot{\gamma}$ on T_c the kink energy was determined to be $U_k = 3.0 \times 10^{-13}$ ergs or 0.19 e.v. Introducing this and the value of τ_p° into Eq. 52 gives a line energy of $\Gamma_o \simeq \frac{Gb^2}{3}$ which is in good agreement with Nabarro's theoretical estimate of $Gb^2/2$. Furthermore, the activation volumes agree exceptionally well with the theoretical deductions as shown in Fig. 25 and using $\nu = 5.1 \times 10^{12}$ and w = 50b gives $\rho L \simeq 300$ which is in the expected range for the Peierls mechanism. Thus, there is little doubt that prismatic slip of Ag_2Al obeys the Peierls mechanism over Region I.

The resolved shear stress for prismatic slip of Ag_2Al over Region II, where an athermal mechanism operates, has the exceptionally high value of about 22,000 psi. Such a high value cannot be ascribed to interactions between dislocations and probably arises from short-range ordering by the mechanism originally suggested by Fisher.[82] As pointed out by Fisher, this mechanism is not thermally activatable at least in the region below about one-half of the melting temperature were diffusion is a negligible factor. Mote, Tanaka and Dorn[50] suggested that the flow stress for prismatic slip controlled by short-range order is given by

$$\tau_p = \frac{8 X_A X_B \mathcal{E} \alpha}{1.61 b^3} \qquad (60)$$

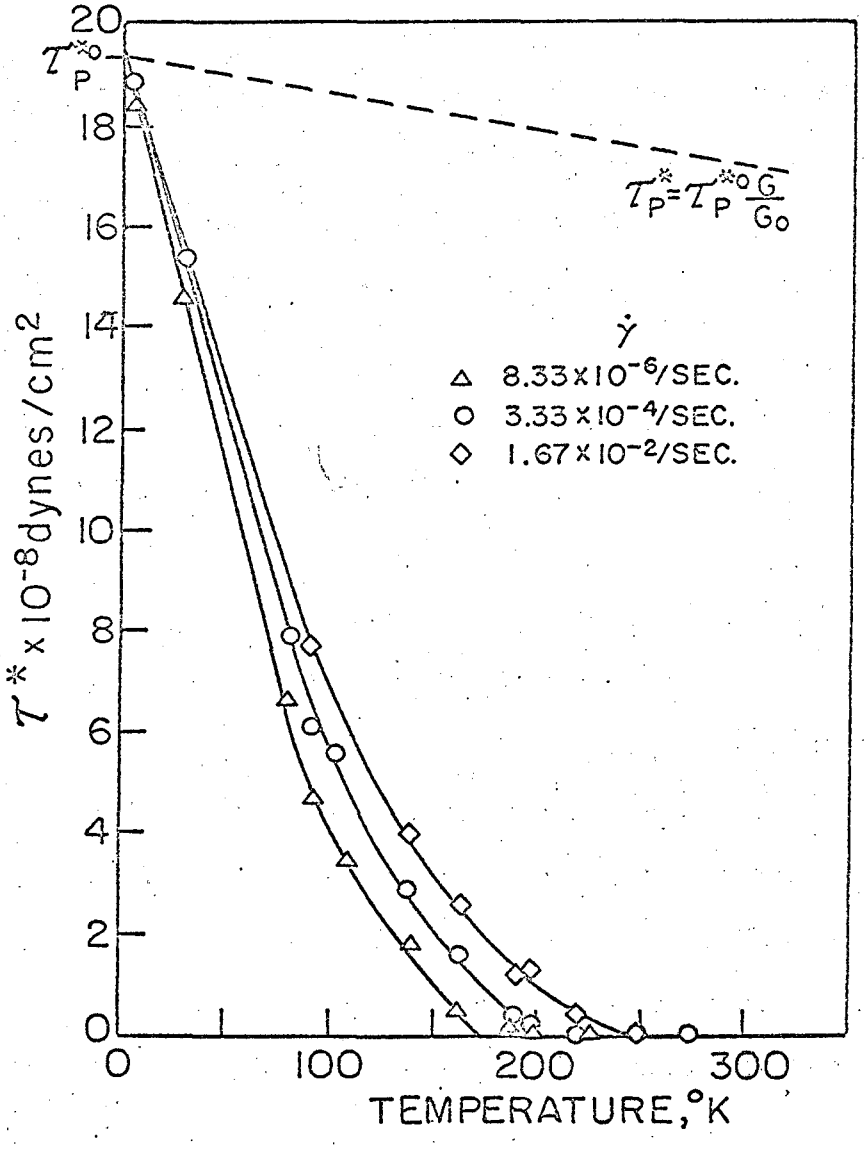

FIG.23 THE THERMALLY ACTIVATED COMPONENT OF THE FLOW STRESS vs. TEMPERATURE FOR DIFFERENT STRAIN RATES FOR PRISMATIC SLIP IN Ag_2Al.

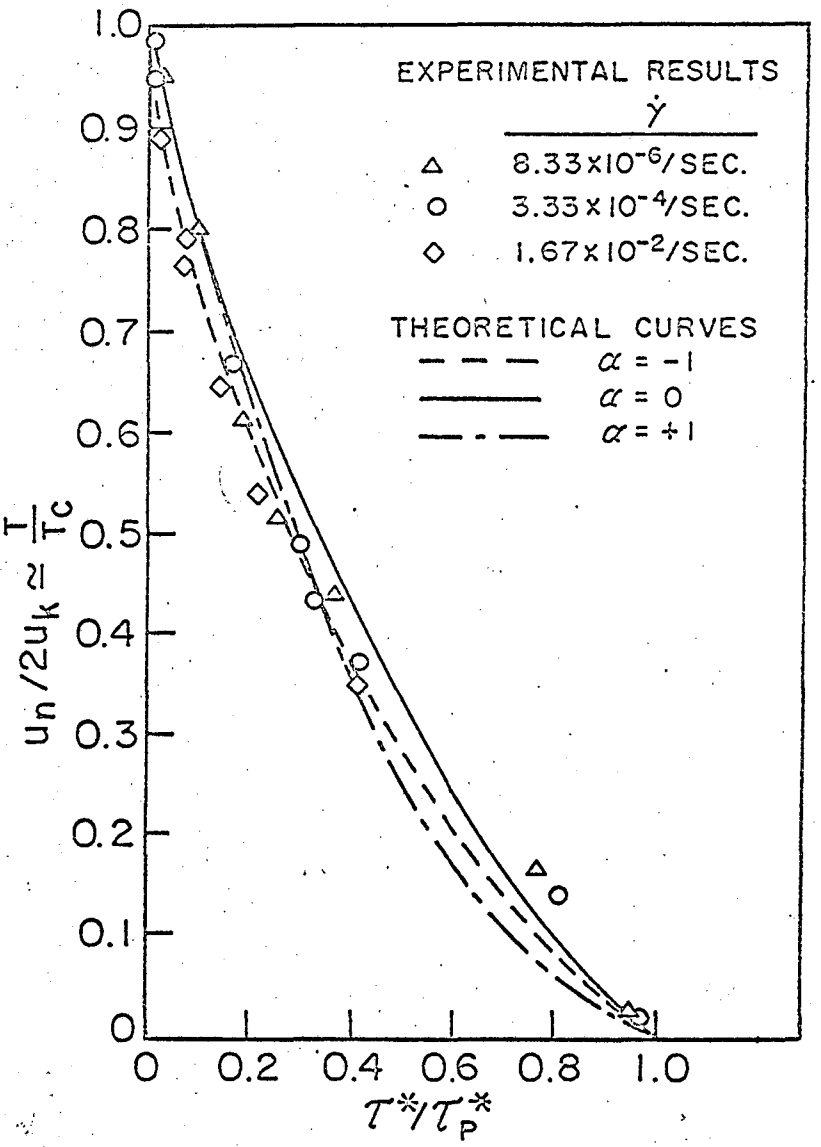

FIG. 24 THE THERMALLY ACTIVATED COMPONENT OF THE FLOW STRESS vs. TEMPERATURE IN DIMENSIONLESS UNITS FOR PRISMATIC SLIP IN Ag_2Al.

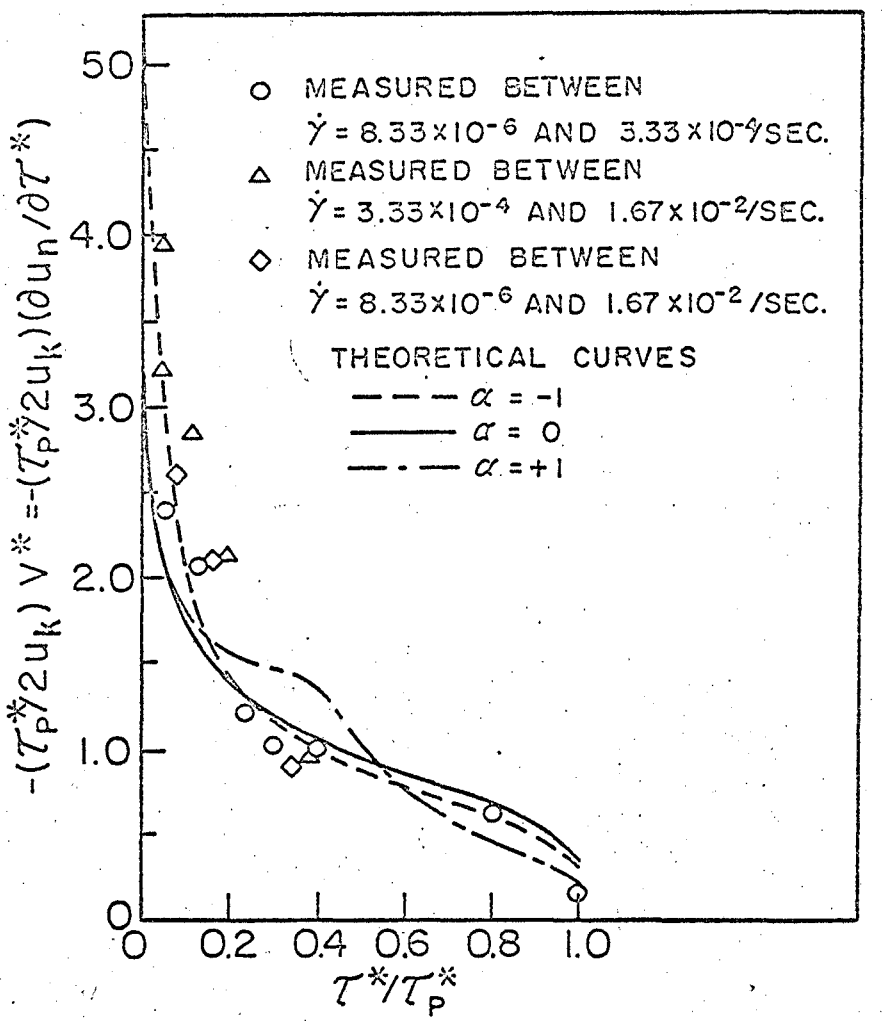

FIG.25 THE THERMALLY ACTIVATED COMPONENT OF THE FLOW STRESS vs. THE ACTIVATION VOLUME IN DIMENSIONLESS UNITS FOR PRISMATIC SLIP IN Ag_2Al.

where X_A and X_B are the mole fractions of the components, α is Cowley's[83] degree of order and $\mathcal{E}$ is the ordering energy

$$\mathcal{E} = \mathcal{E}_{AB} - \tfrac{1}{2}\mathcal{E}_{AA} - \tfrac{1}{2}\mathcal{E}_{BB} \qquad (61)$$

for producing an A-B bond from 1/2 an A-A and 1/2 a B-B bond. As shown by Flinn[84] the equilibrium degree of order, α_o, is given by

$$\frac{\alpha_o}{(1-\alpha_o)^2} = X_A X_B \left\{ e^{2\mathcal{E}/kT} - 1 \right\} \qquad (62)$$

It is expected that the data over Region II refer to the degree of order that is frozen into the alloy at about one-half of the melting temperature, namely about 475°K. Assuming that the equilibrium degree of order was obtained at 475°K and that the total stress τ at 475°K results exclusively from short-range order, simultaneous solution of Eqs. 60 and 62 give $\mathcal{E} = -5.3 \times 10^{-14}$ ergs/atom or -760cal/mole and $\alpha_o = 0.30$. Since these are upper bound values the agreement with theory appears to be good.

A rather thorough investigation was conducted on prismatic slip on Ag_2Al over Region III by Howard, Barmore, Mote and Dorn.[85] Following a short duration and small inverted transient it was found that the creep rate was given by

$$\dot{\gamma} = 3.8 \times 10^{-18} \tau^{3.6} e^{-\frac{33000}{kT}} \text{ per sec} \qquad (63)$$

where τ is in dynes/cm^2.

Although relationships of this kind, where the activation energy is insensitive to the applied stress and the creep rate is proportional to τ^n(n= 3 to 5), are expected from Weertmans dislocation climb model,[86] it does not necessarily follow that the dislocation climb model is valid in this case. This arises because following climb, the dislocations must glide on the prismatic plane before they can contribute to creep. The

stress necessary to cause this glide without the aid of thermal fluctuations is given by Eq. 60 and is represented by the broken/dot-dash curve in Fig. 18. The actual experimentally observed flow stresses is for slip in Region III are below this value, as shown by the solid curve of Fig. 18. Thus the rate controlling mechanism might be due to glide on the prismatic plane, in which event fluctuations leading to disordering in advance of the dislocation can be expected to be the rate controlling mechanism for prismatic slip. A satisfactory theory for this mechanism has not yet been formulated. In lieu of more sophisticated approaches that need to be developed, we might suggest the following as a crude preliminary approximation to this case: When diffusion occurs locally in the vicinity of the dislocation, the alloy becomes disordered. The activation energy for this disordering is about equal to that for diffusion near the core of the dislocation plus that for disordering the alloy. Thus the frequency for local disordering in the vicinity of the dislocation in the absence of a stress is

$$\nu' = \nu Z e^{\frac{\Delta s}{k}} e^{-\frac{\Delta h + 8\bar{\varepsilon}}{kT}} \tag{64}$$

where ν is about the Debye frequency, Δs and Δh are about equal to the entropy and enthalpy for diffusion and Z is the coordination number equal to 12; $\bar{\varepsilon}$ is the average energy of a bond in the ordered alloy ($\bar{\varepsilon} = 2\ X_A\ X_B\ \alpha_o \varepsilon$, according to Cowley's theory of ordering) of which 12 are broken during diffusion and 4 are restored in close-packed alloys. Under the action of an applied stress on the dislocation, the frequency of forward motion of a dislocation is modified by the factor $e^{+\frac{\tau bA}{kT}}$ and the reverse by a factor of $e^{-\frac{\tau bA}{kT}}$ where A is the area swept out by the dislocation namely $A = 3.22b^2$. Thus the velocity of the dislocation is

$$v = b\nu Z e^{\frac{\Delta A}{k}} e^{-\left(\frac{\Delta h + 16 X_A X_B \alpha_o \varepsilon}{kT}\right)} e^{\frac{3.22\tau b^3}{kT}} - e^{-\frac{3.22\tau b^3}{kT}} \quad (65)$$

and the mobility of the dislocation is

$$B = \frac{v}{\tau b} = 6.44\nu Z b^3 e^{\frac{\Delta A}{k}} e^{-\left(\frac{\Delta h + 16 X_A X_B \alpha_o \varepsilon}{kT}\right)} \quad (66)$$

Introducing this expression for the mobility of a dislocation into Weertman's expression of Eq. 30 for viscous creep suggests that

$$\dot{\gamma} = \frac{12.9\pi(1-\mu)\nu Z b^3 \tau^3}{G^2 kT} e^{\frac{\Delta A}{k}} e^{-\left(\frac{\Delta h + 16 X_A X_B \alpha_o \varepsilon}{kT}\right)} \quad (67)$$

In view of the theoretical approximations, the discrepancy between the experimentally observed relationship $\dot{\gamma} \propto \tau^{3.6}$ and that suggested by Weertmans viscous creep theory $\dot{\gamma} \propto \tau^3$ is not too disturbing. Furthermore, the term $16\, X_A\, X_B \alpha_o \varepsilon$ in the activation energy expression is small relative to Δh and α_o decreases almost linearly with an increase in T so that a fairly constant apparent activation energy is predicted theoretically that is independent of τ and T in harmony with the experimental results. The theoretical value of A in $\dot{\gamma} = A\tau^3 e^{-\frac{\Delta h + 16 X_A X_B \alpha_o \varepsilon}{kT}}$ is estimated to be about 7.9×10^{-18} whereas the experimentally determined value was 3.8×10^{-18}. The nominal agreement of the theory with experiment suggests that the high temperature prismatic slip of Ag_2Al is dependent on diffusion leading to disordering in the locale of the dislocation.

Under dynamic conditions of test where very high strain rates are obtained there is insufficient time for diffusion mechanisms to take place. This fact is illustrated by the dynamic tests on prismatic slip in Ag_2Al reported by Larsen, Rajnak, Hauser and Dorn.[72] Using the Kolsky technique[86] they obtained the critical resolved shear stress for slip as a function of strain rate and temperature as shown by the datum points

of Fig. 18, each of which is documented relative to the strain rate. The solid curves are extrapolated from the previously described data of Rosen, Mote, and Dorn[51] for low temperature prismatic slip assuming the validity of the Dorn-Rajnak[81] formulation of the Peierls mechanism. In view of the experimental difficulties in conducting dynamic tests, the agreement between theory and experiment is excellent. As the strain rate is increased T_c for the Peierls process is increased and the viscous creep process that occurs during creep at high temperatures is replaced by the Peierls mechanism under dynamic straining.

G. Effect of Li Solute Additions on Prismatic Slip in Mg

Solute atom additions to a metal usually result in strengthening. The previously quoted example of the increased critical resolved shear stress for basal slip in Mg with solute addition of 12 at.% Li is somewhat typical of the usual case. The increased value of the stress τ_G to overcome the athermal processes probably arises principally from short-range order hardening and the greater density of dislocations that are grown into the alloy. Furthermore, the thermally activated component of the stress, τ^*, at low temperatures is also believed to increase as a result of the effect of the greater density of frozen-in forest dislocations on the intersection mechanism.

A few years ago, Hauser, Landon and Dorn[48] showed that additions of above about 8 at.% Li in a polycrystalline alloy of Mg resulted in solid solution softening. Whereas pure Mg exhibited principally basal slip and twinning at low temperatures, alloys containing over 8 at.% Li exhibited extensive prismatic slip as well. At that time, it was suggested that Li might serve to reduce the Peierls stress for prismatic slip.

Recently Ahmadieh[8.7] studied in detail the effect of Li additions on the critical resolved shear stress for prismatic slip in Mg. The yield strengths as a function of temperature are recorded in Fig. 26 which also contains the previously discussed data for pure Mg. These curves clearly reveal that Li additions reduce the critical resolved shear stress for prismatic slip in Mg. The curves corresponding to 12.5 and 10.0 at.% Li decrease from 4° to about 300°K in a manner paralleling the expectations of the Peierls process; and between about 300° and 400°K they become substantually horizontal reflecting the operation of an athermal mechanism which is probably due to short-range order strengthening. The data for these alloys was analyzed in terms of the Peierls mechanism where in lieu of more accurate information the shear modulus of the alloys was estimated to decrease with increasing temperature in the same way as that for pure Mg. The Peierls plot for these alloys is shown in Figs. 27 and 28; and the experimentally determined activation volumes are compared with the theory of Figs. 29 and 30. The following data were then deduced as described previously for the Ag_2Al alloy.

at.% Li	10.0	12.5
τ_p° in dynes/cm	760×10^6	680×10^6
$2U_k$ in ergs (ev)	0.89×10^{-12} (0.55)	0.85×10^{-12} (0.55)
$2\Gamma_o/G^\circ b^2$	4.99	5.09

using in the last comparison the shear modulus of pure Mg since that for the alloys is unknown. The slightly high values of the line energy given in the last row of the above summary is probably attributable to the inaccurate shear modulus of elasticity that was used. The general agreement with the Peierls mechanism is nevertheless quite good.

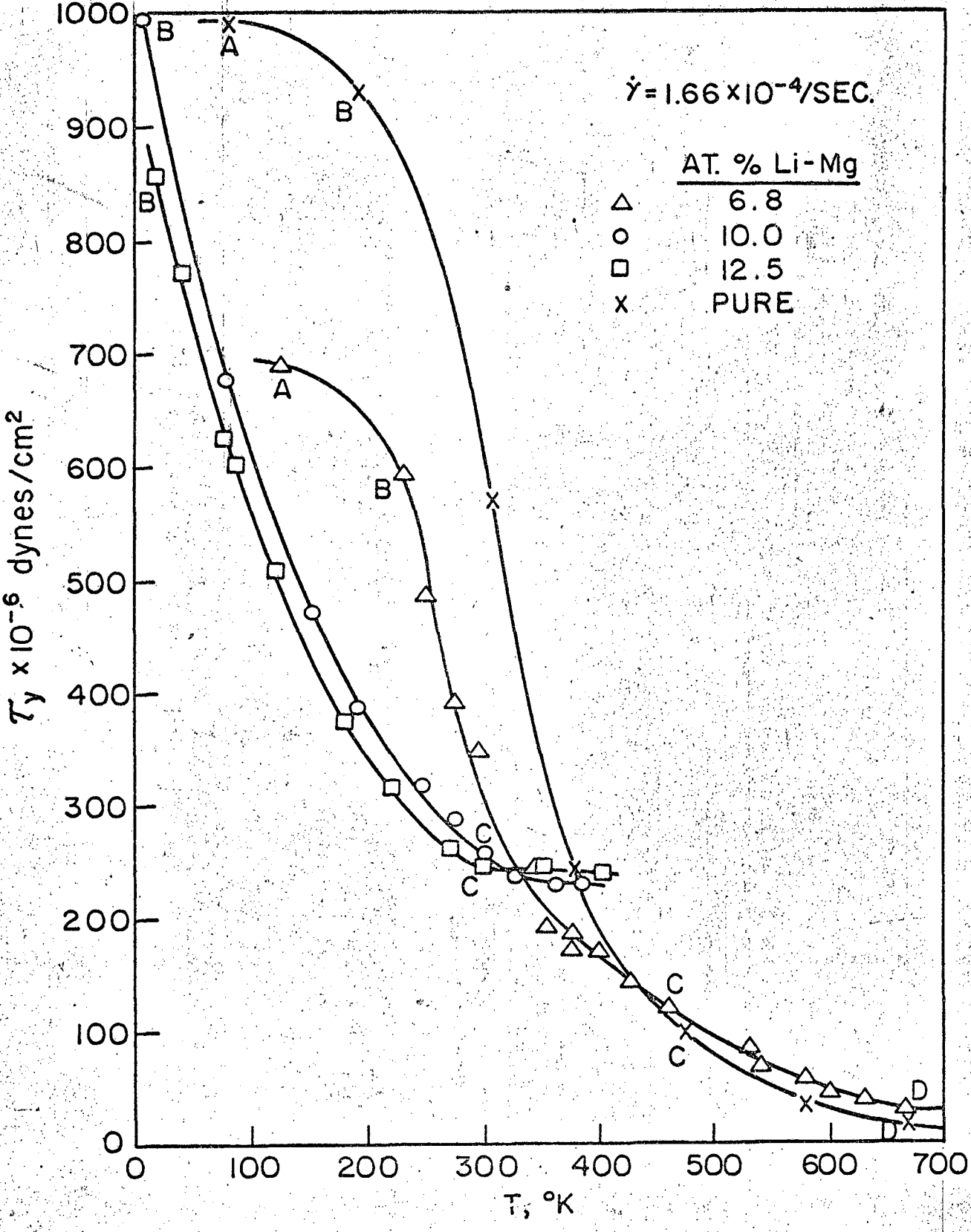

FIG. 26 CRITICAL RESOLVED SHEAR STRESS vs. TEMPERATURE FOR PRISMATIC SLIP IN PURE Mg AND Li-Mg ALLOYS.

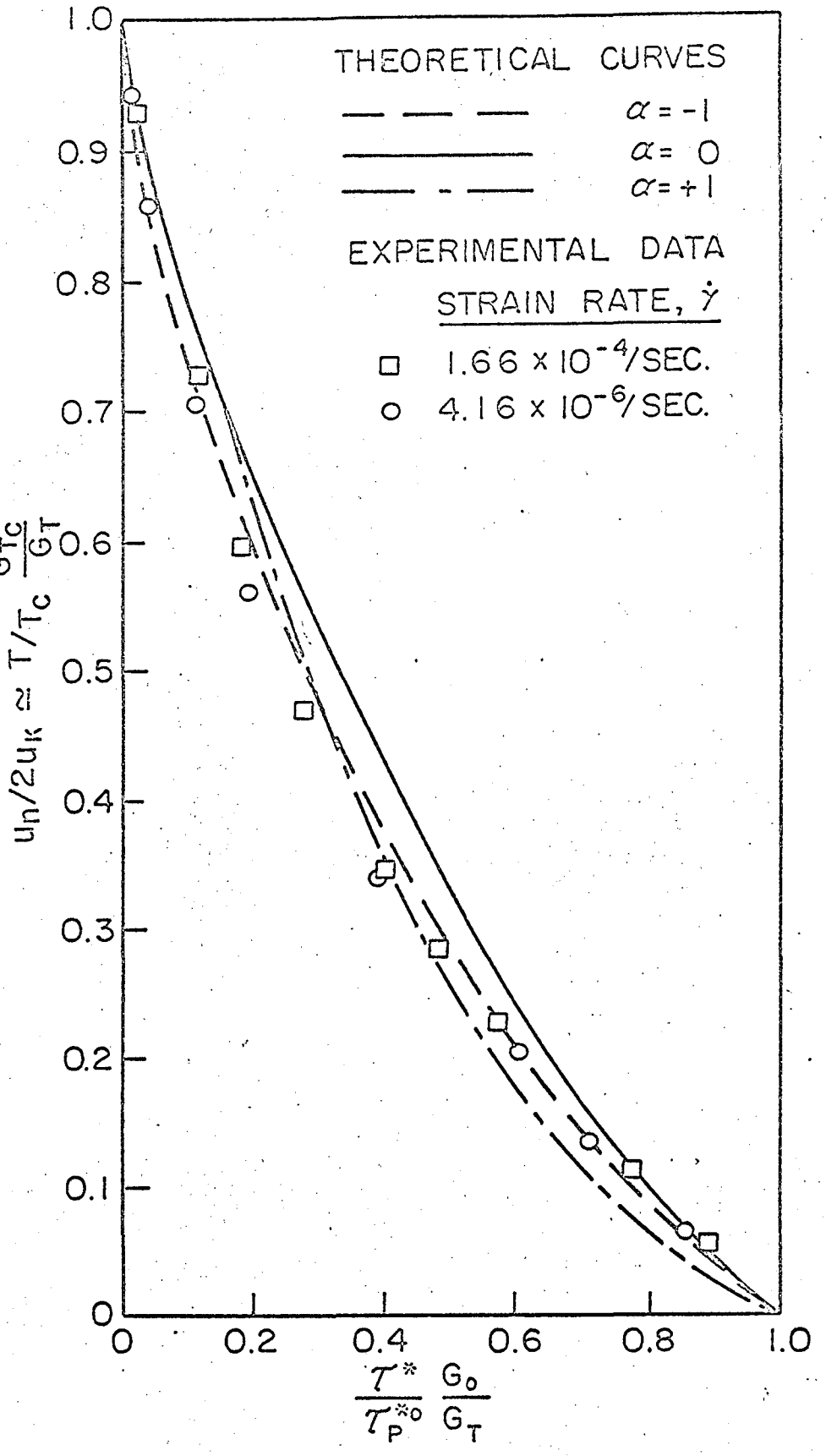

FIG. 27 TEMPERATURE vs. THERMALLY ACTIVATED FLOW STRESS IN DIMENSIONLESS UNITS FOR 10.8 AT. % Li-Mg.

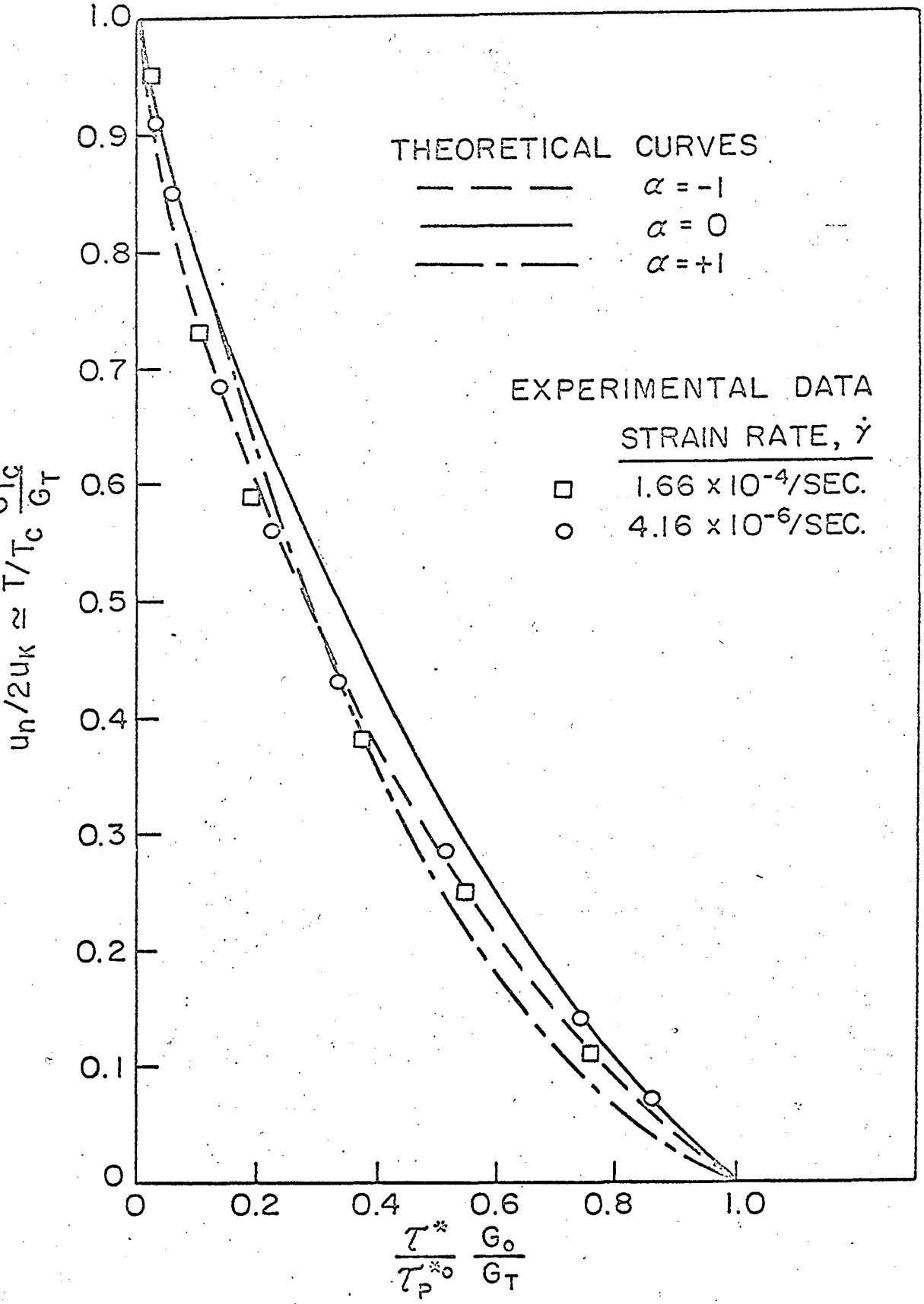

FIG. 28 THERMALLY ACTIVATED FLOW STRESS vs. TEMPERATURE IN DIMENSIONLESS UNITS FOR 12.5 AT. % Li-Mg.

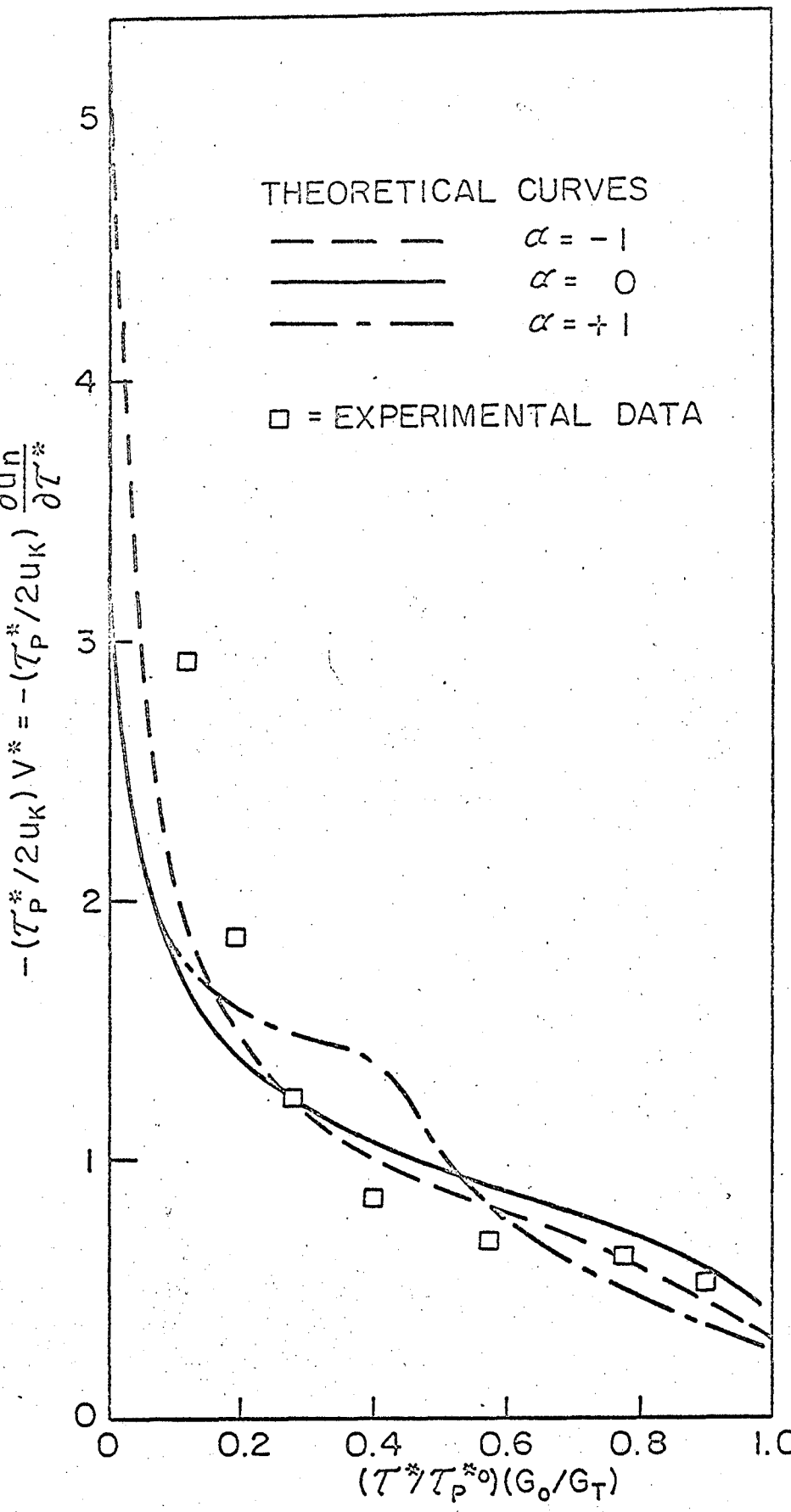

FIG. 29 ACTIVATION VOLUME vs. THERMALLY ACTIVATED COMPONENT OF FLOW STRESS IN DIMENSIONLESS UNITS FOR 10.8 AT. % Li-Mg.

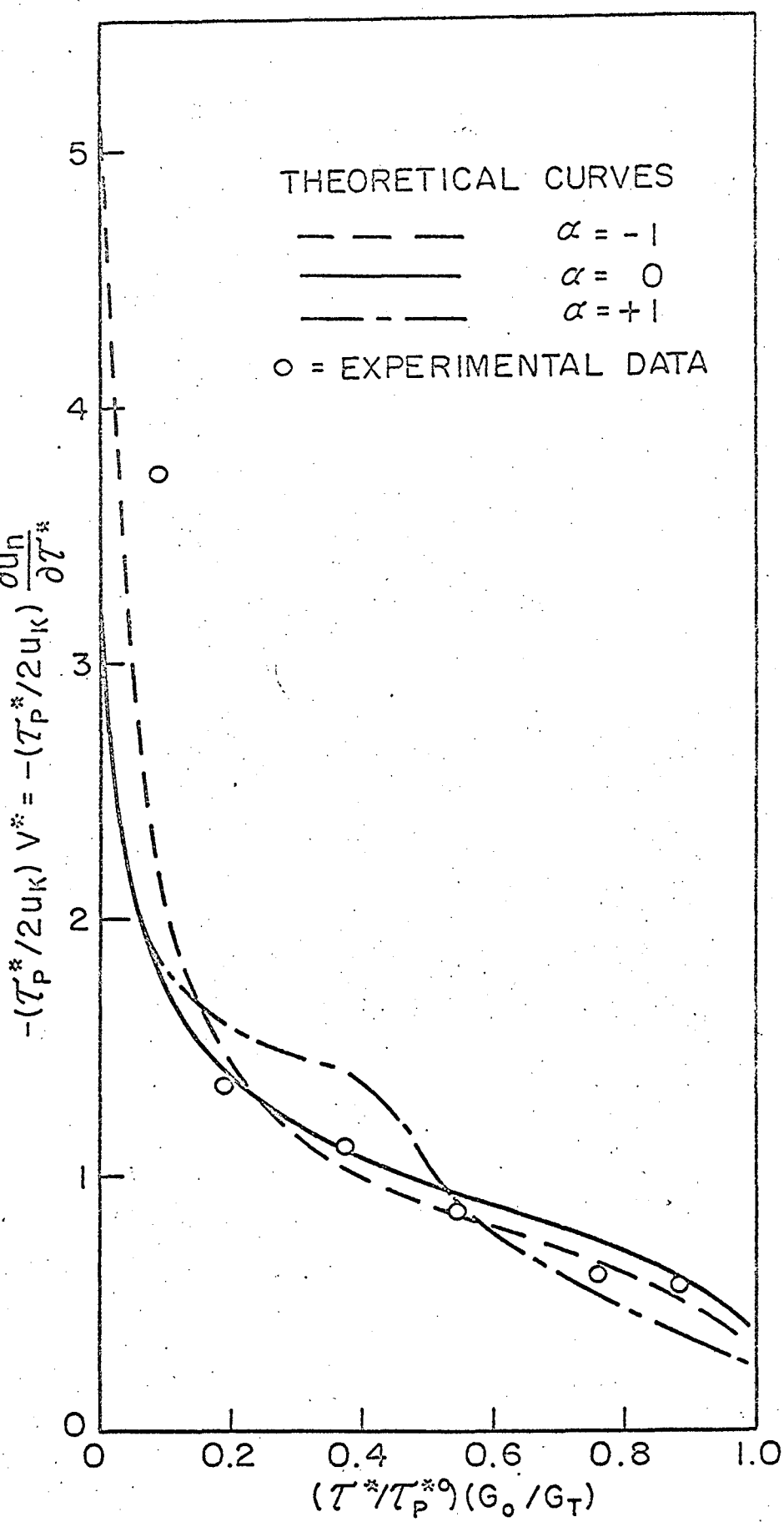

FIG. 30 THERMALLY ACTIVATED COMPONENT OF FLOW STRESS vs. ACTIVATION VOLUME IN DIMENSIONLESS UNITS FOR 12.5 AT. % Li-Mg.

The data for pure Mg and Mg plus 6.8 at.% Li were replotted to compare with Friedel's cross-slip theory as shown in Fig. 31. As discussed previously the linearity of these $\frac{1}{\tau T}$ vs $1/T$ curves suggest that cross slip is the controlling mechanism for prismatic slip at temperature above about 450°K. A comparison of the stacking fault width in the 6.8 at.% Li alloy with that in pure Mg is given below

	From Activation Volume	From Slope $\frac{1}{T\tau}$ vs $\frac{1}{T}$
Mg	~ 7b	~ 3b
Mg + 6.8 at.% Li	~ 6b	~ 3b

The same proceedure was used in calculating the results for the 6.8 at.% Li alloy as that previously employed for pure Mg where G for the alloy is assumed to be that for pure Mg. These data suggest that Li additions up to 6.8 at.% have only a minor effect on the stacking fault width. In view of these correlations, we suggest that the Friedel cross-slip mechanism operates over region CD in Fig. 26. Over region AB twinning and fracturing predominated and only minor amounts of prismatic slip were detected. The trends of the τ - T curves as well as the activation volume suggests that the Peierls process controls over region BC. We suggest that this transition occurs in spite of the higher flow stress for the cross-slip mechanism because more segments of dislocations larger than Friedel's critical length $L_c = 2r \sin \theta_c$ remain on the prismatic plane as the shear stress increases thereby eliminating the necessity for additional thermal activation of cross slip. Thus, the major effect of Li additions on the low-temperature shear stress for prismatic slip appears to be due to its effect in lowering the Peierls stress. The physical origin of this effect has not yet been explored.

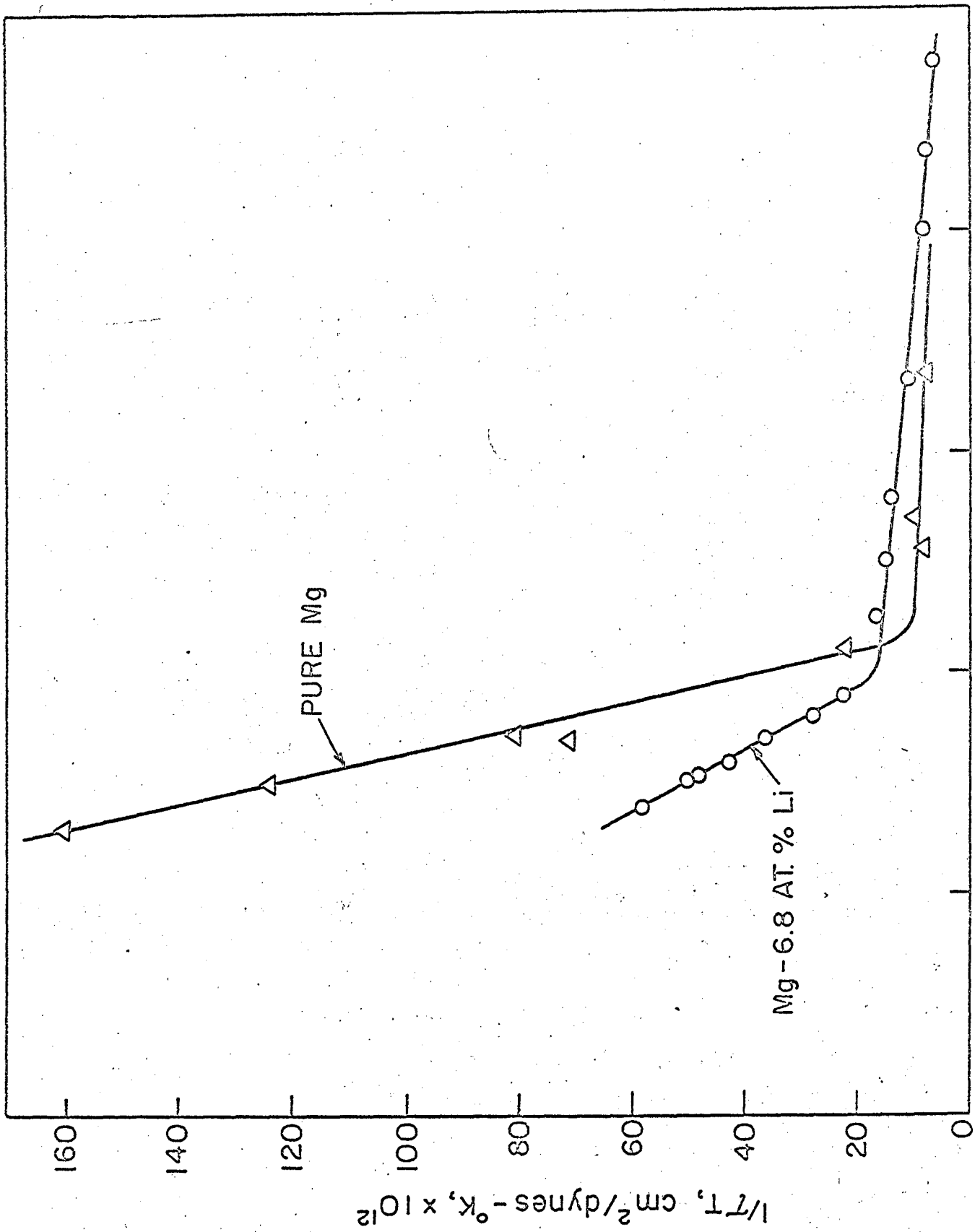

FIG. 31 $1/\tau T$ vs. $1/T$ FOR PRISMATIC SLIP IN Mg AND Mg-6.8 AT. % Li.

V. SUMMARY

Ultra-high strengths have not yet been achieved in polycrystalline aggregates of hexagonal metals because their ductility is so low. Although hexagonal metals contain the needed kinds of dislocations (e.g. c + a) for providing the five independent modes of slip that are needed for continuity of strains at the grain boundaries, the critical resolved shear stress for slip is so high on some modes that they remain inoperative. Because there is no other intrinsic reason for their relatively modest strengths, it should be possible to produce higher strength polycrystalline hexagonal metals by adjusting conditions so as to permit operation of the missing needed modes of slip. To accomplish this difficult objective a clear insight is needed into the operative mechanisms of slip and the factors that might modify these mechanisms.

Close-packed hexagonal alloys, in general, undertake the same kinds of mechanisms of slip that have been identified in face-centered cubic and body-centered cubic alloys. Basal slip in pure hexagonal metals is usually facile and, at low temperatures, it takes place by the dislocation-intersection mechanism. Strain hardening appears to arise principally from interactions between dislocations and from dislocation loop formation due to the condensation of mechanically produced vacancies. Alloying additions (vide Li in Mg) increase the athermal stress principally as a result of short-range order strengthening but also as a result of Cottrell and Suzuki locking. Alloying additions also modify the thermally activated component of the stress in harmony with the concept that the forest dislocation density is increased by solute additions. At higher temperatures (vide Cd in Zn) a viscous creep deformation by the

Weertman-Cottrell mechanism becomes rate controlling. And in some alloys (vide Ag_2Al) the deformation remains athermal over all temperatures as a result of strong Suzuki locking.

The current evidence on mechanisms of prismatic slip $\{10\bar{1}0\}$ $<1\bar{2}10>$ is somewhat less well defined than those for basal slip. At high temperatures, single crystals of Mg and Mg + 6.8 at.% Li obey Friedels cross-slip mechanism whereas Zn, Cd and Zn + 0.1 at.% Cd appear to obey some yet unidentified viscous creep mechanism, having activation energies much in excess of those for self diffusion. At low temperature 10.0 and 12.5 at.% Li alloys of Mg oriented for prismatic slip undertake the Peierls mechanism; and the 6.8 and 0.0 at.% Li alloys appear to exhibit the Peierls mechanism at intermediate temperatures. According to this interpretation, the Peierls stress decreases substantially with increasing Li content. At intermediate temperatures the 12.5 and 10.0 at.% Li alloys of Mg undertake an athermal prismatic slip mechanism that appears to be principally due to short-range order strengthening.

A significant observation concerns the decrease in the critical resolved shear stress for prismatic slip in Mg upon alloying with Li and thus reveals the potentialities of favorably modifying the Peierls stress so as to provide more facile modes of slip. Consequently, there is hope of producing stronger hexagonal alloys with good ductility. Prismatic slip mechanisms in Ag_2Al are controlled by the Peierls mechanism, short-range order strengthening, and fluctuations in short-range order leading to diffusion-controlled viscous creep respectively as the temperature is increased. At high rates of deformation diffusion-controlled mechanisms cannot operate and the Peierls mechanism controls.

The greatest potentiality for strength with adequate ductility in polycrystalline close-packed hexagonal metals rests with the possibility of providing more facile slip on the pyramidal plane by motion of the c + a dislocation because in combination with other modes of slip it provides the mode of slip needed for accomodation of strains at grain boundaries. It appears that this mode of slip is difficult to stimulate excepting in the case of Cd; and even in this case no attempt has yet been made to study the slip mechanisms that might be involved. It is likely that the Peierls mechanism will be found to control pyramidal slip by the c + a Burgers vector, in which event it might be possible to modify the Peierls stress by alloying.

The potentialities of producing high strength hexagonal close-packed alloys are revealed in the exceptionally high critical resolved shear stresses at room temperature of about 11,000 psi for basal slip and about 22,000 psi for prismatic slip in Ag_2Al. Opportunities for producing high strength polycrystalline hexagonal close-packed alloys with good ductility appear to exist but the approach is difficult and uncertain since it appears to center about methods of reducing the Peierls stress for various modes of deformation particularly that for pyramidal slip by the c + a dislocation.

ACKNOWLEDGMENTS

This survey was conducted as part of the activities of the Inorganic Materials Research Division of the Lawrence Radiation Laboratory of the University of California, Berkeley and was done under the auspices of the U.S. Atomic Energy Commission. The authors express their sincere appreciation for this support of their research and also acknowledge the numerous substantial contributions of their colleagues and coworders to this summary.

REFERENCES

1. W. B. Pearson, A Handbook of Lattice Spacings and Structures of Metals and Alloys, (Pergamon Press, 1958).
2. R. von Mises, Z. angew. Math. Mech., 8, 161 (1928).
3. F. C. Frank and J. F. Nicholas, Phil. Mag., 44, 1213 (1953).
4. A. Berghezan, A. Fourdeux and S. Amelinckx, Acta. Met. 9, 464 (1961).
5. P. B. Price, Electron Microscopy and Strength of Crystals, (J. Wiley, New York and London, 1963) pp. 41-130.
6. M. J. Whelan, Proc. Roy. Soc. (London), A249, 114 (1958).
7. A. Seeger, S. Mader and H. Kronmüller, Electron Microscopy and Strength of Crystals, (J. Wiley, New York and London, 1963) p. 665.
8. J. Friedel, Electron Microscopy and Strength of Crystals, (J. Wiley, New York and London, 1963) p. 605.
9. M. J. Marcinkowski, Electron Microscopy and Strength of Crystals, (J. Wiley, New York and London, 1963) p. 333.
10. N. S. Stoloff and M. Gensamer, Trans. AIME, 227, 70 (1963).
11. J. J. Gilman, Trans. AIME, 221, 456 (1961).
12. P. B. Price, Phil. Mag., 6, 449 (1961).
13. F. Kroupa and P. B. Price, Phil. Mag., 6, 243 (1961).
14. P. B. Price, J. Appl. Phys., 32, 1746-1750 (1961).
15. N. S. Stoloff and M. Gensamer, Trans. AIME, 224, 732 (1962).
16. J. H. Wernick and E. E. Thomas, Trans. AIME, 218, 769 (1960).
17. P. B. Price, Phys. Rev. Letters, 6, 615 (1961).
18. A. Seeger and H. Trauble, Z. Metallk., 51, 435 (1960).
19. J. J. Gilman, Trans. AIME, 206, 1326 (1956).
20. H. S. Rosenbaum, Acta. Met., 9, 742 (1961).

21. P. B. Price, Phil. Mag., 5, 873 (1960).

22. P. B. Price, Phil. Mag., 6, 449 (1961).

23. R. L. Bell and R. W. Cahn, Proc. Roy. Soc., (London) A239, 994 (1957).

24. A. F. Kolesnikov, J. of Experimental and Theoretical Physics, 8, 301 (1938).

25. F. E. Hauser, P. R. Landon and J. E. Dorn, Trans. AIME, 48, 986 (1956).

26. P. W. Bakarian and C. H. Mathewson, Trans. AIME, 152, 226 (1943).

27. E. C. Burke and W. R. Hibbard, Trans. AIME, 194, 295 (1952).

28. W. F. Sheely and R. R. Nash, Trans. AIME, 218, 416 (1960).

29. H. Conrad and W. P. Robertson, Trans. AIME, 209, 503(1957).

30. H. Conrad, L. Hays, G. Schoeck and H. Wiedersich, Acta. Met., 9, 367 (1961).

31. G. Thomas, R. B. Benson and J. Nadeau, Proceedings of the Regional Conference on Electron Microscopy, De Nederlandse Vereniging voor Electronenmicroscopic, Delft, 447, (1961).

32. P. Ward Flynn, J. D. Mote and J. E. Dorn, "On the Thermally Activated Mechanism of Prismatic Slip in Magnesium Single Crystals," Trans. AIME, 221, 1148 (1961).

33. E. Schmid and W. Boas, Plasticity of Crystals, (Hughes, London, 1950).

34. R. E. Reed-Hill and W. D. Robertson, Acta. Met., 5, 717 (1957).

35. R. E. Reed-Hill and W. D. Robertson, Acta. Met., 5, 728 (1957).

36. R. E. Reed-Hill and W. D. Robertson, Trans. AIME, 209, 496 (1957).

37. R. E. Reed-Hill and W. D. Robertson, Trans. AIME, 212, 256 (1958).

38. A. T. Churchman, Proc. Roy. Soc., A226, 216 (1954).

39. A. T. Churchman, Nature, (London), 171, 706 (1953).

40. R. D. Rosi, C. A. Dube and B. H. Alexander, Trans. AIME, 197, 257 (1953).

41. E. J. Rapperport, Acta. Met., 162, 208 (1955).

42. E. D. Levine, D. F. Kaufman and L. R. Aronin, (to be published Trans. AIME, 1964).

43. H. T. Lee and R. M. Brick, Trans. ASM, 48, 1003 (1956).

44. R. I. Garber, I. A. Gindin and Yu V. Shubin, Soviet Physics Jet P, 36(9)-2, 260 (1954).

45. R. I. Garber, I. A. Gindin and Yu V. Shubin, Soviet Physics-Solid State, 5, [2] (1963).

46. A. Moore and G. C. Ellin, Abstract of paper presented by Atomic Weapons Research Establishment, Aldermaston, England, at Beryllium Physical Metallurgy Conference at Gatlinbury, Tennessee, April 30-May 1, 1963.

47. P. Bastien and P. Pointu, J. of Nucl. Mat., 5, [1], 153-155 (1962).

48. F. E. Hauser, P. R. Landon and J. E. Dorn, Trans. ASM, 50 856, (1958).

49. R. M. Quimby, J. D. Mote and J. E. Dorn, Trans. ASM, 55 [1], 149 (1962).

50. J. D. Mote, K. Tanaka and J. E. Dorn, Trans. AIME, 221, 858 (1961).

51. A. Rosen, J. D. Mote and J. E. Dorn, (to be published Trans. AIME, 1964).

52. N. S. Stoloff and R. G. Davies, (to be published J. Inst. of Metals, 1964).

53. P. H. Thornton, Phil. Mag., 8, 2013 (1963).

54. R. G. Davies and N. S. Stoloff, Trans. AIME, (in press, 1964).

55. R. Peierls, Proc. Phys. Soc. (London), 52, 34 (1940).

56. F. R. N. Nabarro, Proc. Phys. Soc. (London), 59, 256 (1947).

57. J. Friedel, "Dislocations Interactions and Internal Strains," Physiques des Solides, Sorbonne, Paris, 220-262 (1959).

58. G. W. Groves and A. Kelly, Phil. Mag., 3, 877 (1963).

59. E. Schmid, Z. Electrochem., 37, 447 (1931).

60. W. Fahrenhorst and E. Schmid, Z. Physik, 64, 845 (1930).

61. W. Boas and E. Schmid, Z. Physik, 57, 575 (1929).

62. P. I. Trehorne and A. Moore, J. Less-Common Metals, 4, 275 (1962).

63. J. Washburn and E. R. Parker, Trans. AIME, 194, 1076 (1952).

64. G. Saada, Acta. Met., 8, 841 (1960).

65. A. Seeger, Z. Naturforsch, 9A, 758, 810, 856 (1954).

66. J. Friedel, Les Dislocations, (Gauthier-Villars, Paris, 1956) p. 2056.

67. Z. S. Basinski, Phil. Mag., 4, 393 (1959).

68. H. Suzuki, Dislocations and Mechanical Properties of Crystals, (J. Wiley, New York, 1957) p. 361.

69. A. H. Cottrell, Report of Conference on Strength of Solids, The Phys. Soc., 30 (1948).

70. J. Weertman, J. Appl. Phys., 28, 1185 (1957).

71. A. H. Cottrell and M. A. Jaswon, Proc. Roy. Soc. (London), A199, 104 (1949).

72. T. Larsen, S. L. Rajnak, F. E. Hauser, and J. E. Dorn, University of California, Materials Research Laboratory, Technical Report No. 2 (1962)

73. J. E. Dorn and F. E. Hauser, Proceedings of Symposium on Structural Dynamics Under High Impulse Loading, Technical Documentary Report No. ASD-TDR-63-140 (May, 1963).

74. J. E. Dorn and J. B. Mitchell, J. of Spacecrafts and Rockets, 1, 48 (1964).

75. J. P. Neumann, Acta. Met., 10, 984 (1962).

76. A. Seeger, Phil. Mag., 1, 651 (1956).

77. A. Seeger, H. Donth and F. Pfaff, Discussion Faraday Soc., 23, 197 (1957).

78. J. Lothe and J. P. Hirth, Phys. Rev., 115, 543 (1959).

79. A. Seeger and P. Schiller, Acta. Met., 10, 348 (1962).

80. T. Jøssang, K. Skylstad and J. Lothe, "Theory of Thermal Activation of Dislocations over the Peierls Barrier in a Revised Seeger-Donth Formulation," Presented at the Conference on the Relation Between Structure and Strength in Metals and Alloys, National Physical Laboratory, Teddington, Middlesex, England, (Jan.,1963).

81. J. E. Dorn and S. Rajnak, "Nucleation of Kink Pairs and the Peierls Mechanism of Plastic Deformation," (to be published Trans. AIME, 1964).

82. J. C. Fisher, Acta. Met., 2, 9 (1954).

83. J. M. Cowley, Phys. Rev., 5, 77 (1950).

84. P. A. Flinn, Phys. Rev., 104, 350 (1956).

85. E. Howard, W. Barmore, J. Mote and J. E. Dorn, "On the Thermally-Activated Mechanism of Prismatic Slip in the Ag-Al Intermediate Phase," (to be published Trans. AIME, 1964).

86. H. Kolsky, Proc. Phys. Soc., 62, 677 (1949).

87. A. Ahmadieh, "Lithium Alloying and Dislocations Mechanisms for Prismatic Slip in Magnesium," Ph.D. Thesis, University of California, (May, 1964).

88. C. S. Roberts, Magnesium and Its Alloys, (J. Wiley, New York, 1960).

89. A. N. Stroh, Proc. Phys. Soc. (London) B, 67, 427 (1954).

90. J. Friedel, Internal Stresses and Fatigue in Metals, (Elsevier Publishing Co., Amsterdam, London and New York, 1959) p. 220.

91. J. E. Dorn, "Energetics of Dislocation Mechanics," NRC Seminar on Energetics in Metallurgical Phenomena, University of Denver (July, 1962), to be published.

APPENDIX I

Force-Displacement Diagram for the Mechanical Formation of a Constriction

Although several investigators have already calculated the activation energy for the mechanically assisted formation of a constriction during intersection,[1,2,3,4] the following approximate analysis of the equivalent information on the force-displacement diagram during the formation of a constriction was nevertheless deemed interesting because it employs a different mathematical procedure and gives a simple analytical expression for the force necessary to form a partial constriction.

If L is the average spacing of the forest dislocations that thread the slip plane, a force $F = \tau^* Lb$ acts at their point of contact restraining the forward motion of the glide dislocation. The stress τ^* is the local shear stress on the slip plane in the direction of the total Burger's vector, b, of the glide dislocation. At low stresses, the action of the force $F = \tau^* Lb$ causes a partial constriction to form in the glide dislocation, as shown somewhat schematically in Fig. A1. The local force $\tau^* Lb$, displaces the leading partial from its original equilibrium separation of y_o from the second partial to a smaller separation, λ at its point of contact. The completion of constriction, as shown by the broken curve in the figure requires the aid of an appropriate thermal fluctuation. It is the purpose of this calculation to estimate in terms of a line energy model the saddle-point energy that must be supplied by a thermal fluctuation in order to complete constriction. The total activation energy will then be the constriction activation energy plus the activation energy for the jogs that are produced.

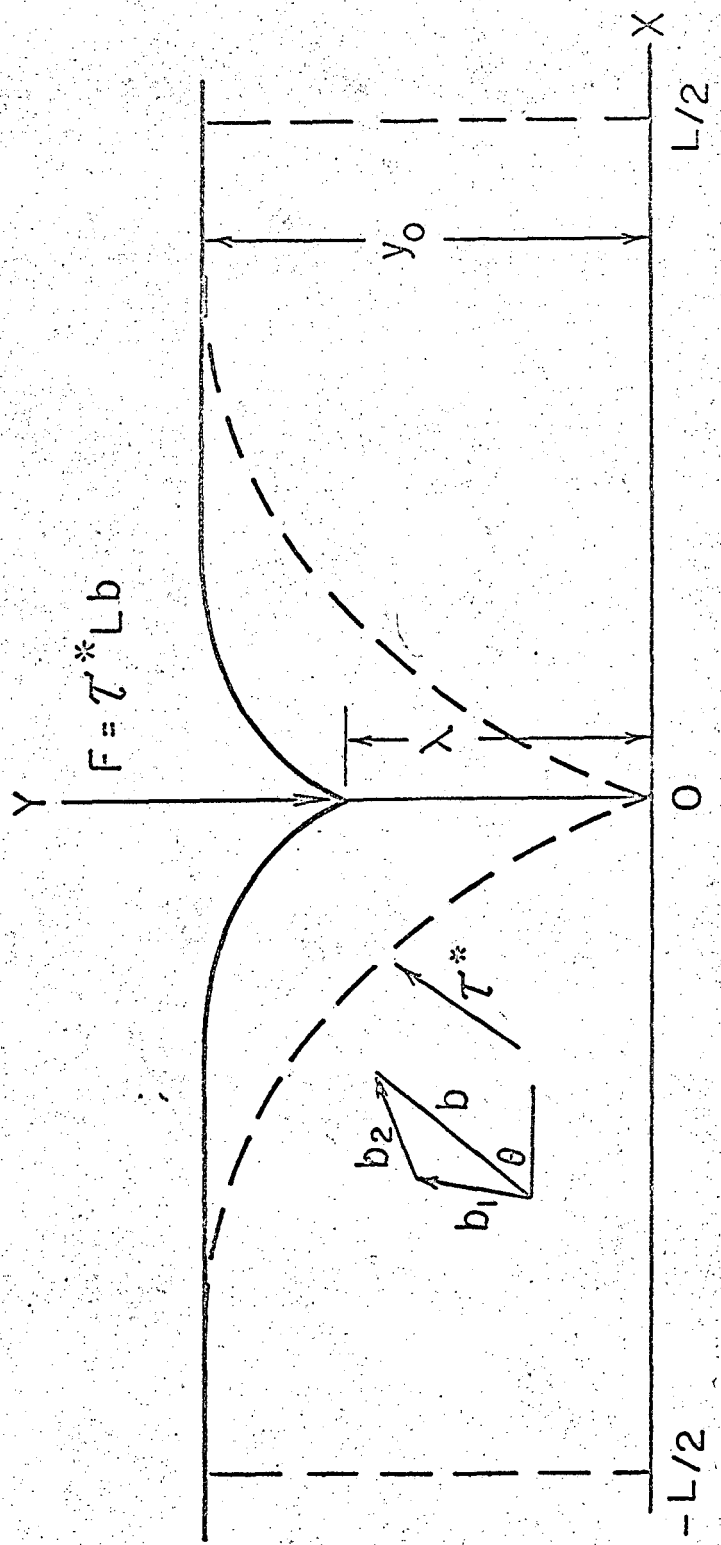

FIG. A1 CONSTRICTION DUE TO A POINT FORCE.

The calculation of the activation energy to complete a constriction will be based on the following steps. First the energy $U\{\lambda\}$ will be determined as a function of λ for the partially formed constrictions. This will be done from energy considerations by arbitrarily selecting each λ and demanding that $\frac{\partial y}{\partial x} = 0$ at $x = \pm L/2$. Furthermore, the true shape of the leading partial will be determined by minimizing the energy. Consequently the force $F = \tau^* Lb$ can be equated to $-\frac{\partial U_c}{\partial \lambda}$ and thus the force will be established as a function of λ. The activation energy for completion of a constriction is then given by

$$U^* = U_c\{\lambda = 0\} - U_c\{\lambda\} + \left(\frac{\partial U_c}{\partial \lambda}\right)_\lambda \lambda \qquad \text{(A1)}$$

where the difference between the first two terms gives the additional energy required to complete the constriction and the last term refers to the extra work done by the constant force F in aiding the formation of the constriction. Consequently, the entire problem is solved when $U_c\{\lambda\}$ is determined.

The change in energy due to the formation of a partial constriction for a displacement from $y = y_o$ to $y = \lambda$ at $x = 0$ is estimated to be

$$U = \int_{-L/2}^{+L/2} \left[\Gamma_p \left\{ 1 + \left|\frac{dy}{dx}\right|^2 \right\}^{1/2} - \Gamma_p + \gamma\left|y - y_o\right| + \frac{Gb^2Q}{24\pi}\ \phi\{y\} \right] dx \qquad \text{(A2)}$$

where Γ_p is the energy per unit length of a partial dislocation, γ is the stacking fault energy per unit area, G is the shear modulus, b is the total Burger's vector of the dislocation and Q is the orientation factor given by

$$Q = \left(3 - \frac{1}{1-\mu}\right) \cos^2\theta + \left(\frac{3}{1-\mu} - 1\right) \sin^2\theta \qquad \text{(A3)}$$

where u is the Poisson's ratio and θ is defined in Fig. A1. $\phi\{y\}$ gives the dependence of the repulsion potential energy due to the interaction of the

partial dislocations. The line energy of a partial dislocation is assumed to be given by

$$\Gamma_p \sim \alpha \frac{G\bar{b}_1 \cdot \bar{b}_1}{2} = \frac{\alpha G b^2}{6} \tag{A4}$$

regardless of the orientation of the partial dislocation in order to preserve the symmetry of the constriction and thereby simplify the problem. The factor α thus serves as a factor that accounts in part for the orientation of the partial dislocation, the effect of curvature on the line energy and the fact that the interaction energy between the two branches of the constricted partial dislocation will be neglected. Thus α should be slightly less than 1 when the bowed partial dislocation is in screw orientation and slightly less than $1/(1 - u)$ when it is in edge orientation.

Whereas the force of repulsion for two partial dislocations a distance y apart is given by[5]

$$R = - \frac{Gb^2 Q}{24\pi y} \qquad \text{for } y \gtrsim b \tag{A5}$$

the force will be assumed to be

$$R = - \frac{Gb^2 Q}{24\pi b} \qquad \text{for } y \lesssim b \tag{A6}$$

in order to avoid infinite repulsion forces at the point of completion of the constriction. Therefore

$$\phi\{y\} = \begin{cases} 1 - y/b + \ell n\, y_o/b & y \leq b \qquad \text{(A7)} \\ \ell n\, y/y_o & y \geq b \qquad \text{(A8)} \end{cases}$$

Consequently, the first two terms under the integrand of Eq. A2 give the increase in line energy, the third term represents the change in

stacking fault energy, and the last term refers to the change in interaction energy.

At their original equilibrium positions both partial dislocations will be straight lines at a distance y_o apart. Under these conditions the first two terms of the integrand of Eq. A2 will be zero, whence the equilibrium conditions, given by $\partial U/\partial y = 0$, is

$$y_o = \frac{Gb^2Q}{24\pi\gamma} \tag{A9}$$

As shown by Eqs. A4 and A9

$$\gamma/2\Gamma_p = Q/8\pi\alpha y_o = c/y_o \tag{A10}$$

where c is defined as $Q/8\pi\alpha$. Therefore Eq. A2 can be rewritten as

$$U = 2\Gamma_p y_o \int_o^{L/2} \left[\left\{1 + \left|\frac{dy}{dx}\right|^2\right\}^{1/2} - 1 + 2c\left|\frac{y}{y_o} - 1 + \phi\{y\}\right|\right] dx \tag{A11}$$

In order to facilitate the integration, the dimensionless variables

$$z = y/y_o \tag{A12}$$

$$t = x/y_o \tag{A13}$$

$$\dot{z} = \frac{dz}{dt} = \frac{dy}{dx} \tag{A14}$$

will be adopted, whence Eq. A11 reduces to

$$\frac{U}{2\Gamma_p y_o} = \int_o^{L/2y_o} \left[\left(1 + \dot{z}^2\right)^{1/2} - 1 + 2c\left|z - 1 + \phi\{z\}\right|\right] dt \tag{A15}$$

where in this case

$$\phi\{z\} = \begin{cases} 1 - zy_o/b + \ell n y_o/b & z \leq b/y_o \qquad (A16) \\ -\ell n z & z \leq b/y_o \qquad (A17) \end{cases}$$

and the boundary conditions become

$$y = \lambda \text{ at } x = 0 \text{ or } z = z_1 = \lambda/y_o \text{ at } t = t_1 = 0 \tag{A18}$$

and

$$\left|\frac{dy}{dx}\right| = 0 \text{ at } x = \frac{L}{2} \text{ or } \dot{z} = 0 \text{ at } t = t_2 = L/2y_o \tag{A19}$$

The minimum energy curve is then given by Euler's equation, which for this case is

$$\frac{\partial f}{\partial z} = \frac{d}{dt}\left(\frac{\partial f}{\partial \dot{z}}\right) \tag{A20}$$

where f is the integrand of Eq. A15. Therefore, Euler's equation is

$$2c\left(1 + \frac{\partial \phi\{z\}}{\partial z}\right) = \frac{\ddot{z}}{\left(1 + \dot{z}^2\right)^{3/2}} \tag{A21}$$

which can now be integrated once to give

$$2c\left(z + \phi\{z\}\right) = -\frac{1}{\left(1 + \dot{z}^2\right)^{1/2}} + \text{constant} \tag{A22}$$

At $t = t_2 = L/2y_o$, where the boundary conditions given by Eq. A19 apply, we let $z = z_2 = a$, where from the physics of the problem it is obvious that $a \leq 1$. In terms of these boundary conditions, the constant of integration is given by

$$2c\left(a + \phi\{a\}\right) = -1 + \text{constant} \tag{A23}$$

and Eq. A22 becomes

$$\frac{1}{\left(1 + \dot{z}^2\right)^{1/2}} = 1 - 2c\left(2 + \phi\{z\}\right) + 2c\left(a - \ell n a\right) \tag{A24}$$

where the last term arises because the calculations will be restricted to values of a greater than b/y_o for which $\phi\{a\} = -\ell n a$.

It is now necessary to determine what values of a should be employed in any selected example. Eq. A24 can be rewritten as

$$\int_{\lambda/y_o}^{a} \frac{dz}{\sqrt{\frac{1}{[1 - 2c\,(z - a + \phi\{z\} + \ell na)]^2} - 1}} = \int_{o}^{t^*} dt = t^* \qquad \text{(A25)}$$

for $a < 1$, $t^* = L/2y_o$ and thus it is seen that $a = a\{\lambda/y_o,\ L/2y_o\}$. To solve the integral equation, Eq. A25, for a, we selected a and λ/y_o and integrated mechanically to obtain $L/2y_o$. These data reveal that $a = 1$ when $L/2y_o > 15$.

The energy of a partial constriction can now be written in terms of Eq. A15 which, upon change of the independent variable from t to Z gives

$$\frac{U_c}{2\Gamma_p y_o} = \int_{\lambda/y_o}^{a} \left[\left(1 + \dot{z}^2\right)^{1/2} - 1 + 2c\left(z - 1 + \phi\{z\}\right)\right] \frac{dz}{\dot{z}} \qquad \text{(A26)}$$

The value of $\dot{z}$ must be expressed as a function of z, as given by Eq. A24 in order to refer to the least energy constriction. When this is done Eq. A26 becomes

$$\frac{U_c}{2\Gamma_p y_o} = \int_{\lambda/y_o}^{a} \left\{\sqrt{1 - [1 - 2c\,(z + \phi\{z\} - a + \ell na)]^2} + \frac{[1 - 2c\,(z + \phi\{z\} - a + \ell na)]\ 2c\,(a - 1 - \ell na)}{\sqrt{1 - [1 - 2c\,(z + \phi\{z\} - a + \ell na)]^2}}\right\} dz \qquad \text{(A27)}$$

For values of $L/2y_o > 15$ where a becomes unity, this integral simplifies since the last term in the integrand vanishes for these conditions.

Rather than record U_c as a function of λ/y_o, the frequently quoted force-displacement (F-λ) diagram that was originally introduced by Basinski[6] will be derived first. Toward achieving this objective we note that

$$\tau^* Lb = F = -\frac{\partial U_c}{\partial \lambda} = -\frac{1}{y_o}\frac{\partial U_c}{\partial (\lambda/y_o)} \qquad \text{(A28)}$$

for the case where $L/2y_o \gtrsim 15$ and $a = 1$, only differentiation with respect to the lower limit of the integral of Eq. A27 is involved and the simple result is

$$\frac{F}{2\Gamma_p} = \sqrt{1 - [1 - 2c\,(\lambda/y_o + \phi\{\lambda/y_o\} - 1)]^2} \qquad \text{(A29)}$$

Several $F/2\Gamma_p$ vs λ/y_o curves are shown in Fig. A2. The curve for $2c = 0.24$ refers to the force-displacement diagram for the formation of a constriction when the total dislocation being constricted is in edge orientation whereas that for $2c = 0.12$ gives the force-displacement diagram for constriction when the total dislocation is in screw orientation. The F-λ diagram for Mg assuming $y_o = 2b$ is given in Fig. 10 of the text.

The total energy for the completion of a constriction is

$$U_c = 2\Gamma_p y_o \int_o^1 F/2\Gamma_p \, d\,(\lambda/y_o) \qquad \text{(A30)}$$

Examples are given in Fig. 9 of the text.

The energy to form incomplete constrictions for various cases can easily be deduced from Eq. A27 and A25 where $\phi\{Z\}$ is defined by Eqs. A16 and A17.

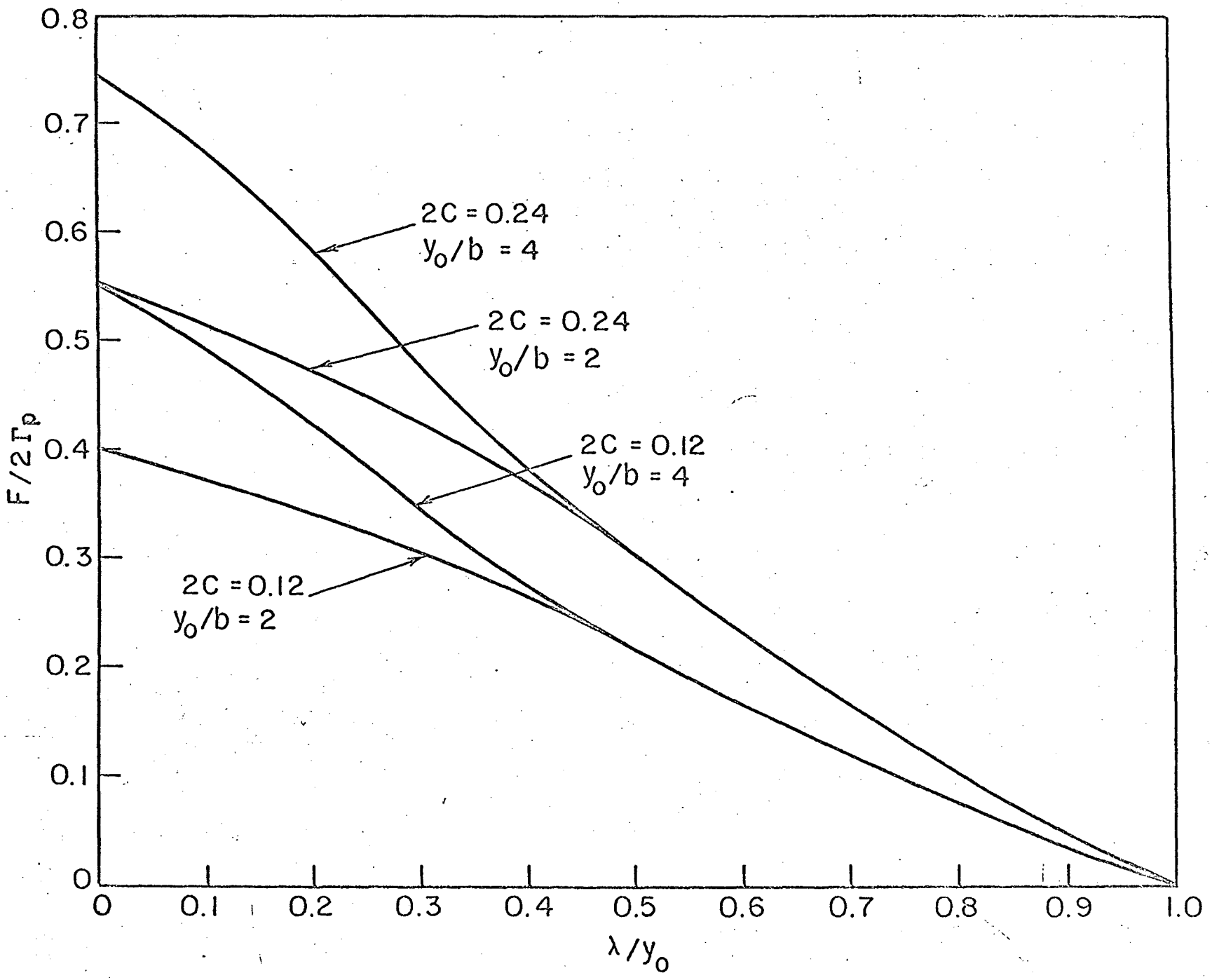

FIG. A 2 FORCE-DISPLACEMENT DIAGRAMS FOR DIFFERENT VALUES OF $C = Q/8\pi\sigma$ AND y_o/b

APPENDIX REFERENCES

1. A. Seeger, Z. Naturforsch, 9a, 856 (1954); Defects in Crystalline Solids, (London Physical Society) (1955).
2. A. N. Stroh, Proc. Phys. Soc. B, 67, 427 (1954).
3. G. Schoeck and A. Seeger, Report of Conference on Defects in Crystalline Solids, Bristol, (1954), London Physical Society, 340 (1955).
4. A. Seeger and H. Wolf, See A. Seeger, S. Mader and H. Kronmüller, Electron Microscopy and Strength of Crystals, (J. Wiley, New York and London) 665 (1963).
5. A. H. Cottrell, Dislocations and Plastic Waves in Crystals, (Oxford) 74 (1956).
6. Z. S. Basinski, Phil. Mag., 4, 393 (1959).